Master Thesis

Formation Breakdown Pressure Prediction Models and Their Applicability in Various Rock Types and Wellbores

Written by:
Akos Kiss, BSc.
1335418

Advisor:
Univ.-Prof. Dipl.-Ing. Dr.mont. Herbert Hofstätter

Leoben, 20.10.2015

EIDESSTATTLICHE ERKLÄRUNG

Ich erkläre an Eides statt, dass ich die vorliegende Diplomarbeit selbständig und ohne fremde Hilfe verfasst, andere als die angegebenen Quellen und Hilfsmittel nicht benutzt und die den benutzten Quellen wörtlich und inhaltlich entnommenen Stellen als solche erkenntlich gemacht habe.

AFFIDAVIT

I hereby declare that the content of this work is my own composition and has not been submitted previously for any higher degree. All extracts have been distinguished using quoted references and all information sources have been acknowledged.

Danksagung / Acknowledgement

I wish to thank OMV Aktiengesellschaft and Devon Energy Corporation for providing hydraulic fracturing treatment data for the study.

I owe my deepest gratitude to

- Reinhard Pongratz
- Robert Maier
- Luigi Corvatta
- Thomas Finkbeiner
- Dwyann Dalrymple

from OMV Aktiengesellschaft for their guidance and for their critical view on the problems challenged throughout this work.

Special thanks to Jeff Dahl for his help to use data from Devon Energy Corporation.

Furthermore, I deeply appreciate the endless technical support from Dipl.-Ing. Dr.mont. Rudolf Fruhwirth (NGS - Neuro Genetic Solutions, Montanuniversität Leoben) as well as providing cVision neural networks for the study.

Special thanks to

- Univ.-Prof. Dipl.-Ing. Dr.mont. Herbert Hofstätter
- Univ.-Prof. Dipl.-Ing. Dr.mont. Gerhard Thonhauser

for teaching the theoretical backgrounds.

Furthermore, thanks to Barree & Associates LLC for providing a student license for GOHFER, the 3D frac simulator software and to all Production Technology employees of OMV Aktiengesellschaft and to Abbas Zamani (Montanuniversität Leoben) who were always happy to help in case any problem encountered.

Akos Kiss

Kurzfassung

Die Diplomarbeit beschreibt den Vergleich errechneter hydraulischer Druckwerte die zum Aufbrechen von Gesteinsschichten notwendig sind (FBP) mit den tatsächlich gemessenen Werten. Die Berechnungen für 141 Behandlungen wurden ausgewertet. Die zum Vergleich bereitstehenden Daten stammen aus verschiedenen Gas- und Ölfelder der OMV Aktiengesellschaft und der Devon Energy Corporation. Das Ziel der Diplomarbeit war die Untersuchung der Genauigkeit und Gültigkeit der Ergebnisse der verschiedenen Modelle unter der Annahme, dass die Modelle als allgemein gültig für die verschiedensten Lagerstätten entwickelt wurden. Die untersuchten Daten decken eine breite Palette von verschiedenen Sandsteinformationen, einige Felder mit Kalkgestein und eine Shale Gas Formation ab. Diese Bandbreite an verschiedenen Lagerstätten und Lagerstättengesteinen verursacht, dass die gemessenen Formation Breakdown Pressures (FBP) im Bereich von 4333 bis 16707 psi liegen und somit sowohl „schwache“ als auch „starke“ Formationen untersucht wurden.

Alle Modelle, die zur FBP - Druckvorhersage eingesetzt werden, sind veröffentlicht und ausführlich in technischen Publikationen erläutert. Die Berechnungsmodelle basieren auf Theorien die elastische, linear-elastische, porenelastische, Punkt Stress und thermo-porenelastische Bruchmechanik beschreiben. Die Korrelationen wurden über ein Error Analysis Framework verglichen und die Genauigkeit und Präzision der Modelle identifiziert und klassifiziert. Sechs verschiedene Analysemethoden wurden angewendet, um eine möglichst objektive Klassifizierung der Modelle zu erreichen. Das Modell, das am besten abschnitt, wurde einer Sensitivitätsanalyse der Eingabeparameter unterzogen, um die gesteinsmechanischen Eigenschaften, die das Modell am stärksten beeinflussen, zu bestimmen. Als zweites sollte diese Analyse auch zeigen welche Parameter den größten Einfluss auf die Druckvorhersage und deren Genauigkeit haben.

Da die Berechnungsergebnisse der untersuchten Modelle keine ausreichende Vorhersagequalität zeigten und keine einfache und konsistente Aussage über die beeinflussenden Datenzusammenhänge erlaubten, wurde ein Computerprogram, das auf dem Prinzip von künstlichen neuronalen Netzwerk basiert, eingesetzt. Es wurde überprüft wie weit mit den vorhandenen Daten eine genaue FBP-Vorhersage möglich ist. Bei dieser Methode wird Informationstechnologie mit Geologie und Erdöltechnik kombiniert, um möglichst verlässliche Ergebnisse zu erzielen und es ist eine Methode die mehr und mehr Bedeutung auch in der Öl- und Gasindustrie gewinnt. Die Gültigkeit dieser Methode wurde mit erstaunlichen Ergebnissen nachgewiesen, da die Vorhersagegenauigkeit eine unerwartete niedrige Fehlerquoten von <10 % erzielte. Der Autor ist der Auffassung, daß zukünftig der Einsatz von künstlichen neuronalen Netzwerken sowohl in der die Ölindustrie, als auch in vielen anderen Industriezweigen ausgeweitet wird, da der integrierte Selbstlernprozess der Programme, die auf künstlichen neuronalen Netzenwerken passieren, zu einer permanente Verbesserung der Berechnungsergebnisse führen beziehungsweise eine große Toleranz gegenüber Unsicherheiten bei Eingabedaten beobachtet wurde.

Abstract

The thesis describes the comparison of predicted Formation Breakdown Pressures (FBP) calculated from industry wide accepted models to actual measured pressure values. Data from 141 hydraulic fracturing treatments were evaluated coming from different gas and oil fields of OMV Aktiengesellschaft and Devon Energy Corporation. The aim of the thesis work was to investigate the accuracy and validity of the various models in a holistic approach examining formations covering a wide range of different sandstone formations, some fields with carbonate formation and one shale gas play. Therefore the calculated and measured bottomhole FBP values range from weak to strong formations with FBP's from 4333 psi to 16707 psi.

All employed models are published and described in detail in technical papers and classified as elastic, linear elastic, poroelastic, linear elastic fracture mechanics, point stress and thermoporoelastic models. The correlations were compared using an error analysis framework and their accuracy and precision was identified. Six error analysis parameters were determined and by using them a ranking mechanism was established. Followed by a sensitivity analysis of the input parameters for the most accurate model. Based on this sensitivity analysis the principal rock parameters which influence most the accuracy of FBP prediction were identified.

Since the results of the study did not allow individuating an easy and consistent prediction model which is valid for all investigated formations, one of the commercially available artificial neural network software was tested, if it is capable to provide accurate FBP prediction for all types of reservoir formations. This approach, where information technology is combined with petroleum engineering, is an emerging technology and interpretation technique in the oil and gas industry. The validity of this method has been proven by predicting the Formation Breakdown Pressure with reasonable low error margins of <10 %. The author believes that the petroleum industry (as well as many other industries) will use the auto-learning process of neural networks because it can greatly improve the required interpretation techniques.

List of Tables

List of Figures

Abbreviations

a	fracture half-length, ft
C, K	Poisson's scaling terms, [-]
C_b	rock bulk compressibility, psi^{-1}
C_r	rock matrix compressibility, psi^{-1}
d	borehole diameter, in
d_{pipe}	pipe inside diameter, in
d'	radial distance, ft
E	modulus of elasticity (Young's modulus), psi
EEF	Euclidean Error Function, [-]
f	friction factor, [-]
FBP	Formation Breakdown Pressure, psi
g	gravitational acceleration, ft/s^2
k_1, k_2	function of borehole diameter d and half crack length a, [-]
K_i	stress intensity factor, psi-sqrt(in)
K_{ic}	fracture toughness, psi-sqrt(in)
L	length of the fracture, in
L_{pipe}	length of the pipe, ft
N_{Re}	Reynold's number, [-]
P_{co}	breakdown pressure under zero initial pore pressure, psi
P_f	pressure within the fracture, psi
P_{head}	hydrostatic head, psi
P_{inj}	injection pressure, psi
P_o	far-field pore pressure at true vertical depth, psi
P_{ob}	overburden pressure, psi

$P_{pipefriction}$	pipe friction pressure, psi
P_w	wellbore fluid pressure, psi
q	flow rate, bpm
r	distance from wellbore, in
r_w	borehole radius, in
$S_{H,max}$	maximum horizontal in-situ stress, psi
$S_{h,min}$	minimum horizontal in-situ stress, psi
S_0	cohesive strength (cohesion), psi
S_r	radial stress, psi
S_t	tangential (hoop) stress, psi
S_v	vertical (intergranular) stress, psi
T	borehole temperature, °C
t	thickness of filter cake, in
TS	tensile strength, psi
T_{init}	virgin in-situ temperature, °C
UCS	Unconfined Compressive Strength, psi
v	fluid velocity, ft/sec
w_{bo}	breakout width, °
Y	yield strength of filter cake particles, psi
z	depth, ft

Greek letters

α	Biot poroelastic parameter, [-]
β	porosity dependent parameter, [-]
γ_{fluid}	specific gravity of the fluid, [-]

ε	strain, [-]
θ	angle from direction of minimum in-situ stress, °
κ	coefficient of linear thermal expansion, $°C^{-1}$
μ	coefficient of friction, [-]
μ_f	fluid viscosity, cP
μ_i	coefficient of internal friction, [-]
v	Poisson's ratio, [-]
ρ	rock density, lb/in^3
ρ_w	water density, lb/in^3
σ	effective stress, psi
$\sigma^{\Delta T}$	thermal stress, psi
τ	shear stress, psi

Table of Contents

1. Introduction

OMV Aktiengesellschaft faced stimulation challenges in three wells in a tight gas environment. Hydraulic fracturing was not possible; even though the completion was designed according to company standard procedures and recommendations based on the estimated rock mechanics with presumed sufficient safety margin. As a result, the pressure limitation of the completion was reached without a fracture initiation. The wells in this reservoir need to be hydraulically fracture stimulated to produce commercially. For wells, where production enhancement interventions are necessary or planned, it is vital to predict the Formation Breakdown Pressure (FBP) as accurate as possible to help ensure that problems such as this do not occur.

Precisely knowing the FBP required during hydraulic fracturing is fundamental for the completion design. OMV Aktiengesellschaft uses the 3D frac simulator software GOHFER for the planning and evaluation purposes of hydraulic fracturing treatments. But as the above mentioned example shows, in this case the model build into the software under predicted the required FBP. The company pursued the evaluation of the different FBP prediction models which had been published in technical papers and were widely accepted in the industry. The FBP prediction results of the various models were compared to measured data to determine which model should be used for different formations. In this thesis eleven existing models were examined and validated using real field data from over 141 hydraulic fracturing treatments. Since no easy and clear result was determinable, a different approach was established. It consisted of using a combination of IT and petroleum technology expertise and employing self-learning artificial neural networks for data interpretation and FBP prediction. The innovative technique proved to provide a more accurate prediction of the Formation Breakdown Pressure value, which is essential in order to design an appropriate well completion.

The first two chapters of the thesis give an overview of (1) common definitions of the different pressure points usually seen during hydraulic fracturing operations and (2) important rock mechanics parameters which play a significant role in the prediction and determination of the FBP.

The following chapter gives a brief overview about the diagnostic pump tests which includes the basis for collecting important information on the formations and fracturing treatments.

The fifth chapter presents the Formation Breakdown Pressure models chronologically according to the dates they were developed and published. The first and simplest model dates back to 1898 and describes the findings of Kirsch. The last was developed by Aadnoy and Belayneh in 2008 and includes a vast variety of rock mechanic parameters and formation temperatures.

Chapter six is a summary about the geomechanical database which was created for the study and an overview of a Mechanical Earth Model workflow. Using actual field data from OMV Aktiengesellschaft and Devon Energy Corporation reservoirs, the models accuracies were validated and the results described in chapter seven. This is followed by the compendium of the factors influencing Formation Breakdown Pressure prediction.

The following two chapters talk about an alternative innovative FBP prediction method using the emerging technology of a self-learning artificial neural networks and presents the conclusions drawn, ending with general recommendation for operative applications.

Chapter 11 and 12 are dedicated to the economic impact of the study and HSE aspects of hydraulic fracturing focusing on techniques and best practices.

In the last chapter the major findings are summarized.

2. Description of Induced Fracture Generation

Hydraulic fracturing is an important completion method for improving the flow of hydrocarbons by the creation of conductive fractures in low permeability reservoirs. As such it is critical to understand the processes involved downhole in generating an induced fracture – from initiation at the wellbore wall, followed by propagation of the fracture away from the wellbore into the far field, to the final shut-in and closure once pumping is stopped.

Below is an idealized, schematic figure from Gaarenstrom et al. (published in 1993) illustrating pressure as a function of pumped volume; assuming a certain interval of intact rock is subject to this kind of treatment.

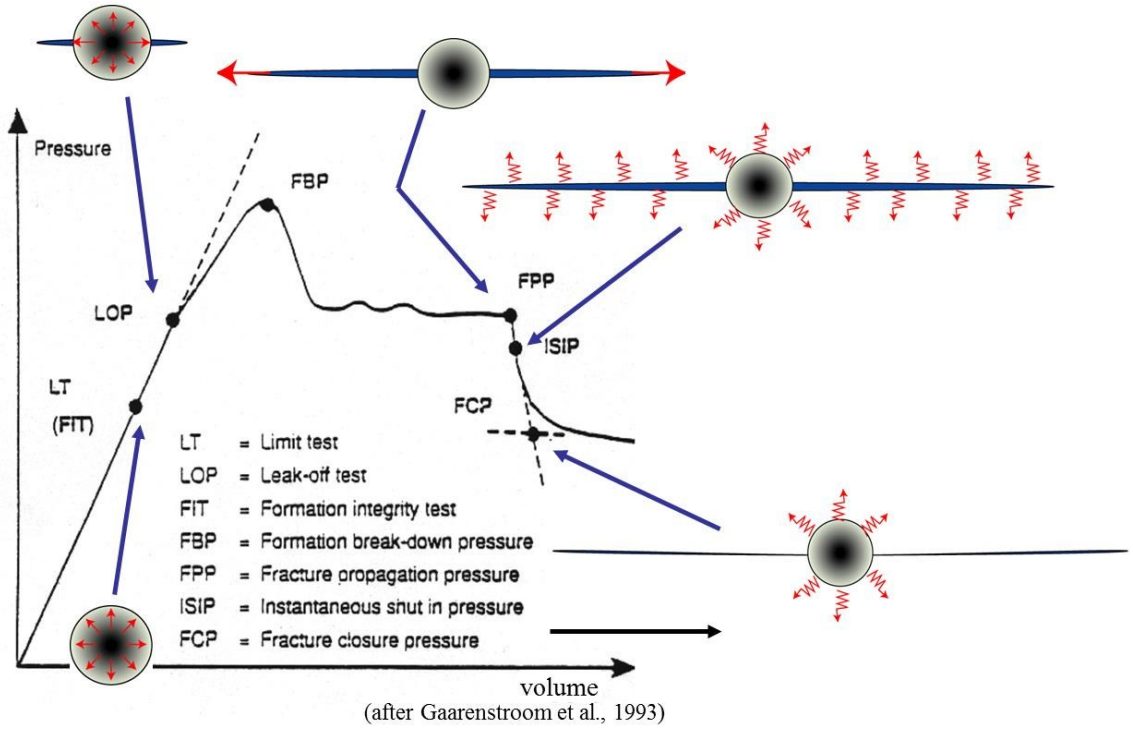

Figure 1: Pressure versus volume curve for an extended leak-off test (XLOT) or minifrac (Gaarenstrom et al., 1993)

Once pumping begins the pressure increases linearly. The slope being a function of the fluid compressibility with increasing volume of fluid pumped. No mechanical failure of the rock formation will occur until the slope changes. The pressure point where the slope is changing is called Leak Off Pressure (LOP). If the test is stopped during this stage it is called a Formation Integrity Test (FIT). This test does not contain tangible information about the fracturing behavior or least principal stress of the treated rock formation. As pumping continues and pressure exceeds the LOP either a pre-existing natural fracture opens or an entirely new fracture is induced. When the latter happens in response to the pressure the LOP can be called Fracture Initiation Pressure (FIP). These induced fractures are generated

at the wellbore wall and the pressure required for these to occur is dependent on the tensile strength of the rock and subject to the stress concentration around the well.

In wellbores that are inclined with respect to the present day stress field – either because the wells are deviated, the stresses rotated, or both, – the induced fractures are often inclined with respect to the wellbore axis and do not have the capability to admit appreciable volumes of fluid. In order to do so, and then to propagate away from the wellbore wall into the far field, they need to connect (link-up) first. Depending on the well trajectory and the far field stresses, this Fracture Link-Up Pressure may be above or below the FIP.

As pumping continues and more pressure is delivered into the linked-up induced fractures, they will begin to open and admit fluids and simultaneously begin to propagate away from the wall of the wellbore into the far field. This is the point which can be defined as Formation Breakdown Pressure (FBP). This FBP is difficult to predict as it depends on the tensile strength of the rock, the stress concentration around the wellbore, the complexity of the fracture being created, and the frictional losses of the fluids moving from the wellbore into the fracture.

Unless pumping occurs into a highly permeable or loosely consolidated formation, the pressure begins to drop from the FBP as the induced fracture continues to propagate further into the far field away from the wellbore. Assuming a constant pumping rate, a rock formation that is relatively homogeneous (i.e. constant tensile strength, fracture toughness, and no interference from natural fracture systems), and non-changing fluid properties the pressure that propagates the fracture remains more or less constant and is a function of frictional losses, the permeability of the formation, how far the wellbore/pumping fluid penetrates into the tip of these induced wellbore wall features as well as the least principal stress in the far field against which the fracture is begin opened. This fracture opening pressure is referred to as Fracture Propagation Pressure (FPP).

Once pumping is stopped and friction effects disappear, the pressure generally drops instantly to the Instantaneous Shut-In Pressure (ISIP). At this stage, the generated fracture is still open, as the fluid pressure inside the fracture should be above the least principal stress. Depending on formation permeability, the fluid in the open fracture will now dissipate into the matrix causing the pressure to drop until it reaches a point where the least principal stress trying to close the fracture becomes greater and, hence, the fracture closes; this point is called Fracture Closure Pressure (FCP).

2.1 Definition of Pressure Points

Two pressure points are often confused, namely the Fracture Initiation Pressure and the Formation Breakdown Pressure. In order to clarify this terminology the definitions used in this study can be seen below.

2.1.1 Fracture Initiation Pressure (FIP)

The pressure required to induce an entirely new fracture at the wellbore wall. These induced features occur only at the wall of the well and do not propagate away from the wall than a fraction of an inch.

2.1.2 Formation Breakdown Pressure (FBP)

The pressure required to link-up and open induced fractures at the wellbore wall such that they begin to admit fluids and simultaneously begin to propagate away from the wall of the wellbore into the far field. The FBP is difficult to predict as well as to measure since the volume of the opening which is created by the fractures is small compared to the volume of the well. An accurate pressure drop from the pressure gauges which show the treatment pressure on surface is often not easy to read.

Unless bottomhole pressure gauges are run bottomhole pressure (BHP) is calculated from surface pump pressure as follows:

$$BHP = P_{inj} + P_{hyd} - P_{fric} \qquad \text{Eq.1}$$

where $\mathbf{P_{inj}}$ is the injection pressure (also referred to as wellhead pressure, surface treating pressure or simply treating pressure), $\mathbf{P_{hyd}}$ is the hydrostatic head (also referred to as hydrostatic pressure or fluid head) and $\mathbf{P_{fric}}$ is the friction pressure (mainly consists of tubing friction pressure, $\mathbf{P_{pipefriction}}$, and a small amount of friction across the perforations).

To calculate the pipe (tubing) friction pressure which is the pressure loss due to friction effects in the wellbore as fluids are injected, the following Fanning's method can be applied:

$$P_{pipe\ friction} = 0.325\ \frac{\gamma_{fluid}\, L v^2 f}{d_{pipe}} \qquad \text{Eq.2}$$

where **L** is the length of the pipe in ft, **v** is the velocity in ft/sec, $\mathbf{d_{pipe}}$ is the pipe inside diameter in inches and **f** is the friction factor.

The friction factor (turbulent flow for smooth pipes) is determined using

$$f \approx \frac{0.0303}{N_{Re}^{0.1612}} \qquad \text{Eq.3}$$

$\mathbf{N_{Re}}$ is the Reynold's number and for Newtonian fluids it can be calculated by using:

$$N_{Re} = 132624 \frac{\gamma_{fluid} q}{d \mu_f} \quad \text{Eq.4}$$

where γ_{fluid} is the specific gravity of the fluid, **q** is the flow rate in bpm, **d** is the inside diameter in inches and μ_f is the fluid viscosity in cP (Economides, 2007).

Since formation breakdown occurs at the beginning of the fracturing process, the equation which applies to Newtonian fluids can be used for Reynold's number calculation since water (or brine) with small amounts of chemicals and friction reducers are used. In case the wellbore is filled with gels the power law model needs to be used.

3. Rock Mechanical Characteristics

3.1 Basic Definitions

The most important rock mechanical parameters which were used in this study are listed in this chapter.

3.1.1 Poisson's Ratio

The Poisson's ratio, **v**, is a measure of how much a material will deform in a direction perpendicular to the direction of the applied force (see Fig.2).

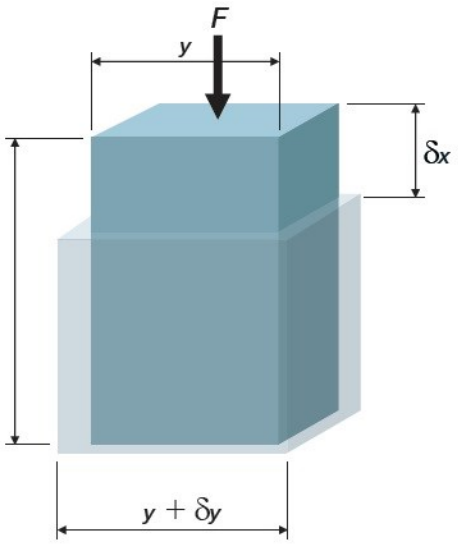

Figure 2: Application of force F in the x-direction will also produce a deformation in the y-direction (Economides et al., 2007)

The Poisson's ratio, **v**, is defined by:

$$\nu = -\frac{\varepsilon_y}{\varepsilon_x} \qquad \text{Eq.5}$$

where $\boldsymbol{\varepsilon_x}$ and $\boldsymbol{\varepsilon_y}$ is the strain in the x and y direction, respectively and can be calculated as:

$$\varepsilon_x = \frac{-\delta x}{x} \qquad \text{Eq.6}$$

$$\varepsilon_y = \frac{-\delta y}{y} \qquad \text{Eq.7}$$

Strain is the measure of how much the material has been deformed when stress is applied to it. As the force, **F**, is applied in the x-direction, the original height of the block of material, **x**, changes by **δx** (so that the new height is **x - δx**).

Note that this value is negative, due to the fact that how the forces and the direction forces are determined. In this case, compressive strain is positive, while tensile strain is negative.

By definition, the Poisson's ratio is always less than 0.5 (otherwise a uniaxial compressive stress would result in an increase in volume) and typical **v** values for rocks are between 0.2 and 0.35. The Poisson's ratio is, of course, dimensionless.

3.1.2 Young's Modulus

Young's modulus, **E**, (also known as modulus of elasticity or elastic modulus) is defined as the ratio of stress over strain:

$$\mathrm{E} = \frac{\sigma}{\varepsilon} \qquad \text{Eq.8}$$

Because strain is dimensionless, **E** has the same units as stress. Young's modulus is a measure of how much a material will elastically deform under a load. This is another term for hardness (Bourgoyne et al., 1986).

In fracturing, Young's modulus is a measure of how much a rock will elastically deform when a pressure is applied to it. Because pressure is stored energy, **E** is also a measure of how much energy it takes to make the rock deform.

Rocks with a high Young's modulus tend to be very hard and brittle (susceptible to brittle fracture). Conversely, materials with a low **E** tend to be soft and ductile (resistant to brittle fracture). In fracturing, Young's modulus will typically have values ranging from as low as 50,000 psi (for a shallow, very soft chalk or weak sandstone) to as high as 6,000,000 psi for deep, tight, shaley sandstone. It should be noted that Young's modulus may not be constant in weak or unconsolidated formations.

3.1.3 Compressional Strength

Materials have a compressive strength, which is the compression load beyond which a material will fail. Failure mechanisms are more complex because the material is often compressed in several directions at once. Strength is typically measured via either uniaxial or triaxial tests. Uniaxial compressive tests ($\mathbf{S_1>0}$, $\mathbf{S_2=S_3=0}$) are those in which one simply compresses a sample axially (with no radial stress) until it fails at a value defined as the unconfined compressive strength (usually termed either the **UCS** or $\mathbf{C_0}$). Figure 3 shows the usual ranges of **UCS** for different rock types (ResGeo202 Reservoir Geomechanics Course – Stanford University).

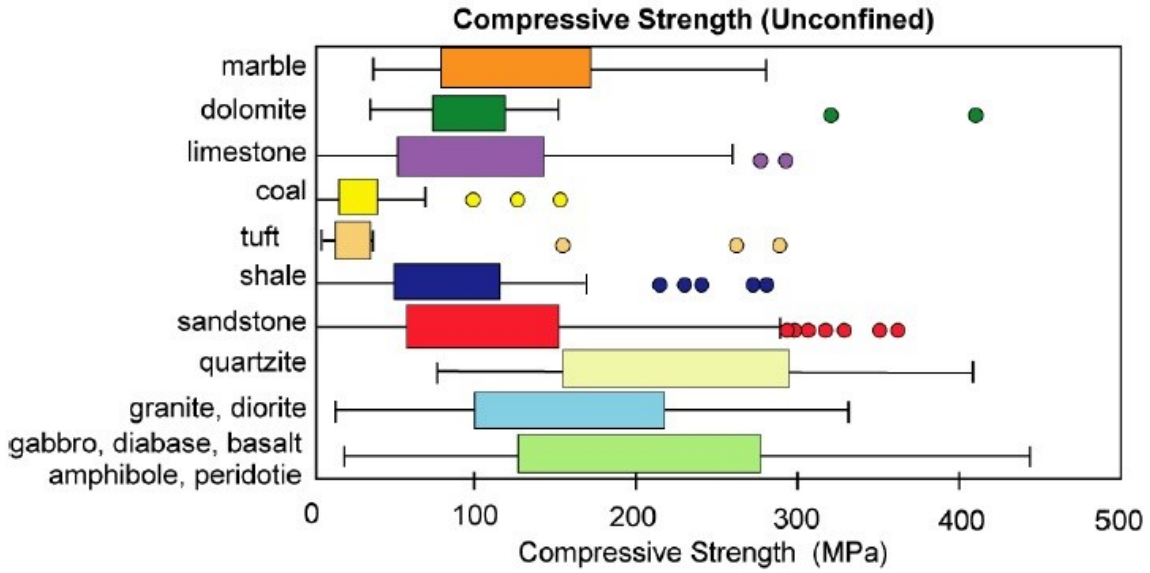

Figure 3: Unconfined Compressive Strength of variable rocks (ResGeo202 Reservoir Geomechanics Course – Stanford University)

Generally, rocks are much stronger in compression than in tension, a fact of which is taken advantage during fracturing. Usually the **UCS** is determined in the laboratory, but when core samples are unavailable for testing, it is possible to estimate rock strength from geophysical log data.

3.1.3.1 Mohr-Coulomb Failure Criterion

Conducting a series of triaxial tests defines an empirical Mohr-Coulomb failure envelope that describes failure of the rock at different confining pressures. Allowable stress states are those that do not intersect the Mohr-Coulomb failure envelope. For most rocks it is possible to consider the change of strength with confining pressure in terms of a linearized Mohr-Coulomb failure envelope (see Fig. 4) defined by two parameters: μ_i, the slope of the failure line, termed the coefficient of internal friction, and the unconfined compressive strength. One could also describe the linear Mohr failure line in terms of its intercept when $\sigma_3=0$ which is called the cohesive strength (or cohesion) S_0. The linearized Mohr failure line can be written as:

$$\tau = S_0 + \sigma_n \mu_i \qquad \text{Eq.9}$$

where τ is the shear stress and σ_n is the effective normal stress (which can be calculated by subtracting pore pressure from normal stress) on the fault that forms during the failure process in terms of the applied effective principal stresses σ_1 and σ_3. Shear and normal stress can be calculated as:

$$\tau = 0.5(\sigma_1 - \sigma_3)\sin 2\beta \qquad \text{Eq.10}$$

$$\sigma_n = 0.5(\sigma_1 + \sigma_3) + 0.5(\sigma_1 - \sigma_3)\cos 2\beta \qquad \text{Eq.11}$$

where **β** is the angle between the fault normal and $\boldsymbol{\sigma_1}$.

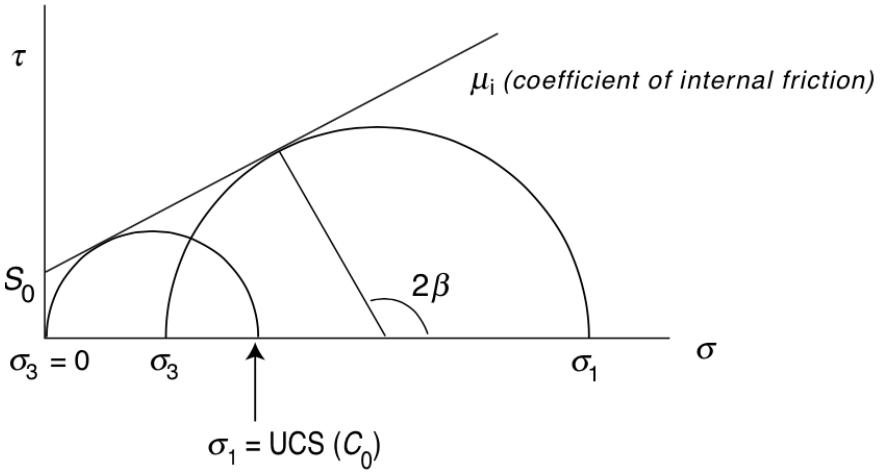

Figure 4: Linearized Mohr-Coulomb failure envelope (Economides et al., 2007)

3.1.4 Tensile Strength

The tensile strength of a material is the level of tensile stress that is required to make the material fail. This property is important in hydraulic fracturing because this stress level has to be overcome in order to split the rock. Usually, the frac pressure is led by two components: the stresses induced by the overburden, and the tensile strength of the rock.

The tensile strength of rocks is quite low, on the order of just a few MPa and when pre-existing flaws exist in the rock (as is the case when considering any appreciable rock volume), tensile strength would be expected to be near zero. Hydraulic fracturing is a form of tensile failure that occurs when fluid pressure exceeds the local least principal stress. The extension of a tensile fracture occurs when fluid pressure is intentionally raised above the least principal stress to propagate a fracture which is then filled with proppant to increase formation permeability. In case of hydraulic fracture propagation the rock strength in tension is essentially unimportant in the fracture extension process. Figure 5 shows the usual ranges of tensile strength (**TS**) for different rock types (ResGeo202 Reservoir Geomechanics Course – Stanford University).

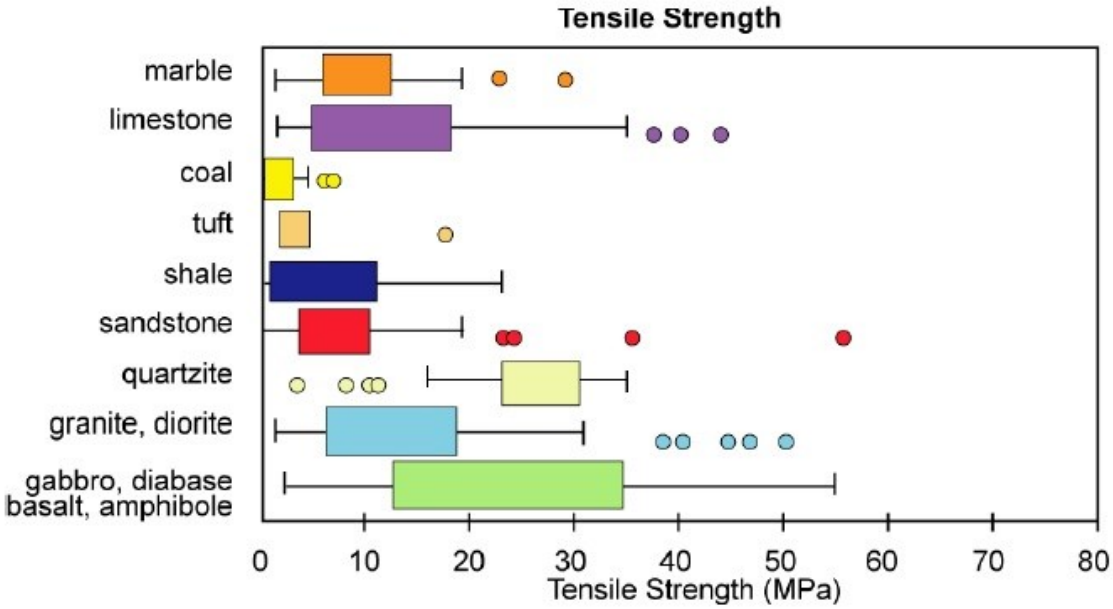

Figure 5: Tensile strength of variable rocks, usually about 10 % of UCS (ResGeo202 Reservoir Geomechanics Course – Stanford University)

3.1.4.1 Griffith Failure Criterion

In terms of fracture mechanics, the stress intensity at the tip of an opening mode planar fracture (referred to as a Mode 1 fracture) is given by:

$$K_i = (P_f - S_3)\pi L^{1/2} \qquad \text{Eq.12}$$

where $\mathbf{K_i}$ is the stress intensity factor, $\mathbf{P_f}$ is the pressure within the fracture, **L** is the length of the fracture and $\mathbf{S_3}$ is the least principal stress. Fracture propagation will occur when the stress intensity factor $\mathbf{K_i}$ exceeds $\mathbf{K_{ic}}$, the critical stress intensity, or fracture toughness. While the fracture toughness is important to initiate and initially extend a fracture, once a fracture reaches a length of a few tens of inches, small pressure in excess of the least principal stress is required to make the fracture grow, regardless of the rock's fracture toughness. This means, that the principal control on fracture propagation is that $\mathbf{P_f}$ exceed $\mathbf{S_3}$ by only a small amount. Once the Mode 1 fracture starts to grow, the strength of the rock in tension is irrelevant.

The different failure modes for linear elastic fracture mechanics are illustrated in Fig. 6. Failure Mode 1 is the "opening mode," Mode 2 the "sliding mode" and Mode 3 the "tearing mode." In hydraulic fracturing, we are usually concerned only with failure Mode 1.

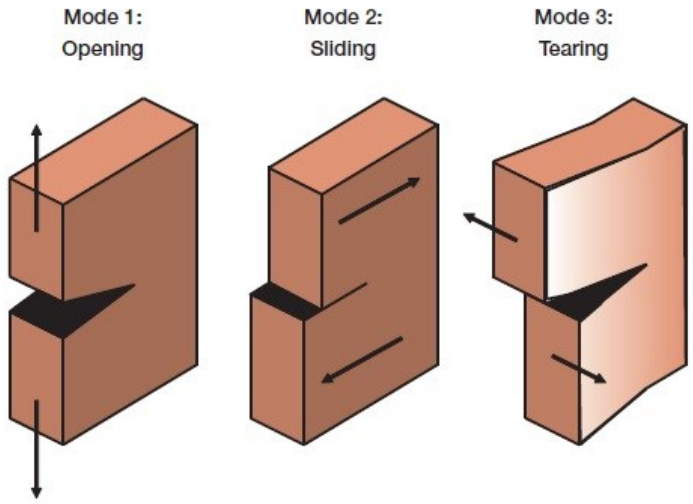

Figure 6: Failure modes for linear elastic fracture mechanics (Economides et al., 2007)

3.1.5 Pore Pressure

Pore pressure (P_o) is defined as a scalar hydraulic potential acting within an interconnected pore space at depth. The value of pore pressure at depth is usually described in relation to hydrostatic (or normal) pressure, the pressure associated with a column of water from the surface to the depth of interest. Hydrostatic pore pressure increases with depth at the rate of 10 MPa/km or 0.44 psi/ft (depending on salinity). Hydrostatic pore pressure implies an open and interconnected pore and fracture network from the earth's surface to the depth of measurement:

$$P_o = \int_0^z \rho_w(z) g dz \approx \rho_w g z_w \qquad \text{Eq.13}$$

where $\mathbf{P_o}$ is the pore pressure, **z** is depth, $\boldsymbol{\rho_w}$ is the water density and **g** is the gravitational acceleration

A reservoir can be hydrological subdivided (compartmentalized) into distinct pressure and flow units and in such a case pore pressure can exceed hydrostatic values in a confined pore volume at depth. Conceptually, the upper bound for pore pressure is the overburden stress, $\mathbf{S_v}$. Lithostatic pore pressure means that the pressure in the pores of the rock is equivalent to the weight of the overburden stress, $\mathbf{S_v}$. Because of the negligibly small tensile strength of the rock, pore pressure will always be less than the least principle stress, $\mathbf{S_3}$.

Direct measurement of pore pressure in relatively permeable formation is done by using a variety of commercially available technologies conveyed either by wireline (samplers that isolate formation pressure from annular pressure in a small area at the wellbore wall) or pipe (packers and drill-stem testing tools that isolate sections intervals of a formation). Similarly, mud weight are sometimes used to estimate pore pressure in permeable formations as they tend to take drilling mud if the mud pressure is significantly in excess of the pore pressure

and produce fluids into the well if the converse is true. Furthermore, pore pressure is frequently estimated from geophysical logs or seismic data.

3.1.6 In-situ Principal Stresses

Knowledge of the current state of stress is a key component of a geomechanical model. In order to fully describe the state of the stress at depth, four parameters have to be defined: three principal stress magnitudes, $\mathbf{S_v}$, the vertical stress, $\mathbf{S_{h,min}}$, the minimum principal horizontal stress and $\mathbf{S_{H,max}}$, the maximum principal horizontal stress and one stress orientation, usually taken to be the azimuth of the maximum horizontal stress.

3.1.6.1 Vertical Stress

The stresses due to the overburden (also called the vertical stress) are simply the integration of rock densities (obtained typically from a density log) from the surface to the depth of interest. Therefore, if there have been no external influences – such as tectonics – and the rocks are behaving elastically, the vertical stress, $\mathbf{S_v}$, at any given depth, **z** can be calculated as follows:

$$S_v(z) = \int_0^z \rho(z) g dz \approx \bar{\rho} g z \qquad \text{Eq.14}$$

where **ρ(z)** is the density of rock as a function of depth, **g** is the gravitational acceleration, $\bar{\rho}$ is the mean overburden density and **z** is depth.

For offshore operations the vertical stress calculation takes water depth in consideration:

$$S_v(z) = \rho_w g z_w + \int_0^z \rho(z) g dz \approx \rho_w g z_w + \bar{\rho} g (z - z_w) \qquad \text{Eq.15}$$

where $\boldsymbol{\rho_w}$ is the density of water and $\mathbf{z_w}$ is the water depth.

Since $\boldsymbol{\rho_w}$ ~ 1 g/m^3 (1.0 SG), hydrostatic water pressure increases at a gradient of 10 MPa/km (0.44 psi/ft). Most clastic sedimentary rock has an average density of about 2.3 g/cm^3 so the vertical stress increases with depth at a gradient of 23 MPa/km (1 psi/ft).

3.1.6.2 Horizontal Stresses

The two horizontal stresses namely, minimum horizontal in-situ stress, $\mathbf{S_{h,min}}$, and maximum horizontal in-situ stress, $\mathbf{S_{H,max}}$, are 90° apart from each other. The magnitude of $\mathbf{S_{h,min}}$ is obtained from hydraulic fracturing data (mini-fracs), extended leak-off tests (LOTs) and pressure while drilling (PWD) observations. General limit for the magnitude of $\mathbf{S_{H,max}}$ (as a function of depth and pore pressure) can be provided by the frictional strength of faults.

Because earth`s crust contains widely distributed faults, fractures and planar discontinuities at many different scales and orientations, it is self-evident that stress magnitudes at depth (specifically, the differences in magnitude between the maximum and minimum principal stresses) will be limited by the frictional strength of these planar discontinuities. For any

given value of σ_3 there is a maximum value of σ_1 established by the frictional strength of the pre-existing fault (Jaeger and Cook, 1979):

$$\frac{\sigma_1}{\sigma_3} = \frac{S_1 - P_o}{S_3 - P_o} = \left[\left(\mu^2 + 1\right)^{1/2} + \mu\right]^2 \quad \text{Eq.16}$$

Assuming coefficient of friction (μ) to be equal to 0.6:

$$\frac{\sigma_1}{\sigma_3} = 3.1 \quad \text{Eq.17}$$

The equation becomes the following for the different faulting environments:

Normal faulting:
$$\frac{\sigma_1}{\sigma_3} = \frac{S_v - P_o}{S_{h,min} - P_o} = \left[\left(\mu^2 + 1\right)^{1/2} + \mu\right]^2 \quad \text{Eq.18}$$

Strike-slip faulting:
$$\frac{\sigma_1}{\sigma_3} = \frac{S_{H,max} - P_o}{S_{h,min} - P_o} = \left[\left(\mu^2 + 1\right)^{1/2} + \mu\right]^2 \quad \text{Eq.19}$$

Reverse faulting:
$$\frac{\sigma_1}{\sigma_3} = \frac{S_{H,max} - P_o}{S_v - P_o} = \left[\left(\mu^2 + 1\right)^{1/2} + \mu\right]^2 \quad \text{Eq.20}$$

If the value for $\mathbf{S_{h,min}}$ or $\mathbf{S_v}$ is known in case of strike-slip or reverse faulting the above equations can be used to put an upper bound on $\mathbf{S_{H,max}}$. This is important since there is currently no direct method known to measure this value. Although, when observation of wellbore failures (breakouts and drilling induced tensile fractures) are available, a more precise estimate of $\mathbf{S_{H,max}}$ is possible.

In case of wellbore breakouts the required magnitude of $\mathbf{S_{H,max}}$ causing breakouts is calculated according to the following:

$$S_{H,max} = \frac{\left(C_o + 2P_o + \Delta P + \sigma^{\Delta T}\right) - S_{h,min}\left(1 + 2\cos 2\theta\right)}{1 - 2\cos 2\theta} \quad \text{Eq.21}$$

$$2\theta = \pi - w_{bo} \quad \text{Eq.22}$$

where $\mathbf{C_o}$ is the unconfined compressive strength of the rock, $\mathbf{\Delta P}$ is the difference between the mud weight in the wellbore and the pore pressure, $\mathbf{P_o}$. $\mathbf{\sigma^{\Delta T}}$ represents thermal stresses arising from the difference between the mud temperature and formation temperature ($\mathbf{\Delta T}$), $\mathbf{\theta}$ is the angle from direction of minimum in-situ stress, $\mathbf{w_{bo}}$ is the observed breakout width in degrees.

When information about drilling induced tensile fractures is available the necessary magnitude of $\mathbf{S_{H,max}}$ to cause tensile fractures is calculated according to equation 23:

$$S_{H,max} = 3S_{h,min} - 2P_o - \Delta P - TS - \sigma^{\Delta T} \quad \text{Eq.23}$$

Industry wide it has been recognized that the most difficult component of the stress tensors to estimate accurately is the maximum horizontal principal stress, $\mathbf{S_{H,max}}$, However, the widespread use of wellbore imaging devices allows more often to constrain the possible $\mathbf{S_{H,max}}$ magnitude (Zoback, 2007). Appendix A demonstrates a formation microimager (FMI) log for one of the wells which were investigated in the study. The recognizable borehole breakouts and drilling induced fractures were used for stress determination.

Further information about relative stress magnitudes as well as E. M. Anderson´s classification scheme about the different faulting environments can be found in Appendix B.

Stresses around the wellbore is described in detail in Appendix C as well as the orientation of hydraulic fractures.

4. Diagnostic Pump Tests

Breakdown tests, step rate tests and minifracs are collectively referred to as diagnostic pump tests or calibration tests. These are fluid injections before a fracture treatment, designed to collect important information to help calibrate the fracture simulator and hence provide a more accurate prediction of fracture geometry. They can also provide some important information about near-wellbore restricted flow. Step rate tests come in two varieties, step up and step down.

Analyzing diagnostic pump test plots and reports of the fracturing treatments were the source of the observed breakdown pressure magnitudes. In order to understand the importance of such tests their theory is briefly described in this chapter.

4.1 Breakdown Tests

The wellbore fluid is displaced into the formation with brine at a constant rate until formation breakdown is observed. The pressure decline is monitored until closure is observed. The post closure pressure behavior is analyzed to verify the formation transmissibility properties.

4.2 Step-Up Tests

Step-up tests are performed with the fracture initially closed. The objective of the test is to obtain the fracture extension pressure, P_{ext}, by injecting into the formation in a series of increasing rate steps and then by analyzing the data on a pressure against rate cross-plot. Figure 7 shows the pressure readings of a step-up test by the orange dots. It is important to perform a minimum of three steps at matrix rate (steep line on Fig. 7) and three steps as fracture rate (shallow line on the plot). This test is typically followed by a step down test.

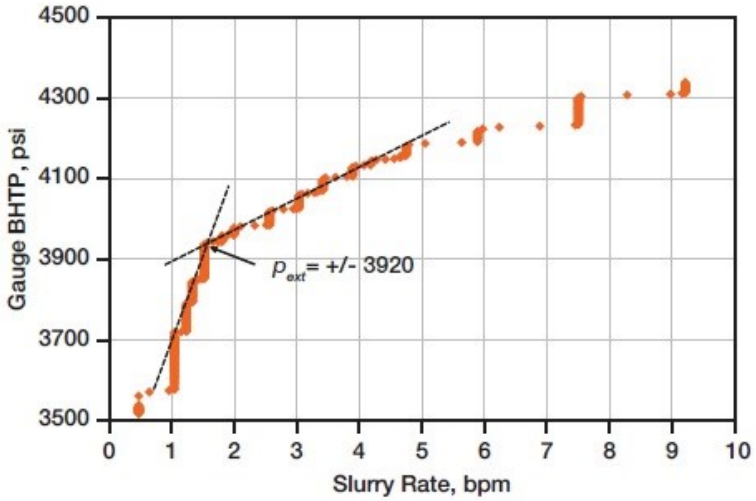

Figure 7: Typical pressure-rate cross-plot from a step-up test (Economides et al., 2007)

4.3 Step-Down Tests

A step down analysis is performed in order to analyze wellbore friction, perforation friction and near wellbore friction mainly due to tortuosity (a measure of the geometric complexity). Furthermore, a proper step down test can help determine total number of perforations open. It is important that the test is performed quickly, because the fracture must remain open throughout the test. The test starts at fracturing rates with a significant volume already pumped into the fracture. Then the rate has to be reduced rapidly in four or five approximately equal steps. Then Bottom Hole Treatment Pressure (BHTP) has to be plot against slurry rate in a similar fashion to the step-up test.

4.4 Minifracs

These tests are typically performed immediately prior to the main fracture treatment to obtain design parameters (i.e.: fracture closure pressure –the point when the fracture closes-, Instantaneous Shut-In Pressure (ISIP), fracture gradient, fluid leakoff, fluid efficiency, formation permeability and reservoir pressure). Once all data is collected and analyzed, the stimulation model is then calibrated in order to predict more accurately the expected fracture geometry and control the theoretic feasibility of proppant placement. The test performed without any significant volumes of proppant and the intent is to break down the formation to create a short fracture during the injection period, and then to observe closure of the fracture system during the falloff period. The minifrac should be pumped using the anticipated treatment fluid, at the anticipated rate and ideally planned pad volume.

Figure 8 shows the parameters which can be derived from a minifrac test.

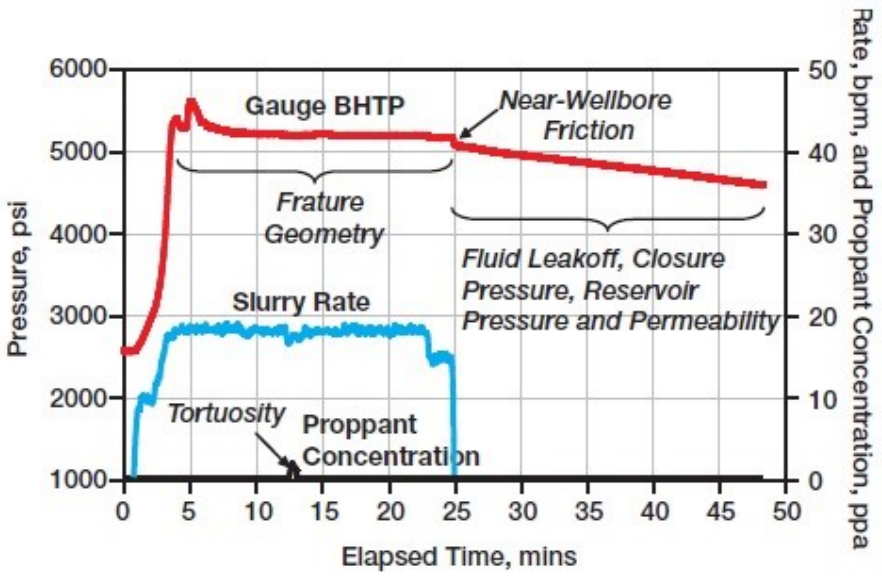

Figure 8: Example minifrac job plot, illustrating the significant parameters that can be derived from its analysis (Economides et al., 2007)

Figure 8 also illustrates a proppant slug with the aim to remove/reduce tortuosity effects since it shall erode the zone where fluid is forced to change direction. As the slug passes into the fracture, the response of the BHTP is observed. Ideally, no pressure rise is seen,

indicating that the near-wellbore flow channels have adequate width. However, if tortuosity is significant, a pressure rise will be observed. In the worst cases, the well will screen out on the proppant slug.

Figure 9 shows a breakdown and step-up test followed by a minifrac for one of the investigated treatments. The Formation Breakdown Pressure can be considered to be at the point of the treating pressure line when the pressure reaches its highest value during the breakdown test.

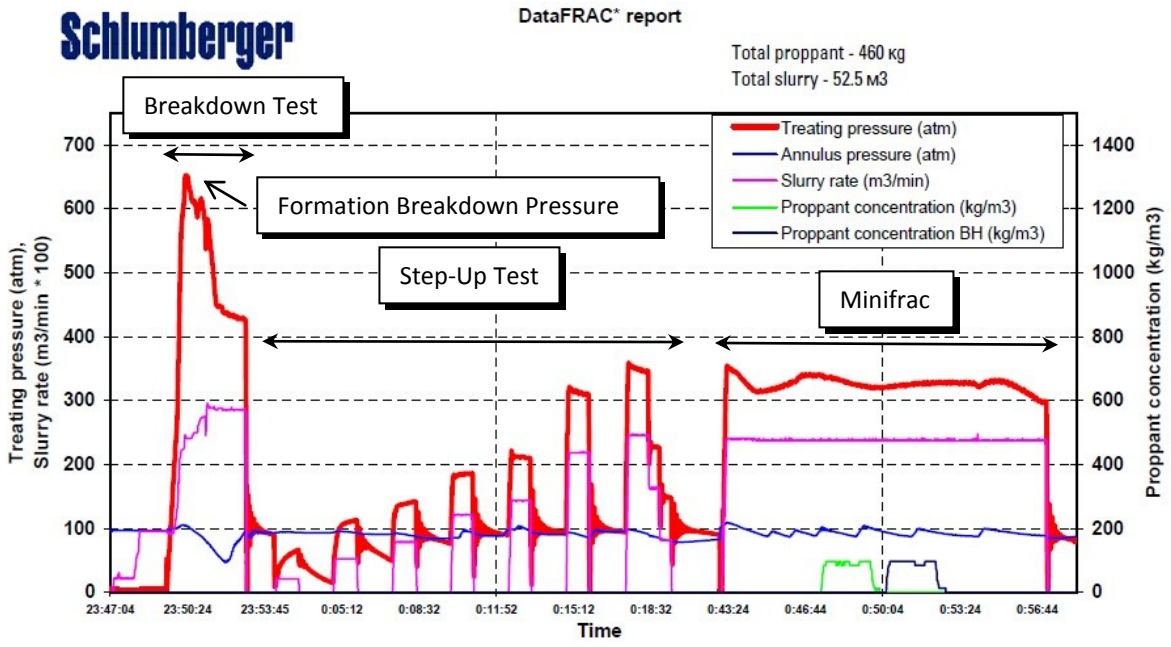

Figure 9: Breakdown, step-up and minifrac test for one of the stimulated wells

Minifrac data are investigated to determine fracture closure pressure using square root of time, G-function, and log-log plot analysis but since these methods are not the main focus of this study the further description of them is not discussed but can be found in Economides and Nolte, 2000.

5. Existing Models for Formation Breakdown Pressure Prediction

5.1 Introduction

In the past many improvements were made in the calculation of Formation Breakdown Pressure. The equations got more complex, but more complex solutions also require more parameters. To determine these parameters is not always easy, even though the capabilities and opportunity to test cores in the laboratories increased. The input data gathering can be highly challenging and difficult if data for new fields are to be determined.

5.2 Description of Formation Breakdown Pressure Models

5.2.1 Elastic Model – Kirsch Solution, 1898

Kirsch published a method for calculation of stresses in a circular hole. Later, borehole mechanics started to apply this in the petroleum industry.

Formation Breakdown Pressure prediction by Kirsch assumes a balanced borehole, where the drilling fluid supports no deviatoric stress but provides pressure on the wellbore that equals the lithostatic pressure.

$$FBP = 2S_{h,min} - P_o \qquad \text{Eq.24}$$

where **FBP** is the formation breakdown pressure, $\mathbf{S_{h,min}}$ is the far-field minimum horizontal stress, $\mathbf{P_o}$ is the pore pressure.

The Kirsch solution is uncomplicated and uses parameters relatively easy to obtain. It results in good prediction of FBP. If only the minimum horizontal stress and the pore pressure are known, this equation can give a worthy estimate (Aadnoy and Belayneh 2008 A). GOHFER is an industry wide used fracture simulation software and it is based on the Kirsch model.

5.2.2 Linear Elastic Model – Hubbert and Willis, 1957

Hubbert and Willis published in 1957 a model which assumes that the rock surrounding the wellbore is linear elastic, homogeneous, isotropic medium, which is impermeable to the fluid injected.

$$FBP = P_{co} + 3S_{h,min} - S_{H,max} - P_o \qquad \text{Eq.25}$$

where **FBP** is the breakdown pressure, $\mathbf{P_{co}}$ is the “zero breakdown pressure” or the breakdown pressure under zero initial pore pressure and zero far-field stresses, $\mathbf{S_{h,min}}$ and $\mathbf{S_{H,max}}$ are the far-field minimum and maximum horizontal stresses, $\mathbf{P_o}$ is the pore pressure.

It is assumed that the maximum tensile strength criterion holds at the borehole wall, so $\mathbf{P_{co}}$ is equivalent to the tensile strength of the rock (**TS**). Thus, this model assumes that the zero breakdown pressure is a constant material property of rock.

5.2.3 Poroelastic Model – Haimson and Fairhurst, 1967

The poroelastic model incorporates the stresses induced as a result of fracturing fluid penetration into the rock. It includes Poisson's ratio and the Biot poroelastic parameter (**α**) which depends on the rock matrix and rock bulk compressibility.

$$FBP = P_{co} + (3S_{h,min} - S_{H,max} - P_o)/A \quad \text{Eq.26}$$

where **A** is a material property equal to

$$A = 2 - \alpha(1 - 2\nu)/(1 - \nu) \quad \text{Eq.27}$$

$$\alpha = 1 - C_r/C_b \quad \text{Eq.28}$$

$\mathbf{P_{co}}$ is the breakdown pressure under zero initial pore pressure and $\mathbf{P_{co}=TS/A}$, which is again assumed to be a constant material property. **v** is the Poisson's ratio of the rock, **α** is the Biot poroelastic parameter, $\mathbf{C_r}$ and $\mathbf{C_b}$ are the rock matrix and rock bulk compressibilities respectively. Theoretically, $\mathbf{0<\alpha<1}$, and $\mathbf{0<v<0.5}$; thus $\mathbf{0<A<\alpha}$. Note, that $\mathbf{\alpha=0}$ in low porosity dense rock without interconnected pores and $\mathbf{\alpha=1}$ for compliant (uncemented) sand.

5.2.4 Linear Elastic Fracture Mechanics – Rummel, 1987

A different approach to the FBP prediction models was made by Rummel in 1987. He assumed the preexistence of a symmetrical double crack of half-length **a**. The model further assumes that fracturing-fluid pressure is applied both to the borehole wall and the preexisting crack, and neglects initial pore pressure

$$FBP = P_{co} + k_1 S_{h,min} + k_2 S_{H,max} \quad \text{Eq.29}$$

$$P_{co} = K_{IC}/f(d,a) \quad \text{Eq.30}$$

where $\mathbf{K_{Ic}}$ is the fracture toughness of tested rock, **f(d,a)** is a function of borehole diameter **d** and half crack length **a**. $\mathbf{k_1}$ and $\mathbf{k_2}$ are fracture coefficients and also functions of **d** and **a**. In the original paper of Rummel 1987 the methods to determine $\mathbf{k_1}$ and $\mathbf{k_2}$ values are discussed in detail. If no pre-existing fractures are present (fractures cannot seen on image logs) $\mathbf{k_1}$ equals 3 and $\mathbf{k_2}$ equals -1.

The crack dimension **a**, like the $\mathbf{K_{Ic}}$, is assumed to be a constant of the material, thus $\mathbf{P_{co}}$ is a function of the borehole diameter. The basic idea is, that a crack will grow if the stress concentration $\mathbf{K_i}$ is bigger than the fracture toughness $\mathbf{K_{IC}}$ (Rummel 1987).

Four different pressure distributions were considered in the crack system along the fracture:

- the pressure in the fracture equals the pressure in the wellbore (Rummel 1, 1987)

- due to the pressure lost which occurs when the fracturing fluid goes into the pre-existing fracture, the pressure in the fracture equals 75 % of the pressure in the wellbore (Rummel 2, 1987)
- assuming linear pressure drop along the crack (Rummel 3, 1987)
- assuming quadratic pressure drop along the crack (Rummel 4, 1987)

Figure 10 shows the wellbore with symmetrical pre-existing fractures parallel with the maximum horizontal stress which is present in the rock. As one can see, the fluid pressure inside the wellbore also acts in the fractures.

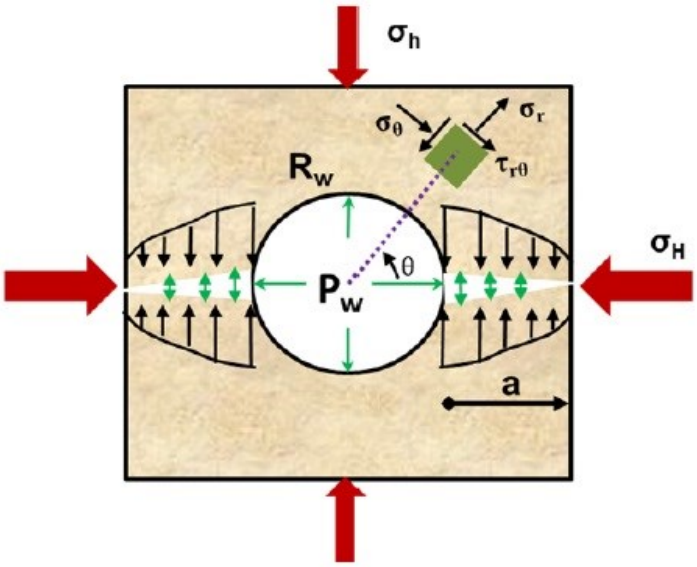

Figure 10: Wellbore with a pre-existing symmetrical double crack (Jin et al. 2013)

5.2.5 Poroelastic Model – Schmitt and Zoback, 1989

The Schmitt and Zoback method is also a poroelastic model. It assumes that the rock is permeable and includes a porosity dependent correction parameter.

$$FBP = \left(P_{co} + 3S_{h,min} - S_{H,max} - \eta P_o\right)/\left(1 + \beta - \eta\right) \qquad \text{Eq. 31}$$

where **β** is a porosity dependent parameter, **0≤β≤1**, **η** is a material property and equal to equation 32.

$$\eta = \alpha(1 - 2\nu)/(1 - \nu) \qquad \text{Eq. 32}$$

$\mathbf{P_{co}}$ is the breakdown pressure under zero initial pore pressure which is in this case equivalent to the tensile strength of the rock. $\mathbf{S_{h,min}}$ and $\mathbf{S_{H,max}}$ are the far-field minimum and maximum horizontal stresses, $\mathbf{P_o}$ is the pore pressure.

The technical difficulty with the equation above is the necessity to determine the porosity dependent material parameter β, since the stress field around a pressurized wellbore is changing permanently and rapidly. Presently, the major tool available to explore the effect of

poroelastic rock behavior on the breakdown pressure is the laboratory simulation under controlled conditions as described by Haimson and Huang 1989.

5.2.6 Point Stress Model – Ito and Hayashi, 1990

A different approach was published by Ito and Hayashi. The point stress model assumes that a finite region of material, and not just a point, must be critically stressed in order to initiate failure. This model is very similar to the linear elastic case in that linear elasticity and maximum tensile strength criterion are used. The difference is that it considers hydraulic fracturing to occur not when the tangential stress at the borehole wall becomes critical, but when the tangential stress over the region between the borehole diameter **d** and a radial distance **d'** into the rock equals or exceeds the tensile strength of the rock formation. The radial distance d' is assumed to be a material property. The model neglects initial pore pressure and is represented by the following equation:

$$FBP = P_{co} + S_{H,max}\left(1 - 3I^2\right)/2 + S_{h,min}\left(1 + 2/I^2 + 3I^2\right)/2 \quad \text{Eq.33}$$

$$I = d/\left(d + 2d'\right) \quad \text{Eq.34}$$

$$P_{co} = TS/I^2 \quad \text{Eq.35}$$

where **TS** is the tensile strength in large boreholes and a parameter considered basically constant, which shows clearly that in the model $\mathbf{P_{co}}$ is dependent on the borehole diameter length. $\mathbf{P_{co}}$ in linear elastic fracture mechanics and in point stress models is size dependent, which means it varies with borehole diameter and rate of loading demonstrated and described by Haimson and Zhao also in 1991.

The zero breakdown pressure which is common in all the above equations should be determined in the laboratory from hydraulic fracturing simulations in boreholes drilled in cylindrical specimens under no far-field stresses and no initial pore pressure (Haimson and Zhao 1991).

5.2.7 Thermoporoelastic Model – Aadnoy and Belayneh, 2008

The latest model by Aadnoy and Belayneh 2008 A includes pressure and temperature load history of the wellbore and its vicinity. Using this approach, a better assessment of the fracture strength is obtained which lead to better predictions.

The model is based on the Kirsch solution for stresses in a circular hole. The starting assumption is that there exists a principal stress state in the rock before the hole is drilled and lowering or increasing the mud pressure from this stress level will result in Poisson's effect on the stresses (borehole is loaded in the radial direction, causing tension in the tangential direction). Figure 11 illustrates a possible load history of a well (Aadnoy and Belayneh 2008 B). In the drilling phase when the borehole is created the loadings from the mud differ from the in-situ stress (note, that swabbing usually occurs when drill pipe is retracted from wellbore). Furthermore, when a leak-off test is carried out even higher loadings take place. The Poisson's effect only acts on the loading that deviates from the

initial stress state (in-situ stresses).

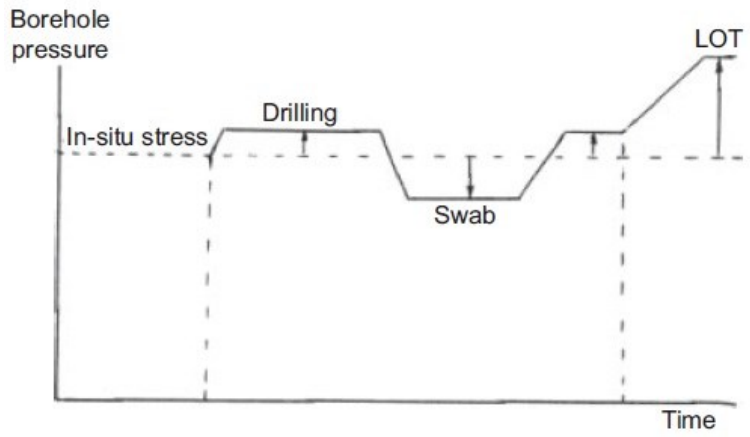

Figure 11: Possible load history of the borehole (Aadnoy and Belayneh 2008 B)

The Poisson's scaling factor leads to a higher fracture pressure than the classical Kirsch equation (which in certain cases under predicts the fracturing pressure).

$$FBP = S_{H,max} + C \cdot \left\{ \frac{3}{2} S_{h,min} - S_{H,max} - P_o \right\} + P_o \qquad \text{Eq.36}$$

where **C** is the Poisson's scaling factor and can be calculated as:

$$C = \frac{(1-\nu)(1-\nu^2)}{3\nu(1-2\nu)+(1+\nu)^2} \qquad \text{Eq.37}$$

If Poisson's ratio is set equal to zero, then is $\mathbf{C = 1}$ and in this model equals the Kirsch solution.

Another important factor in this model is temperature and it's relation to fracturing pressure. If the borehole is heated or cooled, the fracturing pressure will change because of hoop stress change due to expansion or contraction.

In order to include the temperature effect into the model, the following equation was added to Eq. 36:

$$K \cdot E\kappa(T - T_{init}) \qquad \text{Eq.38}$$

where **E** is the Young's modulus, **κ** is coefficient of linear thermal expansion, $\mathbf{T_{init}}$ is the initial temperature, which exist at the in-situ stress conditions, **K** is a correction term for temperature and looks the following:

$$K = \frac{(1-\nu)^2}{3\nu(1-2\nu)+(1+\nu)^2} \qquad \text{Eq.39}$$

Coefficient of thermal expansion has a strong dependence on silica content because the **κ** of quartz is an order of magnitude higher than other rock forming minerals.

The above mentioned **C** and **K** correction factors can be given in graphical or numerical form for different values of Poisson's ratio as it can be seen in Fig. 12 and Table 1.

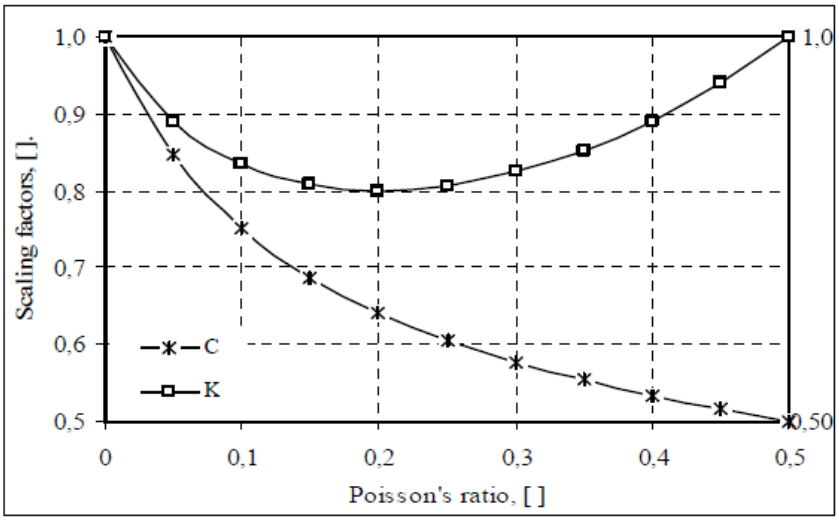

Figure 12: Scaling factors due to Poisson's effect, C for stress and K for temperature (Aadnoy and Belayneh 2008 A)

Table 1: Correction factors for the thermoporoelastic model (Aadnoy and Belayneh 2008 A)

Poisson's Ratio	*C* for Stress $\frac{(1+\upsilon)(1-\upsilon)^2}{3\upsilon(1-2\upsilon)+(1+\upsilon)^2}$	*K* for Temp $\frac{(1+\upsilon)^2}{3\upsilon(1-2\upsilon)+(1+\upsilon)^2}$
0.00	1	1,000
0.05	0.846364	0,891
0.10	0.751034	0,834
0.15	0.686489	0,808
0.20	0.640000	0,800
0.25	0.604839	0,806
0.30	0.577073	0,824
0.35	0.554211	0,853
0.40	0.534545	0,891
0.45	0.516816	0,940
0.50	0.500000	1,000

Incorporating findings of various studies executed, Aadony and Belayneh included the elastoplastic barrier as described in their paper published in 2004. Since the mudcake which left on the wellbore due to the drilling behaves plastically, higher fracture pressures are required, but up to now there is no field method available to measure the magnitude of this phenomenon. Aadnoy and Belayneh calculate the influence of the mudcake with the following equation:

$$\frac{2Y}{\sqrt{3}}\ln\left(1+\frac{t}{r_w}\right) \quad \text{Eq.40}$$

where **Y** is the yield strength of filter cake particles, **t** is the thickness of filter cake, $\mathbf{r_w}$ is the borehole radius.

Including **C** and **K**, the complete model for calculating formation breakdown pressure for anisotropic stress loading was defined as follows:

$$FBP = S_{H,max} + \frac{2(1+\nu)(1-\nu^2)}{3\nu(1-2\nu)+(1+\nu)^2}\left\{\frac{3}{2}S_{h,min} - S_{H,max} - P_o\right\} + P_o + \frac{(1+\nu)^2}{3\nu(1-2\nu)+(1+\nu)^2}E\kappa(T-T_{init}) + \frac{2Y}{\sqrt{3}}\ln\left(1+\frac{t}{a}\right) \quad \text{Eq.41}$$

Since the cooling effect of the fracturing fluid to the wellbore and the surrounding rock is not known in all the cases, the above mentioned combined model was divided into Aadnoy and Belayneh 1, 2008 method which includes only the load history:

$$FBP = S_{H,max} + \frac{2(1+\nu)(1-\nu^2)}{3\nu(1-2\nu)+(1+\nu)^2}\left\{\frac{3}{2}S_{h,min} - S_{H,max} - P_o\right\} + P_o \quad \text{Eq.42}$$

and to Aadnoy and Belayneh 2, 2008 method which includes temperature history too (complete model).

5.3 Summary of Methods

The different FBP prediction methods are listed in Table 2 showing their authors, year of publication, description and assumptions.

Table 2: Summary of Formation Breakdown Pressure prediction methods used in this study

Author(s)	Year	Method	Description	Assumption
Kirsch	1898	Elastic model	First published method for calculation of stresses in a circular hole, equation used in the fracture simulation software	Circular hole, balanced borehole (drilling fluid provides a pressure on the well bore that equals the lithostatic pressure)
Hubbert and Willis	1957	Linear elastic model	Improved Kirsch model	Rock is homogeneous, isotropic, and impermeable, P_{co} is a constant rock mechanical property
Haimson and Fairhurst	1967	Poroelastic model	Incorporating the stresses induced due to fluid penetration into the rock	P_{co} is a constant rock mechanical property
Rummel 1	1987	Linear elastic fracture mechanics model	Preexistence of a symmetrical double crack, neglects initial pore pressure	Pressure in the crack is equal to the pressure in the wellbore
Rummel 2	1987	Linear elastic fracture mechanics model	Preexistence of a symmetrical double crack, neglects initial pore pressure	Pressure in the crack is equal to 75 % of the pressure in the wellbore
Rummel 3	1987	Linear elastic fracture mechanics model	Preexistence of a symmetrical double crack, neglects initial pore pressure	Linear pressure drop along the crack
Rummel 4	1987	Linear elastic fracture mechanics model	Preexistence of a symmetrical double crack, neglects initial pore pressure	Quadratic pressure drop along the crack
Schmitt and Zoback	1989	Poroelastic model	Incorporating the effect of injection fluid flow into the rock and include a porosity dependent correction parameter	Porosity dependent correction parameter is known (can be determine only with laboratory simulation under controlled conditions)
Ito and Hayashi	1990	Point stress model	A finite region of material, and not just a point, must be critically stressed	It neglects initial pore pressure, P_{co} is size dependent
Aadnoy and Belayneh 1	2008	Thermoporoelastic model	Including load history of the wellbore	Poisson's effect arises (the effects in the tangential and axial direction of a radial loading)
Aadnoy and Belayneh 2	2008	Thermoporoelastic model	Including temperature and load history of the wellbore	Poisson's effect arises (the effects in the tangential and axial direction of a radial loading)

The thesis results will demonstrate, that even with the most sophisticated model it is not easy to obtain a satisfying prediction of FBP in all types of reservoirs and rocks. The reason for this is seen in the fact that FBP is considered to be influenced by many parameters which are difficult to quantify and they are not sufficiently reflected in any of the models.

6. Geomechanical Database

In order to compare the different Formation Breakdown Pressure prediction methods and confirm their validity to real measurements, a statistically relevant size database of geomechanical parameters used for modeling formation rock and treatment data of hydraulic fracturing treatments was required. Data quantity and quality was the main target. Furthermore, it was aimed for a variety in field data to investigate if the Formation Breakdown Pressure prediction methods are applicable for all types of formations. The information about the rock properties derived from different available reports used for the study and are listed below:

- Geomechanics studies
- Logs
- Hydraulic treatment design reports
- FracPro and GOHFER files
- Post frac reports
- Pump data
- Completion drawings/schematics

From these reports the parameters used by the different models were collected:

Principal Stress Tensor Components:

- Overburden stress (S_v)
- Minimum principal horizontal stress ($S_{h,min}$)
- Maximum principal horizontal stress ($S_{H,max}$)
- Maximum principal horizontal stress azimuth ($aziS_{H,max}$)
- Pore pressure (P_o)

Rock Properties:

- Rock strength
    - Unconfined compressive strength (UCS)
    - Coefficient of internal friction (μ_i)
- Elastic properties
    - Poisson's ratio (ν)
    - Biot coefficient (α)
    - Young's modulus (E)

Since the geomechanic parameters are the base for fracture modelling the Mechanical Earth Models (MEM) of the individual fields where all the available drilling, logging and general available geological and geomechanical information is combined were the main sources. Nevertheless, understanding the source and accuracy of these data is vital for the QA/QC evaluation.

6.1 Mechanical Earth Model

The goal of a geomechanical study is to develop a reliable understanding of a zone of interest and to achieve ±10 % accuracy for rock mechanical properties and to determine the orientation of the different stresses.

Table 3 provides a general overview of the data required to build a MEM and the output parameters which can be used as a basis for any required application (e.g., stimulation, wellbore stability, sanding tendency, water injection for EOR etc.):

Table 3: Required data and output parameters of a geomechanical model

Work Flow – Geomechanical Model

Parameter		Data
Vertical stress, S_v	←	$S_v(z_0) = \int_0^z \rho\, g\, dz$
Pore pressure, P_p	←	Formation pressure measurements, log-derived (acoustic, resistivity, density), seismic, inflow events
Least principal stress, Fracture gradient S_{hmin},	←	LOT, XLOT, minifrac, PWD, losses
Stress orientation	←	Orientation of wellbore failure, WSM
Rock properties: strength (UCS, friction), Poisson ratio, Biot coefficient	←	Lab, logs, modeling wellbore failure
Max. Horizontal stress, S_{Hmax}	←	Modelling wellbore failure, stress regime – geology- tectonics

The abbreviations are the following in Table 3: PWD=pressure while drilling; LOT= leak-off test; XLOT=extended leak-off test; WSM=world stress map; UCS=unconfined compressive strength.

In addition to this list various data serve to calibrate and verify the constructed model, most of these additional data are reported in the below outlined, but not limited to, documents:

- Drilling morning reports - used to calibrate the geomechanical model against the actual drilling experience
- Wellbore surveys and schematics - to provide information about the position of a borehole or well path and completion
- Caliper logs - to measure the size and shape of the borehole; generally acquired with the bulk density tool
- Image logs - electrical and acoustic to detect stress induced wellbore failures (borehole breakouts, tensile and natural fractures). This information helps constraining orientation and magnitudes of maximum horizontal stress
- Photographs of cuttings and cavings - collected at the shale shakers and reveal/manifest the mechanical behavior of a wellbore during drilling

- Well test data - to calibrate pore-pressure and to predict and later understand well productivity

Figure 13 below shows a workflow about how a geomechanical model develops with the progression of the exploration using the various sources of information. Since more and more information is built into the model the uncertainties are reduced as a consequence.

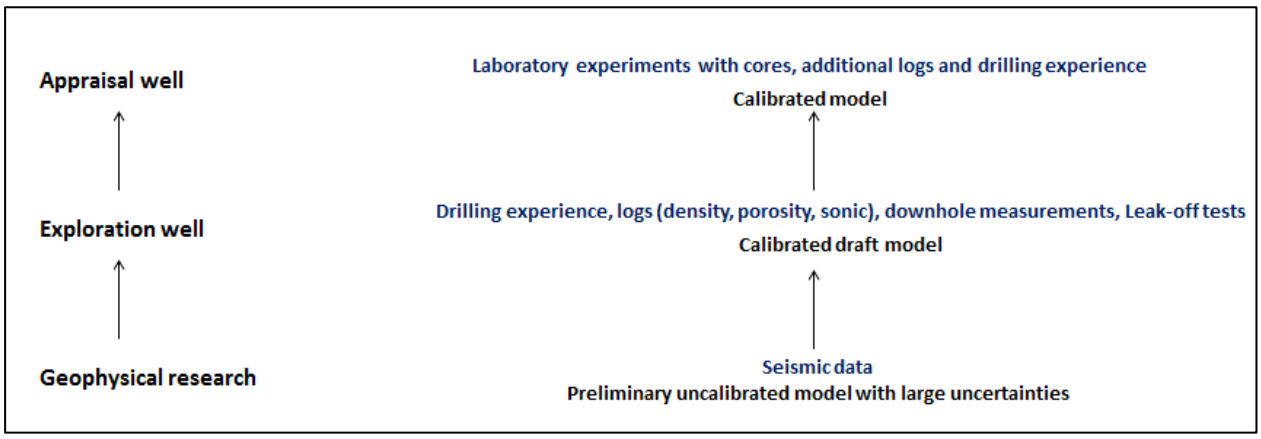

Figure 13: Geomechanical model improvement as field exploration progresses

It can be imagined that building a MEM is a challenging data management task since the information comes from various sources. In Appendix D a table provides the data checklists and formats, which should be completed by the experts in a geomechanical project at OMV Aktiengesellschaft. This list should be filled as accurate as possible to ensure maximum data quality and that a standard is maintained during a project. However, it is understood that not all data listed in this file are available for any given study and engineering needs to be used to verify the input data.

In Appendix E logs about mechanical properties and stress magnitudes, wellbore stability and a final integrated montage can be seen for one of the examined well. This information together with the reports was used to collect the input parameters for the FBP prediction models.

6.2. Database Summary

127 hydraulic fracturing treatments were collected coming from 55 wells from 4 countries and 8 fields (in a later phase of the study additional 14 hydraulic fracturing treatments data were gathered and used for quality check purposes). Figure 14 shows the distribution of the treatment origin in terms of hemispheres of the Earth.

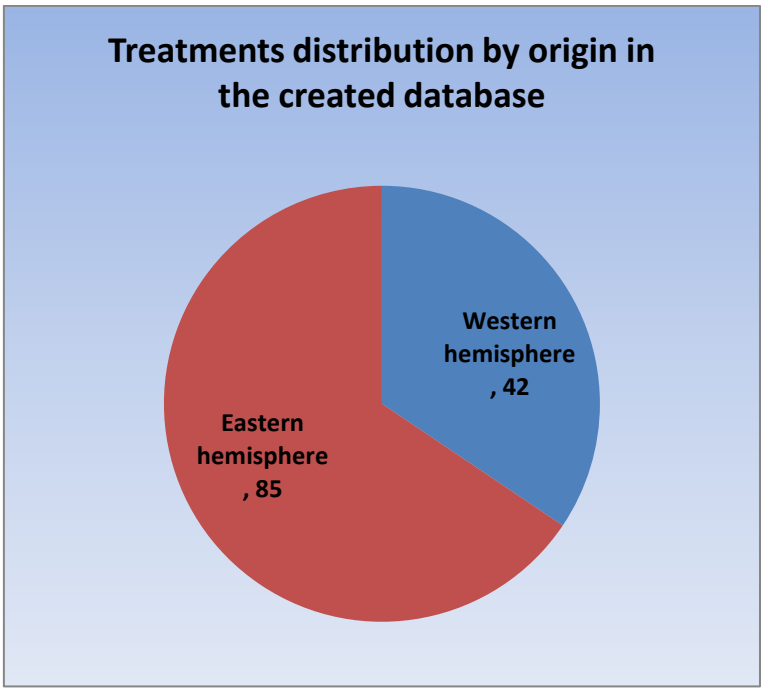

Figure 14: Distribution of treatments by origin in the created database

Table 4 shows the origin of the wells. Please note, that the Wells 10, 11, 12 and 43 are not located inside the main fields investigated. Therefore they are shown in brackets.

Table 4: Database summary

Country	Field	Well name
Country A	Field A	Well 1-4
	Field B	Well 5-9 (10-12)
Country B	Field C	Well 13-17
	Field D	Well 18-30
	Field E	Well 31-42 (43)
Country C	Field F	Well 44-49
	Field G	Well 50-53
Country D	Field H	Well 54-55

The parameters from the various sources of the hydraulic fracturing treatments and the wells were the following:

Break Down Test: FBP

Figure 15 shows distributional characteristics of the measured FBP datasets for the different countries as the origin of the treatments (breakdown data distribution for the identified major fields can be found in Appendix F). For representation purposes of the Formation Breakdown Pressure distribution, a violin plot was combined with a box plot. This enables to show the data density at different values similar to a histogram.

To create the boxplot the sorted data were clustered into four equally sized quartile groups. The middle “box” represents the middle 50 % of the sorted data. The median marks the mid-

point of the data and is shown by the line that divides the box into two parts. Half the scores are greater than this value and half are less.

As in Fig. 15 can be seen, the plot shape of FBP values for Country C and D are comparatively short meaning that the pressures magnitudes for the FBP values are similar for the country. However, in case of Country D, one outlier is present at the lower part of the plot. The contrary is the case for the data measured in Country A and B the boxplots are long-drawn, this indicates the scatter in the dataset. The locations of the boxplots tell about the absolute pressure magnitudes e.g. in case of Country D significantly higher pressures are needed for the treatments to create a fracture in the rock than for Country A, B, C. The uneven size of boxplot for Country A shows that FBP values which are higher than the median vary a lot in magnitude. Although the medians, which are commonly close to the average, are at similar levels for Country A and B, however the boxplots demonstrate the different distributions of pressure values.

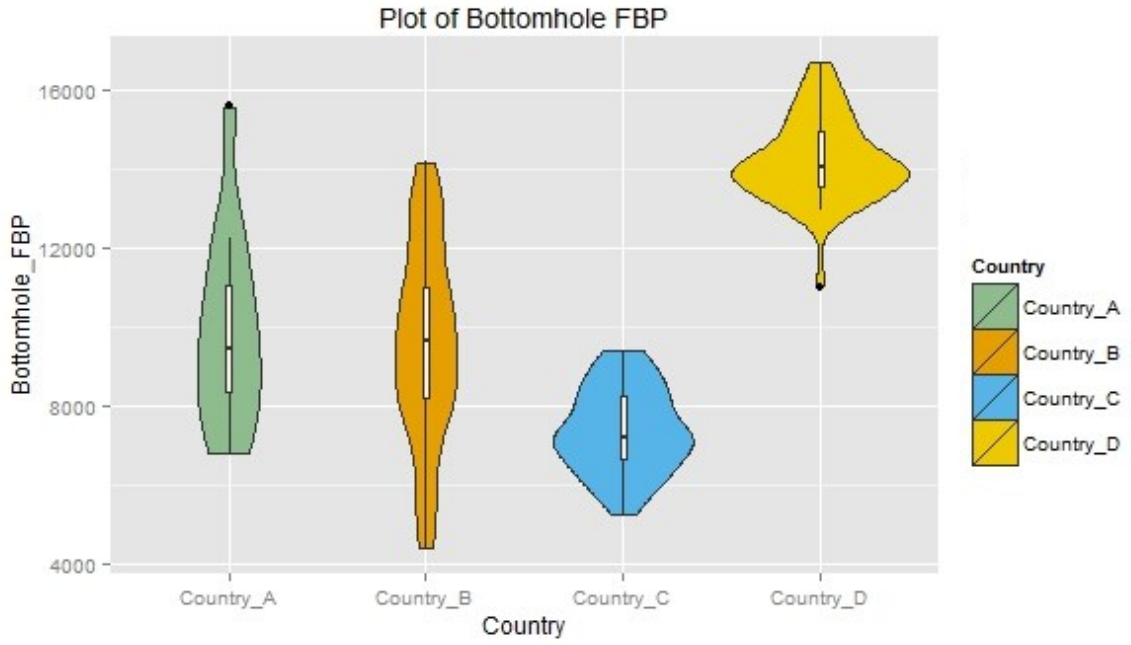

Figure 15: Breakdown data distribution by countries (probability density, median of the data -shown by the horizontal marker- and a box indicating the interquartile range)

Minifrac/Datafrac data: FBP (if not determined in earlier diagnostic pumping tests), closure pressure, net pressure, flow rate, frac fluid properties (fluid type, density, viscosity)

Mechanical Earth Model data: in-situ stresses (magnitude and direction – given by the azimuth of the maximum horizontal stress), pore pressure, rock properties (elastic properties, strength, temperature, compressibility, fracture toughness)

Wellbore and completion data: TVD, MD, borehole diameter, hole deviation and azimuth, tubing diameter

Perforation data (partially available): gun type, phasing, underbalance/overbalance, entry hole diameter, perforation length, shot per foot, propped fracture half-length

Data pre-processing as a data mining technique was used to transfer the raw data into an understandable format. The parameters were converted into a common unit system since several service companies carried out the hydraulic fracturing operations and their style of reporting differs from each other. If any important variable was missing in the reports (like in-situ stresses, pore pressure, elastic parameters) then the treatment was excluded from the database. However, if only such parameters were missing which variance should not change a lot within the field (i.e. temperature), a field averaged value was applied.

Note: Some FBP prediction models require adjustment factors, which were often not available. Based on the model description and stated range values, according to best engineering assumptions and evaluation, valid data ranges for the individual data was established and then the determined value kept constant during the calculations for similar fields.

7. Evaluation of the Formation Breakdown Pressure Prediction Models

To evaluate and prove the validity of the Formation Breakdown Pressure prediction methods, their performance was compared to actual field data. In order to carry out the calculations for the various models, an Excel Spreadsheet was created. To investigate the obtained results as a first approach, the distribution of the datasets were compared using a boxplot. Furthermore, the calculated data points for each model were demonstrated in a cross plot to measured FBP (Figure 18 to 28). In this general approach was observed that the prediction results concentrate for some models in various specific areas. Since this method was not conclusive a comprehensive error analysis was applied following the work as described and applied by Comisky et al. in 2007.

To rank the prediction models, parameters like a) success rate factor, b) mean residual square error, c) standard deviation, d) mean squared error, e) mean absolute error and f) Pearson correlation coefficient for each individual model were calculated and compared. Using statistical parameters like a, b and c were adapted from Comisky et al. 2007 and the analysis was enhanced with parameters like d, e and f. Based on the ranking of the models according to the six statistical parameters the model with the best ranking was chosen. The model, which ranked first, provided results closest to the actual measured data, but since the predictions were not consistently close to the actual data and the “success factors” were still quite far from perfect, none of the models was considered to provide sufficient accurate and precise data to be recommended for general use in all types of reservoirs.

Figure 16 describes as an example the type of data found and the idea of accuracy and precision of data. In the case of FBP prediction, precision means reproducibility and accuracy means distance from true value. Some of the evaluated models in general, or at least for some data sets were more or less accurate but missed precision or if they showed some kind of precision most likely these data could not be classified accurate. The goal was to find the model which is accurate and precise at the same time and it can be only done with carefully chosen statistical characterization (i.e. if one would only consider standard deviation -which gives an idea about the spread of the data- in case of the middle picture, it would be misleading since the model is not accurate at all).

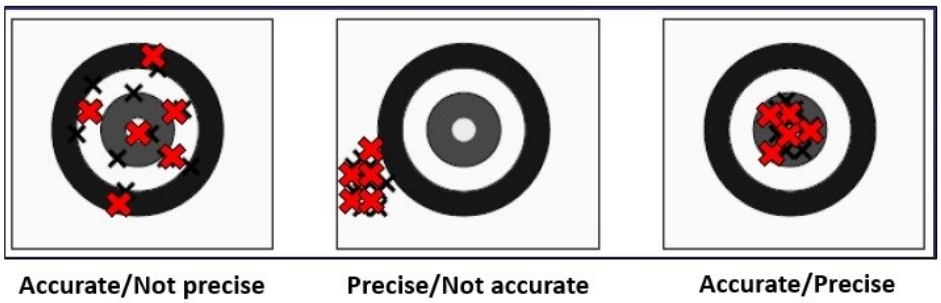

Figure 16: Complexity of the calculated data evaluation

Nevertheless, demonstrating the data points for each model in cross plots of calculated FBP to measure FBP (Figure 18 to 28), prediction results concentrations in specific areas were observed. The unit slope or "perfect correlation" is given by the red trend line in each case. For guidance, high/low (dashed) trend lines are provided which represent a variance factor of ± 2500 psi to each value and which is derived from parallels to the trend line drawn through a ± 15 % criteria on the maximum measured FBP. The graphs provide a visual orientation as to the accuracy of each FBP estimation method taken into account the acceptance criteria. All data points which lay within the criteria bars are considered an acceptable match. The visual observation of result clouds on these plots led to the idea that because different field, area, formation parameters are used by the models and also because the models were developed studying specific formations, grouping/clustering of the data, based on the common parameters might allow refining the outcome. Based on engineering judgment the data were clustered by a) well location, b) well type, c) depth, d) faulting environment, e) formation type and f) fields with the intention to refine the outcome and get more precise and accurate results.

Furthermore, the sensitivity of the best scored model to the different input parameters was investigated. With this technique the most important parameters influencing the model result can be determined. The knowledge of the main influencing parameters was considered important in regards to the efforts necessary to obtain the best quality input data possible.

In Appendix G the measured and calculated FBP values are tabulated for the investigated treatments.

7.1 Comparison of the Models

Figure 17 compares the boxplots of the measured to the calculated FBP pressure of the individual models. For each box all the 127 treatments as listed in Appendix G were investigated. From the shape of the boxes, the upper and lower quartile boundaries, the maximum and minimum values and the closeness of the median line the models from Aadnoy and Belayneh (1 and 2), Schmitt and Zoback and Kirsch are qualified as the most precise and promise to provide the required accuracy.

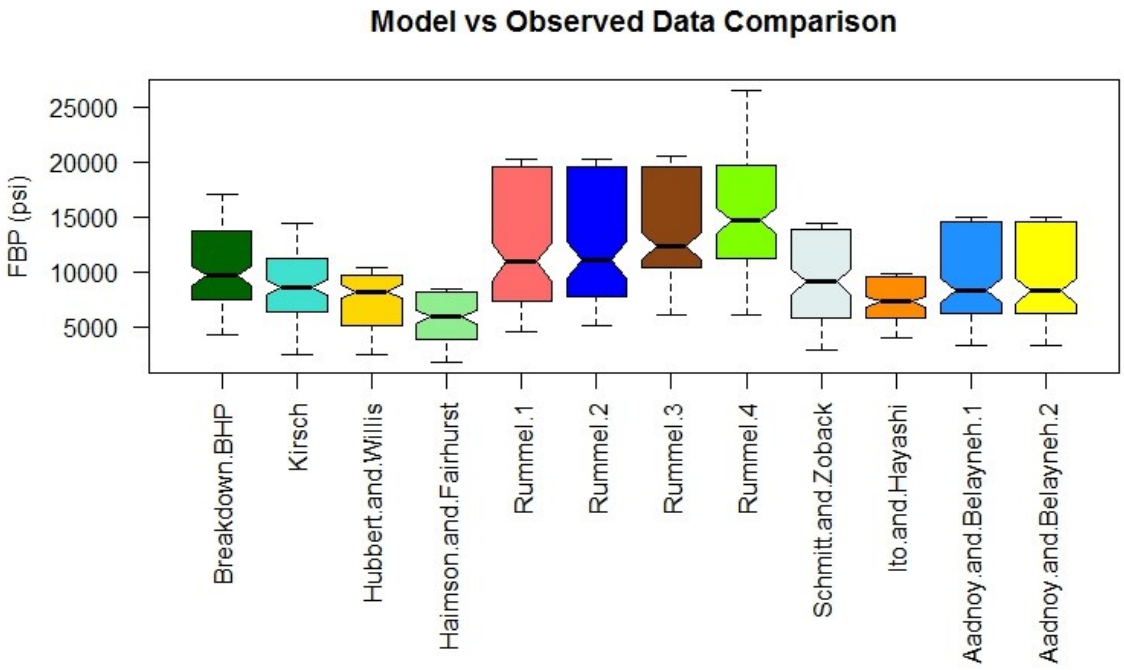

Figure 17: Comparison of the measured breakdown pressure versus the predicted values

For verification of the interpretation of the boxplot the predicted FBP of the individual models were plotted against measured FBP. Figure 18 to 28 list the results and although the data are scattered and do not allow to determine a clear correlation, this visual interpretation confirms that the models which promise best FBP pressure prediction are the same as the ones from the box plot interpretation. The results classification is based on the overall distribution of the data and the fact that most of the calculated data for these models lay within the chosen accuracy criteria as describe above. The other models had significant variances as the point clouds scattered over the complete scale range reducing the confidence in data quality for the calculated data to a minimum.

Figure 18 shows the result of Kirsch method. However the data is scattered, a lot of points are close to the perfect correlation. The result for the Hubbert and Willis method is presented in Fig. 19 and it shows poor accuracy. As one can see, there is a significant point cloud at the upper right corner of the plot (representing Field H with a lot of treatments) which is completely out of the acceptable envelope range. In case of the Haimson and Fairhurst model (Fig. 20) only a group of data (representing one field) is close to the perfect correlation the rest has poor accuracy and an overall underestimation is valid for the predicted points.

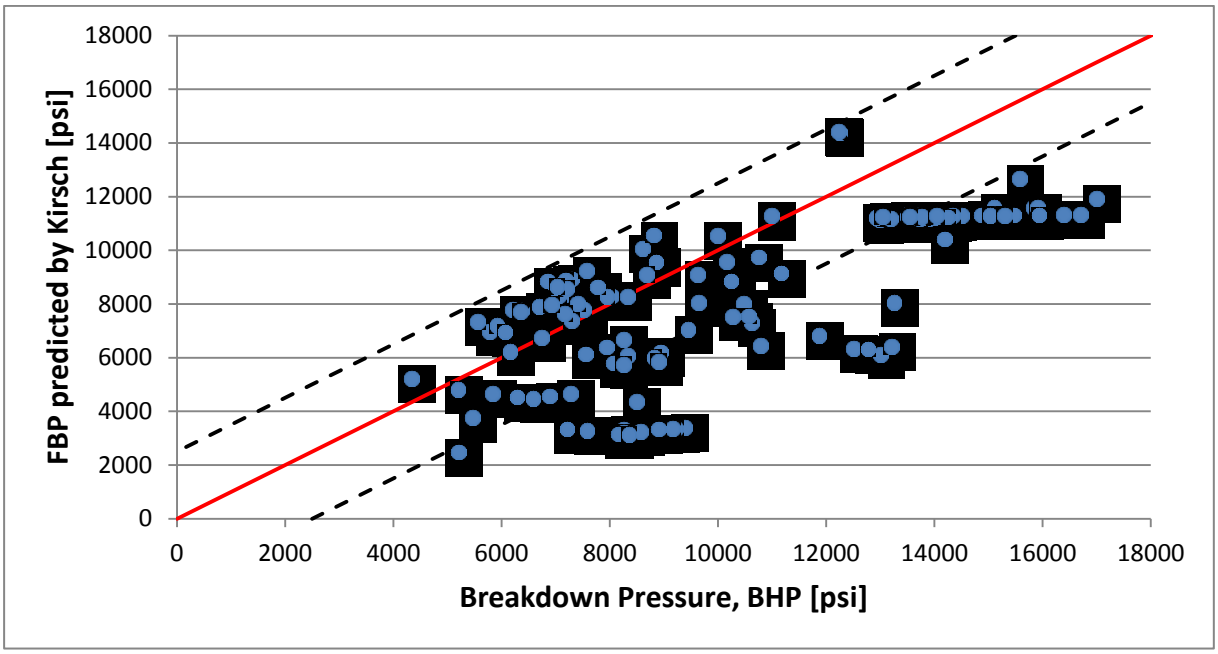

Figure 18: Comparison of the predicted Formation Breakdown Pressure using the Kirsch method to the measured pressure

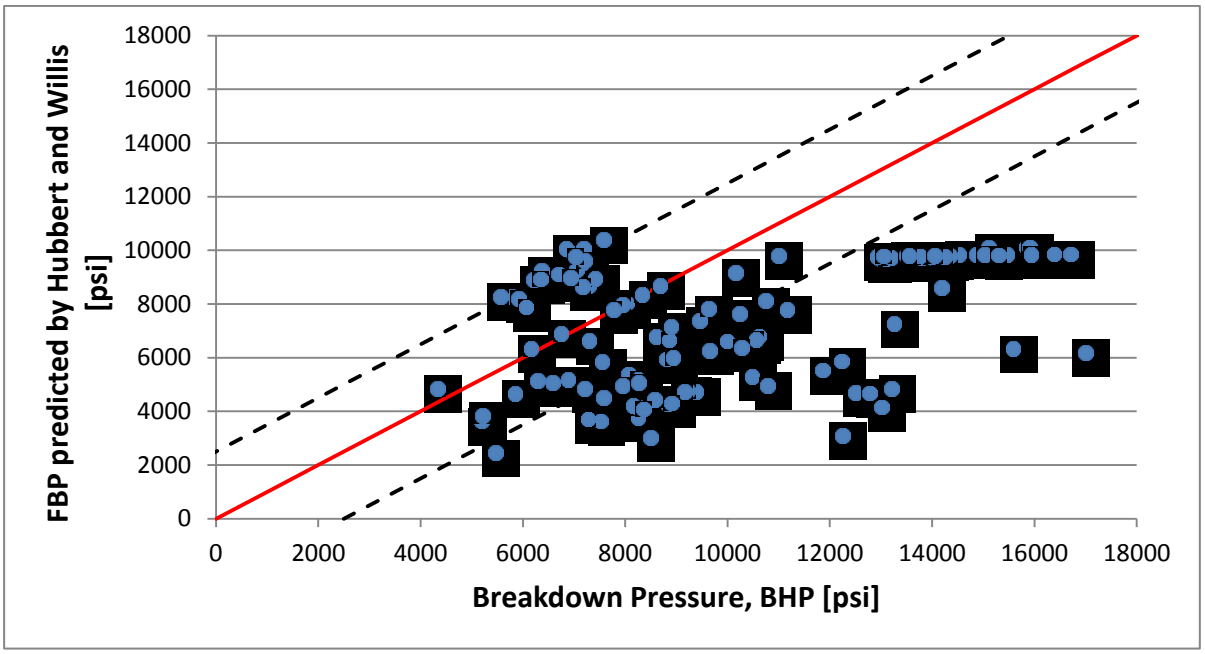

Figure 19: Comparison of the predicted Formation Breakdown Pressure using the Hubbert and Willis method to the measured pressure

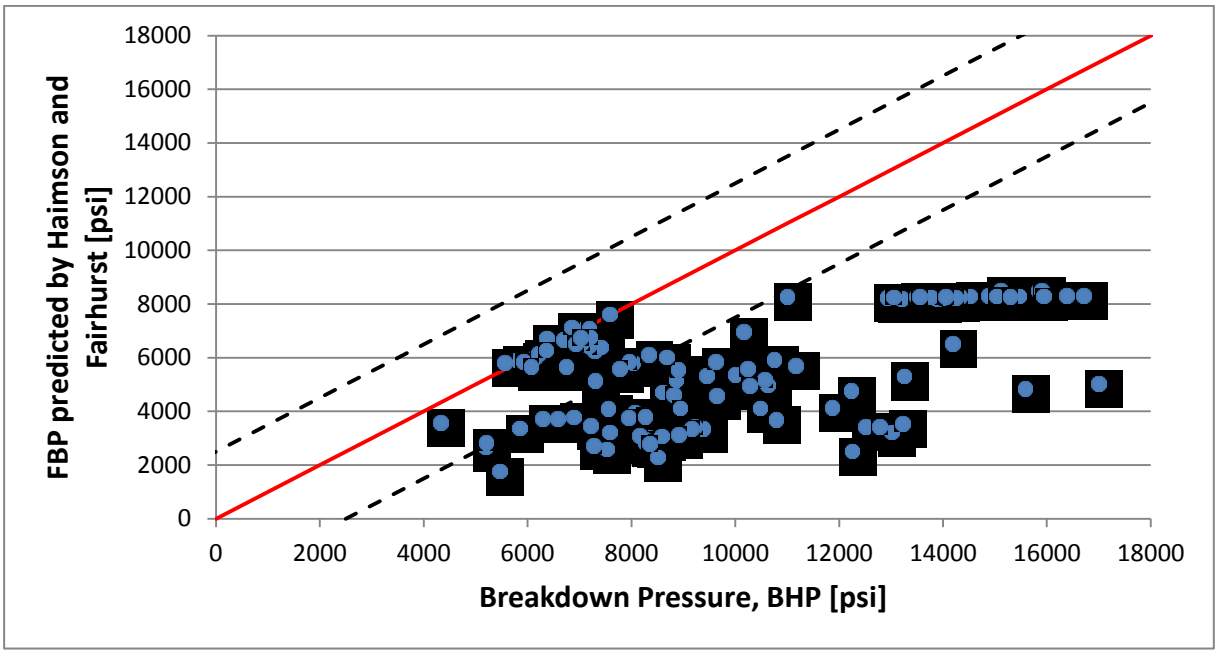

Figure 20: Comparison of the predicted Formation Breakdown Pressure using the Haimson and Fairhurst method to the measured pressure

The result for the four Rummel methods is presented in Fig. 21–24. On the one hand, Rummel 2 method yields the best overall match to measured pressure values out of the four technics; on the other hand, about half of the samples lie completely outside of the acceptable region. Generally speaking all the four methods severely overestimate the values; in case of the treatments from Field H the data cloud is not visible at all. The Rummel 4 correlation (Fig. 23) yields values shifted above the trend lines almost throughout the entire data set.

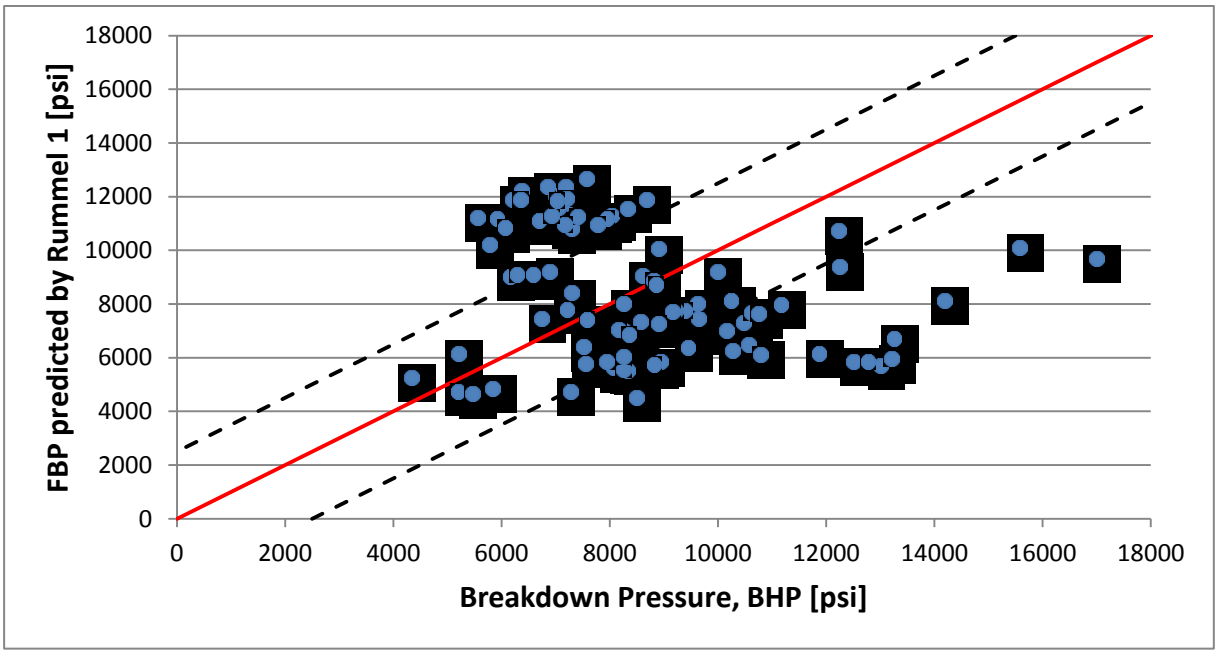

Figure 21: Comparison of the predicted Formation Breakdown Pressure using the Rummel 1 method to the measured pressure

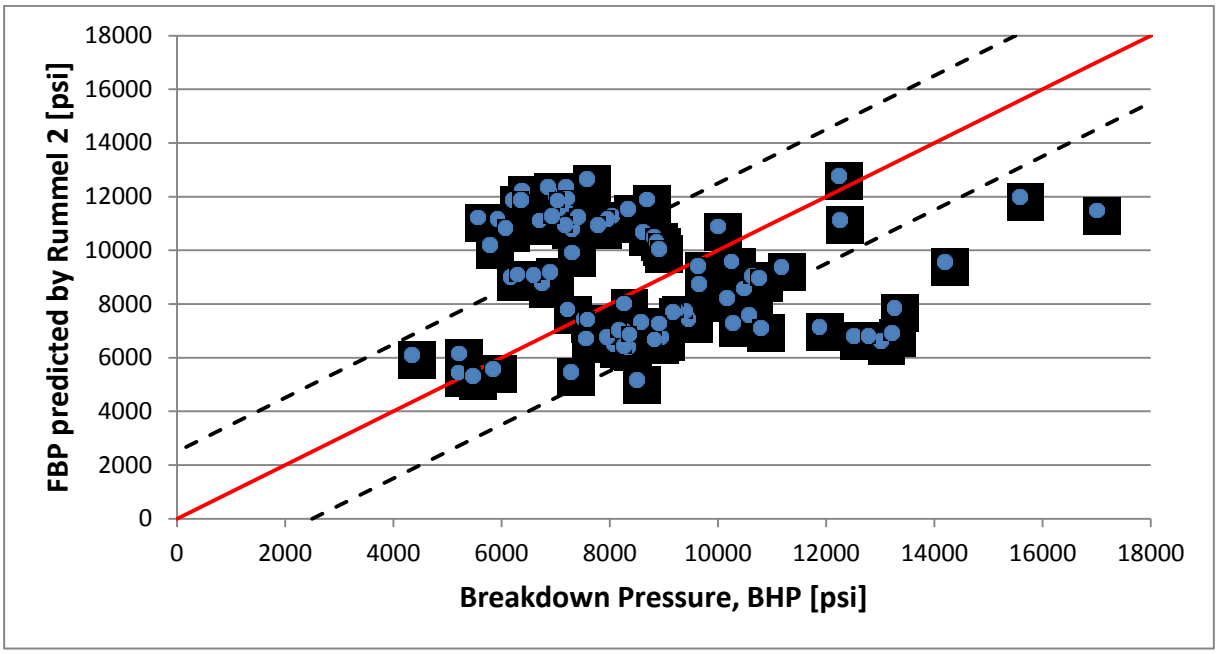

Figure 22: Comparison of the predicted Formation Breakdown Pressure using the Rummel 2 method to the measured pressure

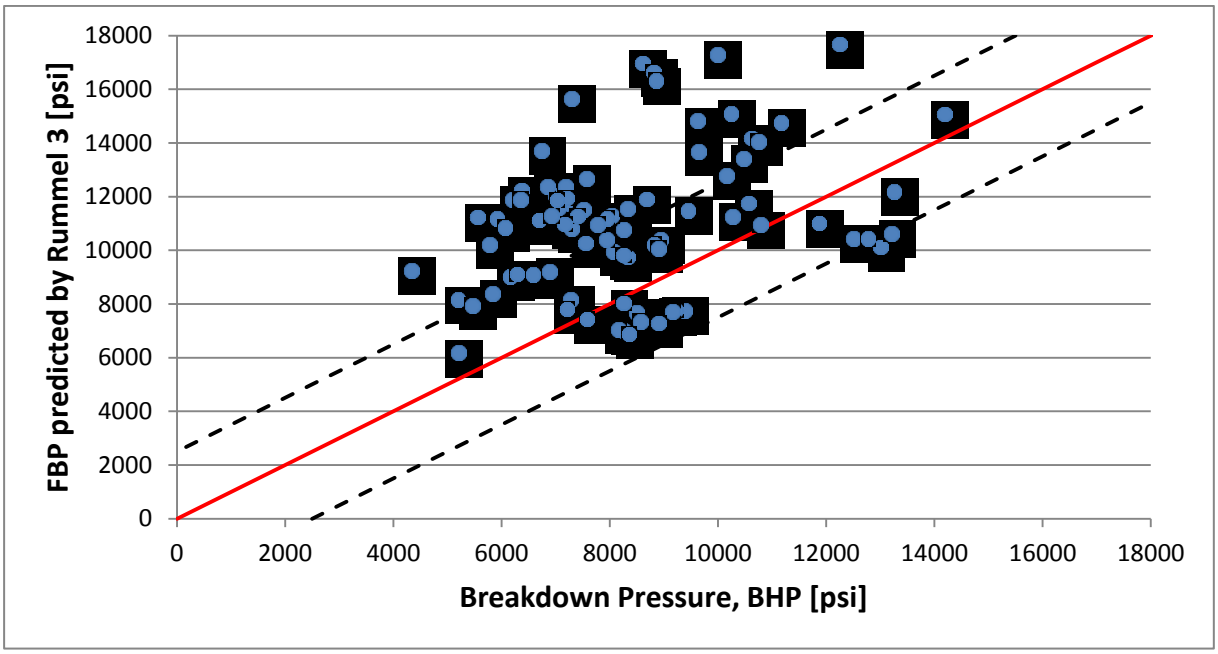

Figure 23: Comparison of the predicted Formation Breakdown Pressure using the Rummel 3 method to the measured pressure

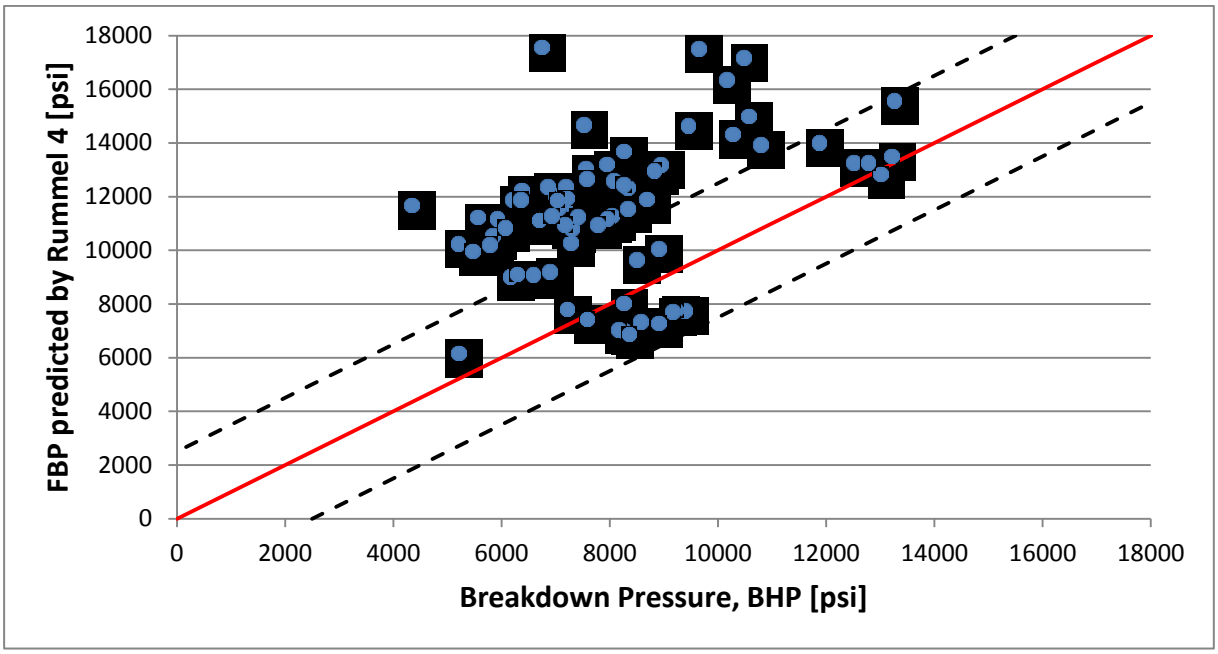

Figure 24: Comparison of the predicted Formation Breakdown Pressure using the Rummel 4 method to the measured pressure

Schmitt and Zoback method is presented in Fig. 25. It shows better accuracy and precision than some of the previously described models. It roughly equally under- and overestimates the predicted pressure compare to the measured ones. The Ito and Hayashi FBP estimation method is shown in Fig. 26. The data is not spread over the whole plot but the accuracy is really poor, the majority of the points are falling into the underestimated region of the plot.

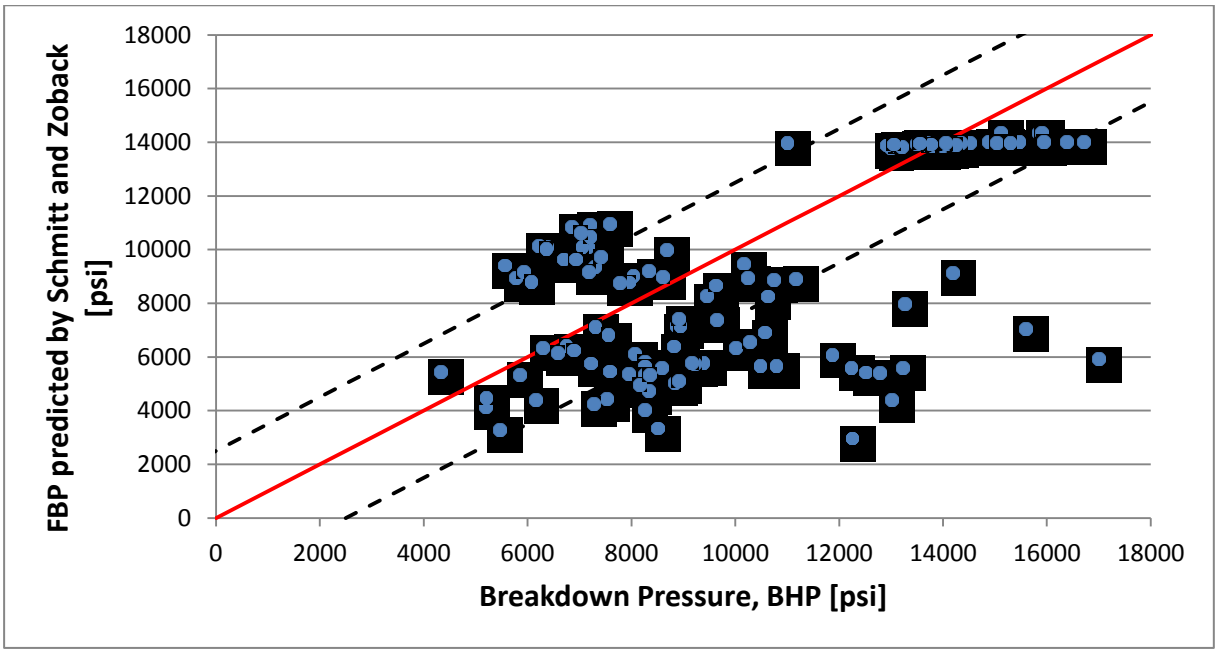

Figure 25: Comparison of the predicted Formation Breakdown Pressure using the Schmitt and Zoback method to the measured pressure

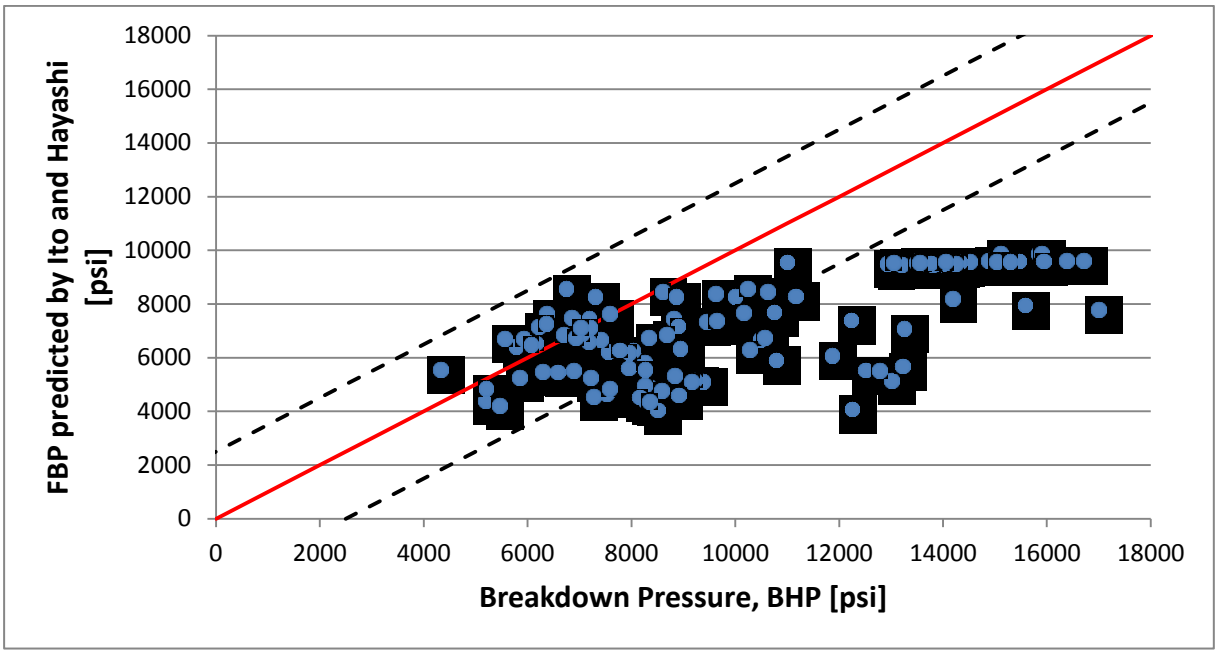

Figure 26: Comparison of the predicted Formation Breakdown Pressure using the Ito and Hayashi method to the measured pressure

Aadnoy and Belayneh 1 and 2 FBP correlations in Fig. 27 and 28 indicate the best precision and accuracy from all the above mentioned methods. The difference between the two models is minimal. Aadnoy and Belayneh 2 method shifts the data points down to a small extent since this model takes into account the cooling of the wellbore and the surrounding rock by the fracturing, but sensitivity analysis showed that this effect is almost negligible.

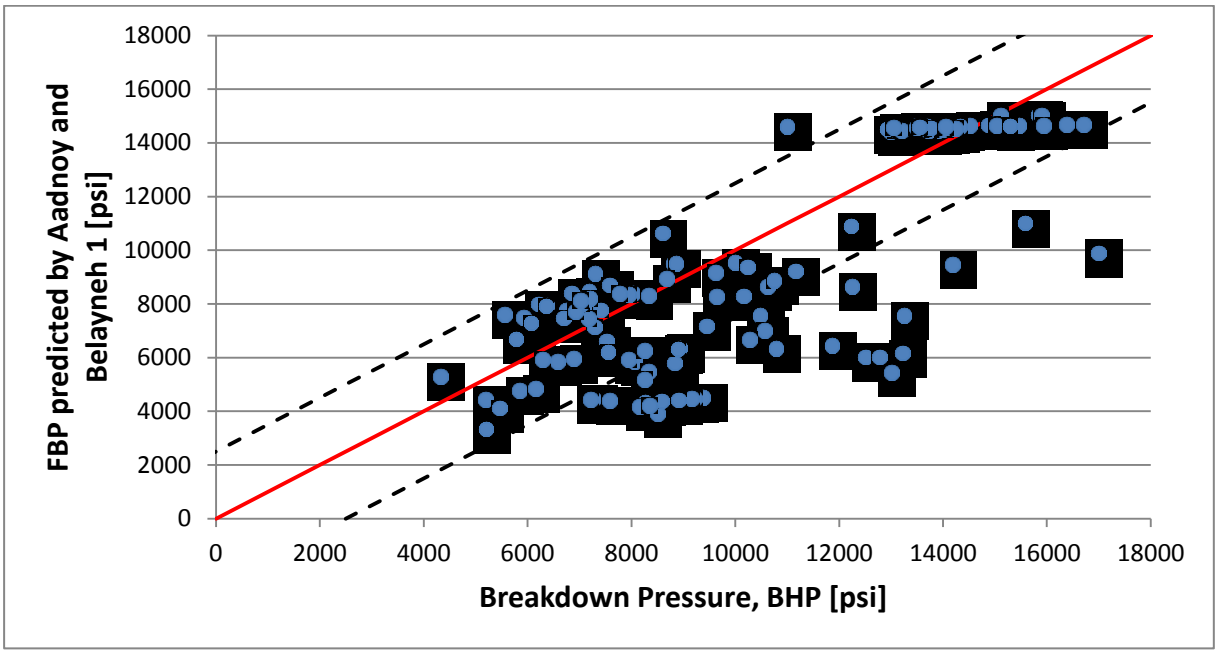

Figure 27: Comparison of the predicted Formation Breakdown Pressure using the Aadnoy and Belayneh 1 method to the measured pressure

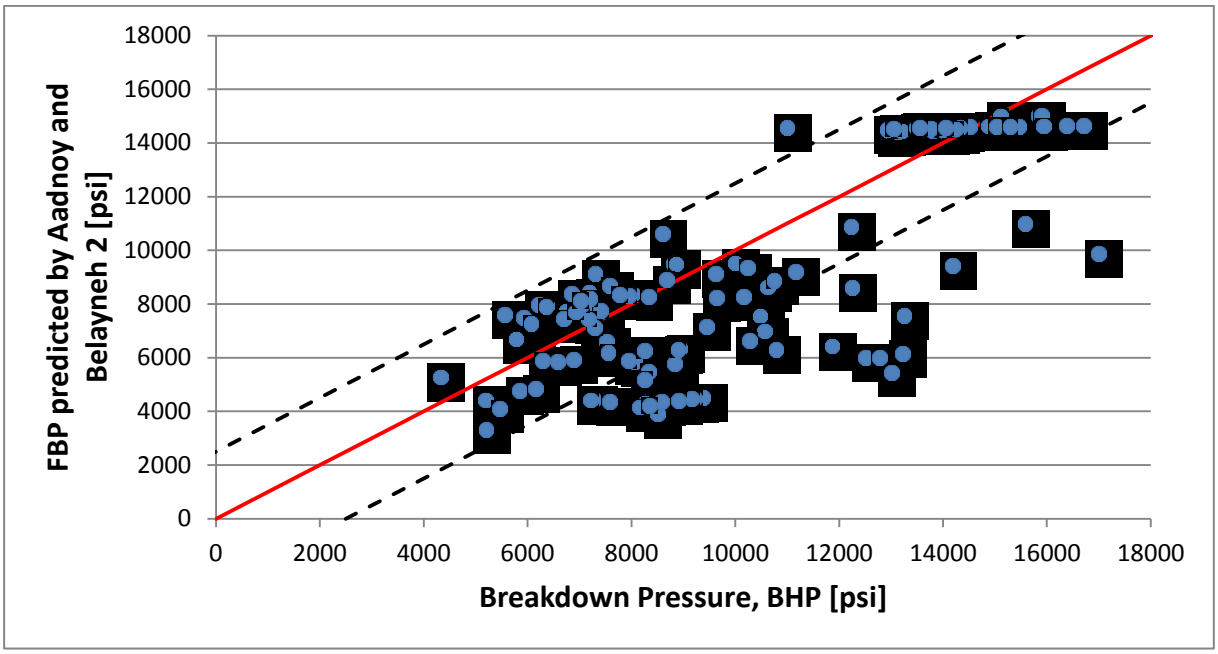

Figure 28: Comparison of the predicted Formation Breakdown Pressure using the Aadnoy and Belayneh 2 method to the measured pressure

7.2 Evaluation Criteria - Error Analysis Details

Overall, the accuracy and precision of the Formation Breakdown Pressure correlations were lower than expected. The poor performance can be caused by the parameter inaccuracies or the theory assumptions. The intention was to qualify the performance of the models using a comprehensive error analysis with six statistical parameters which are described in more detail in this chapter.

7.2.1 Success Rate Criteria

As a first evaluation criteria an acceptable envelope region was used on the cross plot of the predicted and the measured data to assess "goodness-of-fit" for the FBP prediction models. As a ranking mechanism the percentage of number of points which fell inside the criteria was used. The higher the percentage of data points meeting the criteria was the better the model was ranked in this method. Table 5 provides and overview of the ranking with the names of the FBP method as well as the year of the publication. Surprisingly, only four models have a “success” percentage above 50 % and none of them was exceeding 75 %. Using the "percent success" value was understood as a rough comparison, but nevertheless it provided contrasts and an indication of which models perform better in practice.

Table 5: Ranking summary for the Formation Breakdown Pressure prediction methods based on the percentage of the sample population that falls within the acceptable envelope

Rank	Success ratio [%]	FBP Prediction Method
1	74.22	Aadnoy and Belayneh 1, 2008
1	74.22	Aadnoy and Belayneh 2, 2008
2	60.94	Schmitt and Zoback, 1989
3	57.03	Kirsch, 1898
4	41.41	Ito and Hayashi, 1990
5	35.16	Rummel 2, 1987
6	27.34	Hubbert and Willis, 1957
6	27.34	Rummel 3, 1987
7	26.56	Rummel 1, 1987
8	23.44	Haimson and Fairhurst, 1967
9	17.19	Rummel 4, 1987

7.2.2 Mean Residual Square Error

The mean residual square error of an estimator measures the average of the squares of the logarithmic "errors". In this case the estimator is the calculated FBP and what is estimated is the measured FBP value. Equation 43 describes this method mathematically. :

$$S^2 = \frac{1}{n}\sum_{i=1}^{n}\left[\log\left(FBP_{measured,i}\right) - \log\left(FBP_{predicted,i}\right)\right]^2 \qquad \text{Eq.43}$$

Table 6 ranks the result of each FBP correlation using the mean residual square error (MRE-S2) and the ranking is showed by ascending MRE-S2 values. As one can see, the Aadnoy and Belayneh methods yield the lowest errors.

Table 6: Ranking summary for the Formation Breakdown Pressure prediction methods based on the mean residual square error

Rank	MRE-S2	FBP Predicting Method
1	0.0193	Aadnoy and Belayneh 1, 2008
2	0.0195	Aadnoy and Belayneh 2, 2008
3	0.0242	Rummel 2, 1987
4	0.0263	Rummel 3, 1987
5	0.0287	Schmitt and Zoback, 1989
6	0.029	Kirsch, 1898
7	0.0294	Rummel 1, 1987
8	0.0317	Ito and Hayashi, 1990
9	0.0382	Rummel 4, 1987
10	0.0449	Hubbert and Willis, 1957
11	0.0887	Haimson and Fairhurst, 1967

7.2.3 Standard Deviation

To evaluate the precision, amount of variation or dispersion of each method, the standard deviation was calculated, mathematically described in equation 44:

$$\sigma = \sqrt{\frac{1}{n}\sum_{i=1}^{n}\left(x_i - \bar{x}\right)^2} \qquad \text{Eq.44}$$

Table 7 shows the relation of each FBP correlation method based on the standard deviation (σ) calculation. The results are ranked by ascending σ since a low value indicates that the data points are not spread out over a wider range of values. The best ranking is achieved by the Haimson and Fairhurst approach.

Table 7: Ranking summary for the Formation Breakdown Pressure prediction methods based on standard deviation

Rank	Std. Dev.	FBP Prediction Method
1	1090.61	Haimson and Fairhurst, 1967
2	1128.67	Ito and Hayashi, 1990
3	1516.86	Rummel 1, 1987
4	1668.26	Hubbert and Willis, 1957
5	1714.14	Rummel 2, 1987
6	1930.25	Rummel 3, 1987
7	2322.21	Kirsch, 1898
8	2861.51	Rummel 4, 1987
9	3613.12	Schmitt and Zoback, 1989
10	3689.15	Aadnoy and Belayneh 2, 2008
11	3691.65	Aadnoy and Belayneh 1, 2008

7.2.4 Mean Squared Error

The Mean Squared Error (MSE) of an estimator measures the average of the squares of the "errors", that is, the difference between the estimator and what is estimated. The difference occurs because of randomness or because the estimator does not account for information that could produce a more accurate estimate. The method is described in equation 45:

$$MSE = \sum_{i=1}^{n}\left(FBP_{measured,i} - FBP_{predicted,i}\right)^2 \qquad \text{Eq.45}$$

Table 8 demonstrates the accuracy of each FBP correlation method evaluated according to the mean squared error (MSE). Both Aadnoy and Belayneh methods are showing the lowest errors followed by the Kirsch and the Schmitt and Zoback model.

Table 8: Ranking summary for the Formation Breakdown Pressure prediction methods based on mean squared error

Rank	MSE	FBP Prediction Method
1	6.37E+06	Aadnoy and Belayneh 1, 2008
2	6.40E+06	Aadnoy and Belayneh 2, 2008
3	9.36E+06	Kirsch, 1898
4	9.82E+06	Schmitt and Zoback, 1989
5	1.49E+07	Ito and Hayashi, 1990
6	1.73E+07	Hubbert and Willis, 1957
7	1.76E+07	Rummel 2, 1987
8	1.94E+07	Rummel 1, 1987
9	2.03E+07	Rummel 3, 1987
10	2.76E+07	Haimson and Fairhurst, 1967
11	3.27E+07	Rummel 4, 1987

7.2.5 Mean Absolute Error

The Mean Absolute Error (MAE) is a quantity used to measure how close predictions are to the eventual outcomes. As the name suggests, the mean absolute error is an average of the absolute errors. MAE can be expressed as:

$$MAE = \frac{1}{n}\sum_{i=1}^{n}\left|FBP_{predicted,i} - FBP_{measured,i}\right| \qquad \text{Eq.46}$$

Table 9 shows the accuracy of each FBP correlation method using the mean absolute error (MAE) and each method is ranked by ascending MAE. The outcome is similar to mean squared error method with Aadnoy and Belayneh models leading the table indicating the lowest absolute error.

Table 9: Ranking summary for the Formation Breakdown Pressure prediction methods based on mean absolute error

Rank	MAE	FBP Prediction Method
1	889.59	Aadnoy and Belayneh 2, 2008
2	892.48	Aadnoy and Belayneh 1, 2008
3	1089.3	Schmitt and Zoback, 1989
4	1727.65	Kirsch, 1898
5	2039.52	Ito and Hayashi, 1990
6	2245.13	Hubbert and Willis, 1957
7	2711.31	Haimson and Fairhurst, 1967
8	2882.92	Rummel 2, 1987
9	2905.4	Rummel 1, 1987
10	2954.65	Rummel 3, 1987
11	3021.04	Rummel 4, 1987

7.2.6 Pearson Correlation Coefficient

Pearson correlation coefficient (R) expresses the strength of the linear relationship between two variables. R close to 1 indicates a strong positive relationship, a value of 0 indicates no linear relationship in the dataset and a value close to -1 signal a strong negative relationship between the two variables. Pearson correlation coefficient is mathematical described as follows:

$$R = \frac{\sum_i (x_i - \bar{x})(y_i - \bar{y})}{\sqrt{\sum_i (x_i - \bar{x})^2} \sqrt{\sum_i (y_i - \bar{y})^2}} \qquad \text{Eq.47}$$

Where x = measured FBP, $\bar{x}$ = mean measured FBP, y = predicted FBP, $\bar{y}$ = mean predicted FBP

Table 10 represents the outcome of the FBP correlation method using the Pearson correlation coefficient (R). R is ranked according to its positive relationship. As it can be seen, even the models with the highest ranks have only moderate positive correlation due to the outliers in the dataset.

Table 10: Ranking summary for the Formation Breakdown Pressure prediction methods based on Pearson correlation coefficient

Rank	R	FBP Prediction Method
1	0.8234	Rummel 3, 1987
2	0.8028	Aadnoy and Belayneh 1, 2008
3	0.8027	Aadnoy and Belayneh 2, 2008
4	0.7750	Rummel 4, 1987
5	0.7349	Rummel 2, 1987
6	0.7260	Kirsch, 1898
7	0.7196	Ito and Hayashi, 1990
8	0.6975	Rummel 1, 1987
9	0.6435	Schmitt and Zoback, 1989
10	0.6071	Haimson and Fairhurst, 1967
11	0.4816	Hubbert and Willis, 1957

7.3 Error Analysis Summary

The statistical measures were used to assess the accuracy of the Formation Breakdown Pressure prediction methods and indicate the model which promises the most reliable Formation Breakdown pressure prediction. To combine all statistical methods a final ranking is based on a "cumulative" rank of each individual method (using the data from Tables 5–10). The outcome of this ranking scheme is summarized in Table 11. The two models from Aadnoy and Belayneh scored best followed by the model described by Kirsch. Taking this final ranking into consideration it can be concluded that in case good and reliable geomechanical data is available, the most accurate and precise FBP prediction can be expected using one of the Aadnoy and Belayneh models, which represent the latest

improvement in the FBP prediction development. In case only limited data are available the Kirsch solution should be a valid alternative since it requires small amount of input parameters. However, although from the statistical evaluation methods models are indicated, the engineering judgment leaves doubt of the overall prediction data quality since none of the models allow for a more or less consistent result. All models demonstrate a fairly wide scatter with partially high error percentage from the actual data.

Table 11: Final ranking for the Formation Breakdown Pressure prediction methods

Rank	FBP Predicting Method	Success Ratio	MRE -S2	Std Dev	MSE	MAE	R	Cum. Score
1	Aadnoy and Belayneh 1, 2008	1	1	11	1	2	2	18
2	Aadnoy and Belayneh 2, 2008	1	2	10	2	1	3	19
3	Kirsch, 1898	3	6	7	3	4	6	29
4	Ito and Hayashi, 1990	4	8	2	5	5	7	31
5	Schmitt and Zoback, 1989	2	5	9	4	3	9	32
6	Rummel 2, 1987	5	3	5	7	8	5	33
7	Rummel 3, 1987	6	4	6	9	10	1	36
8	Rummel 1, 1987	7	7	3	8	9	8	42
9	Hubbert and Willis, 1957	6	10	4	6	6	11	43
10	Haimson and Fairhurst, 1967	8	11	1	10	7	10	47
11	Rummel 4, 1987	9	9	8	11	11	4	52

Reasons for the wide error range in the results are seen in:

- The structure of the models themselves
- The underlying calibration datasets
- The inaccuracy of calculated parameters such as bottomhole FBP from surface treatment pressure, etc.

7.4 Sensitivity Analysis

For understanding the data quality requirement and the main influencing factors when the best ranked models are used, a sensitivity analysis was made. With changing one single parameter while the rest of the variables were kept constant, it is possible to investigate the impact of this particular parameter for the result, which is in this case the Formation Breakdown Pressure (see Fig. 29).

Each input parameter of the models was investigated, namely:

- Minimum horizontal in-situ stress
- Maximum horizontal in-situ stress
- Pore pressure
- Poisson's ratio
- Young's modulus
- Coefficient of linear thermal expansion
- Bottomhole temperature during fracturing
- Virgin in-situ bottomhole temperature

The result confirmed that the minimum horizontal in-situ stress, the stress which has to overcome while fracturing, has the biggest influence for the FBP. On the plots also the combined effect of changing minimum horizontal in-situ stress ($S_{h,min}$) and with maximum horizontal in-situ stress ($S_{H,max}$) is shown since it should be investigated how a combined change will behave in comparison to the change of the single parameter. The combined value has the second biggest importance followed by the maximum horizontal in-situ stress, pore pressure and Poisson's ratio.

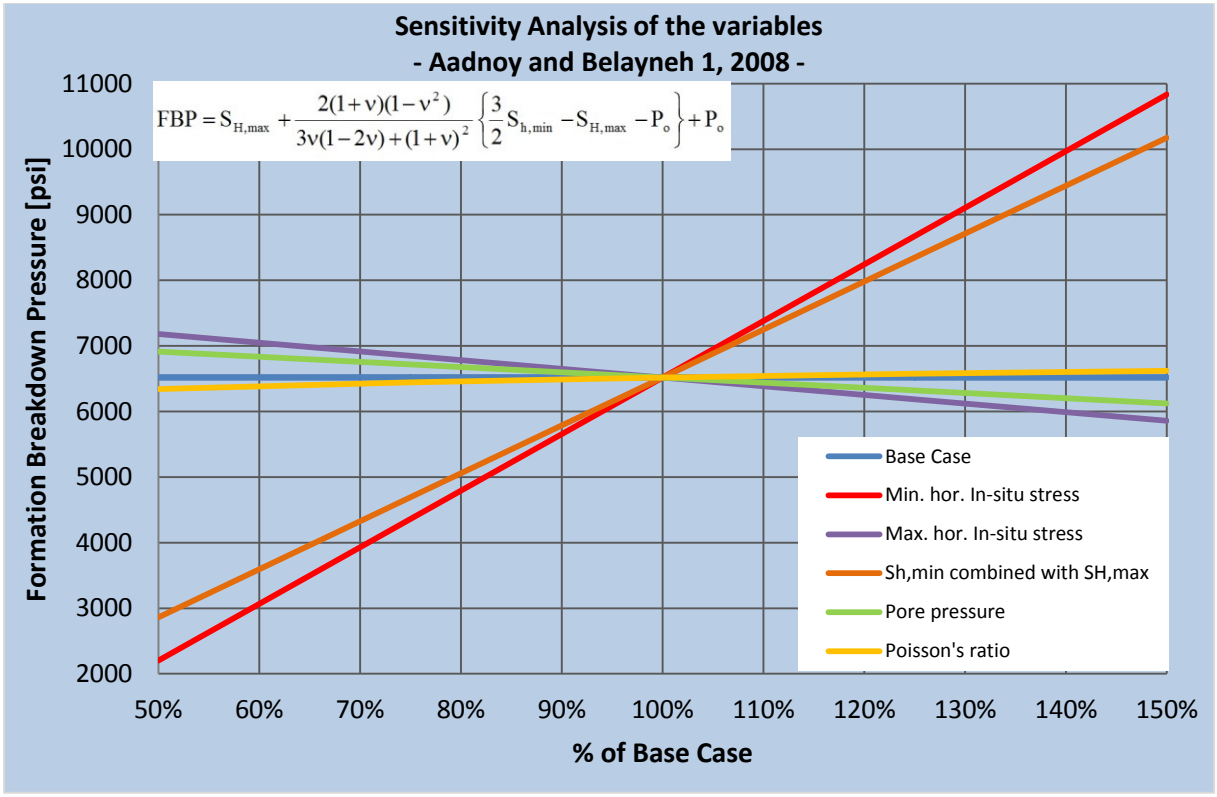

Figure 29: Sensitivity analysis of the variables (Aadnoy and Belayneh 1 method)

In case of Aadnoy and Belayneh 2 method the parameter which has biggest importance remains the minimum horizontal in-situ stress followed by the combination of $S_{h,min}$ and $S_{H,max}$, and the maximum horizontal in-situ stress (Fig. 30). Interesting was that a notable change in FBP prediction was caused by the virgin in-situ bottomhole temperature and bottomhole temperature during fracturing, demonstrating that temperature impacts the model significantly. Pore pressure and Poisson's ratio have moderate impact, while Young's modulus and the coefficient of linear thermal expansion have limited effect for the FBP prediction.

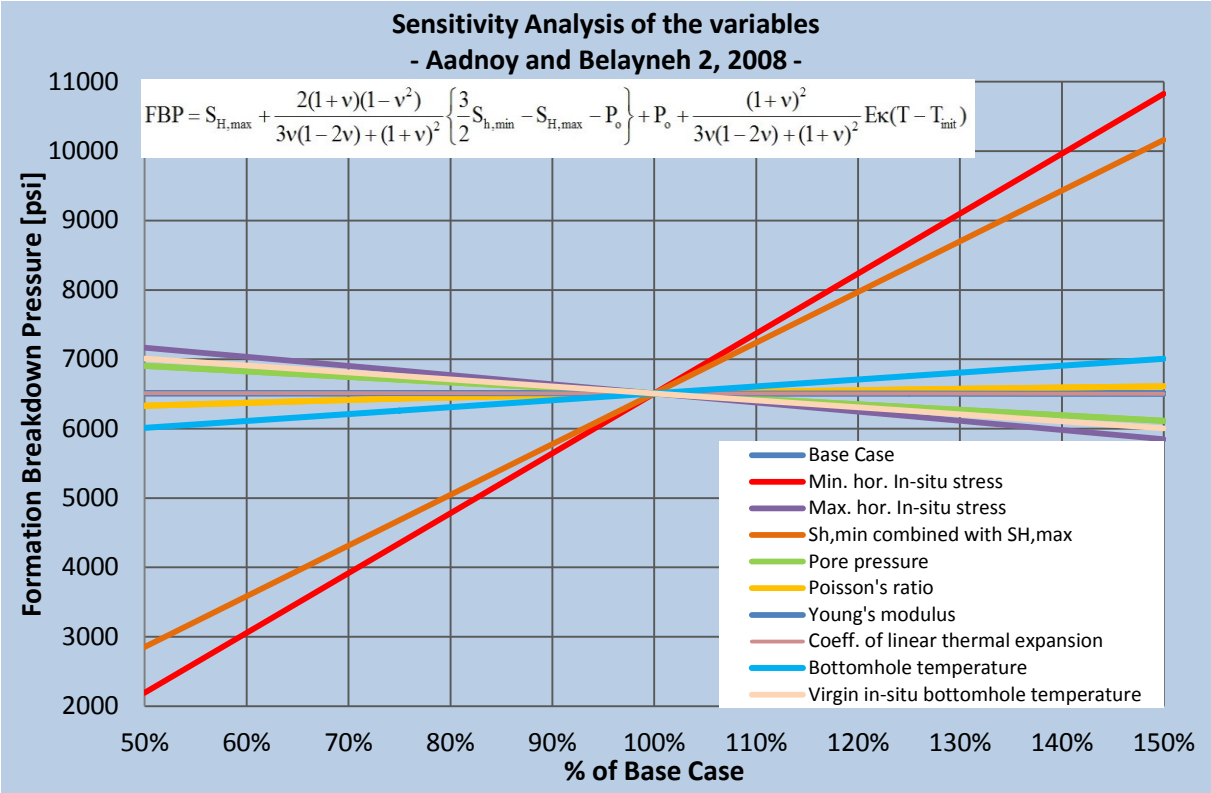

Figure 30: Sensitivity analysis of the variables (Aadnoy and Belayneh 2 method)

7.5 Best Model in Various Environments

Since the study and the statistical error analysis revealed uncertainties that the FBP models are not suitable for all formations and areas, since they were developed from studies of specific fields, it was investigated if applying the models to clustered data sets increases the accuracy and precision of the FBP prediction. Engineering judgment was used to cluster the data into the following groups:

- well location: onshore vs. offshore
- well type: vertical vs. horizontal
- depth: “shallow” vs. “medium deep” vs. “deep”
- faulting environment: normal vs. normal/strike-slip vs. strike-slip
- formation type: sandstone vs. shale vs. carbonate
- fields: different areas and presumed similar formation type

Table 12 and 13 shows a short summary about the well location and type (plots can be found in Appendix H).

Table 12: Well location clusters

Well location	# of treatments
Onshore	89
Offshore	38

Table 13: Well type clusters

Well type	# of treatments
Vertical	46
Deviated	81

The treatments were carried out in different depths. In order to compare the treatments which were at similar depths and have similar FBPs were clustered into the three depth groups: “shallow”, “medium deep” and “deep” (see Fig. 31).

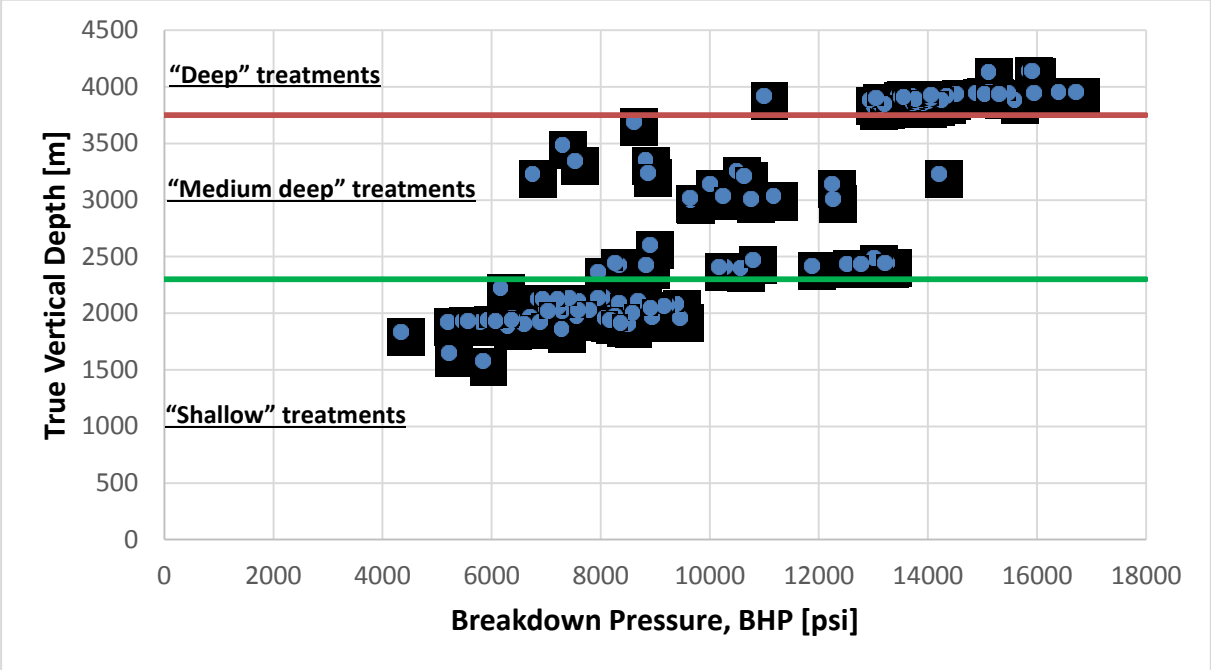

Figure 31: Depth clustering of the data

The following table shows the result of depth clustering of the treatments:

Table 14: Depth clustering of the treatments

Depth group	“Shallow” depth treatments (1500-2300 m TVD)	“Medium deep” treatments (2300-3750 m TVD)	“Deep” treatments (3750-4200 m TVD)
# of treatments	51	33	43

Table 15 gives an overview of the data distribution of the different faulting environments. In order to compare the fracturing jobs which were at the same faulting environment, the treatments were clustered. Since not all types of faulting were present in the used data the clustering was limited to normal faulting, normal/strike-slip intermediate faulting and strike-slip faulting.

Table 15: Faulting environment clustering of the treatments

Faulting environment group	Normal faulting	Normal/strike-slip intermediate faulting	Strike-slip faulting
# of treatments	83	13	31

Three formation types could be identified, namely sandstone, shale and carbonate among the treatments. Their frequency can be seen in Table 16:

Table 16: Formation type clustering of the treatments

Formation type group	Sandstone	Shale	Carbonate
# of treatments	78	42	7

Using the acceptable envelope as it was described in chapter 7.2 the measured and calculated FBP values were cross plotted and a success rate calculated. As success all points which fall into the acceptable region were counted. The results in detail can be seen in:

- in Appendix I for the different well locations
- in Appendix J for the different well types
- in Appendix K for the different depths
- in Appendix L for the different faulting environments
- in Appendix M for the different formation types
- in Appendix N for the different fields

Table 17 summarizes the results for all the investigated environments showing the preferred FBP prediction methods (preferred in terms of accuracy and input data requirements), their success rate and the number of treatments. As one can see, Aadnoy and Belayneh 1 method is the preferred method six times out of thirteen cases.

Table 17: Preferred Formation Breakdown Pressure prediction methods for the investigated environments

Preferred FBP prediction method	Investigated environment	Success rate	# of treatments
Aadnoy and Belayneh 1, 2008	Carbonate	100%	7
	Shale	98%	42
	“Deep” well	95%	43
	Normal faulting	85%	83
	Deviated well	84%	82
	Onshore well	74%	90
Kirsch, 1898	Strike-slip faulting	77%	31
	“Medium deep” well	69%	33
	Sandstone	65%	78
Ito and Hayashi, 1990	Offshore well	76%	38
	“Shallow” well	67%	51
Rummel 2, 1987	Vertical well	70%	46
	Strike-slip/normal faulting	68%	13

Table 18 summarizes the results of the analysis for the major fields showing the most accurate FBP prediction methods, their success rate and the number of treatments. When more preferred models are shown it means that their performance was the same.

Table 18: Formation Breakdown Pressure prediction methods for the different major fields which were investigated

Field name	Preferred FBP prediction method	Success rate	# of treatments
Field A	Kirsch; Rummel 2	80 %	4
Field B	Rummel 2	100 %	5
Field C	Aadnoy and Belayneh 1-2; Kirsch; Ito and Hayashi; Schmitt and Zoback; Rummel 2	100 %	5
Field D	Rummel 3, 1987	85 %	13
Field E	Schmitt and Zoback; Rummel 2	83 %	12
Field F	Rummel 1-4, 1987	68 %	19
Field G	Aadnoy and Belayneh 1-2; Kirsch; Ito and Hayashi	100 %	23
Field H	Aadnoy and Belayneh 1-2	98 %	42

8. Formation Breakdown Pressure Influencing Factors Mind Map

In order to see the complexity of the Formation Breakdown Pressure prediction due to the various parameters which affect the result, a mind map was created (see Fig. 32). This tool enables not only to represent the different variables but also to visualize there connectivity. Two big groups were identified, namely geomechanical parameters and design parameters.

The geomechanical parameters are the independent ones, which are given by nature. For the sake of simplicity, the parameters considered when in situ conditions are present in the formation. If the effect of production would be included, then one would experience that depletion changes the pore pressure, (effective) permeability, principal stresses, closure and fracture pressure with time and additional relations (arrows) would be needed on Fig. 32.

The other big group of parameters is the so called design parameters. These are dependent on the earlier mentioned geomechanical parameters. The variables were further grouped into hydraulics, completion and perforation groups.

There is one additional factor which cannot be clearly characterized by none of the above mentioned two big groups of parameters simply because it is a link between them. This is the phenomenon of stress cage effect. Drilling alters the stress field of the surrounding rock around the wellbore and this case a higher breakdown pressure. Usually this problem is overcome by the perforations which should be long enough to pass through this zone. However, perforations also create an altered stress zone.

Obviously, none of the existing Formation Breakdown Pressure prediction methods which were found in the literature include all these parameters. The most complex one (Aadnoy and Belayneh 2) incorporate 11 parameters. On the other hand, Neural Network software is capable of dealing with as many features (inputs which can be numerical value as well as categorical) as the operator determined. This is one of the huge advantages of such a solution and also one of the reasons why it was believed that this method can lead to a more accurate result.

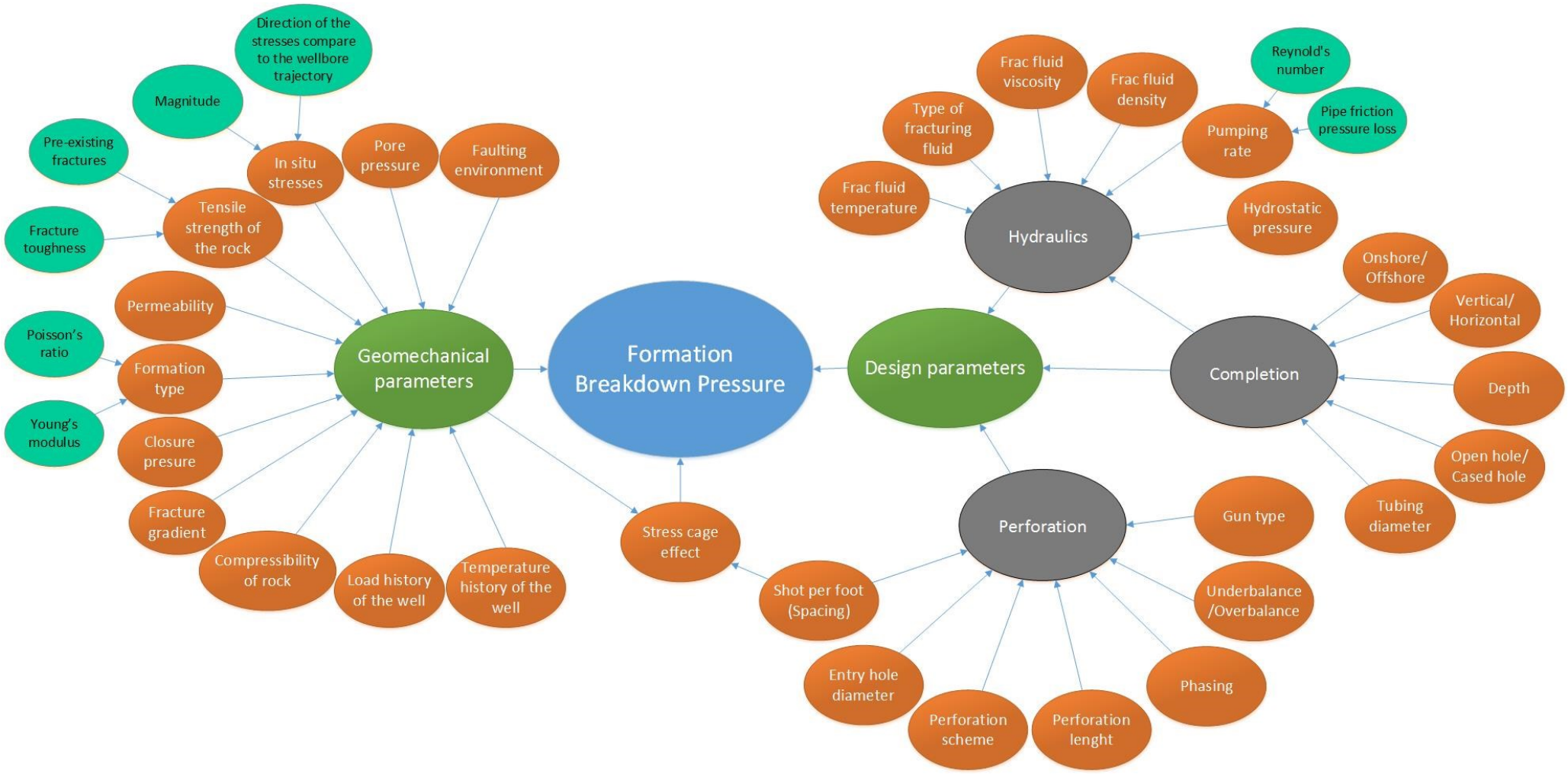

Figure 32: Various influencing factor in the Formation Breakdown Pressure prediction

9. Innovative Approach to Determine Formation Breakdown Pressure

Since the results obtained from the various Formation Breakdown Pressure prediction models were not satisfactory, an alternative method was looked for. Using Artificial Neural Network software, cVision, was a method seen with high potential to provide FBP predictions with improved accuracy and precision.

Artificial Neural Networks (ANNs) are used more frequently over the recent years since the number and fields of application for such software is infinite (i.e. it is used in medical diagnosis, chemistry, image recognition like automatic handwriting or fingerprint recognition, financial applications, speech recognition, e-mail spam filtering). In the last decade, usage of Artificial Neural Networks in the oil and gas industry is emerging as well, applications are reported for many different areas such as reservoir production optimization (Mats, 2009), interpretation of well inflow performance (Muhammad, 2003) and permanent downhole gauge data analyses (Olubusola, 2002).

The working principle of ANNs is inspired by the way biological nervous systems process information. It is an advanced solution for pattern recognition, to create and memorize relationships in data, to store and manage know-how and to support making decisions and predictions. The most important feature is that the software has a capability of learning from a dataset (Data Science and Machine Learning Essentials – Arizona State University).

9.1 Artificial Neural Networks

Artificial Neural Networks resemble the brain in two respects:

- Knowledge is acquired by the network from the data through a learning process.
- Interneuron connection strengths, known as synaptic weights, are used to store the acquired knowledge.

In the human brain a large number of interconnected processing elements (so called neurons) work together to solve a problem. Same as humans, ANNs learn by example and the procedure that is used to perform the learning process is called learning algorithm. The learning algorithm adjusts the synaptic weights of the network to create a required design objective which is in this case an accurately predicted Formation Breakdown Pressure.

ANNs offer a different approach to problem solving than conventional approaches, like predicting FBP's using models. A conventional approach can be applied and will result in accurate and more or less precise predictions, when the algorithm is known and a set of instructions are followed to solve the problem. In this conventional approach it is necessary to understand the problem completely and clarify the steps which have to be followed. These requirements restrict conventional approaches to problems that are already understood and

for which enough and precise data are available allowing correlations to describe and solve them.

A basic requirement of any data analysis is to study relationships between variables. When the relationship among variables is complex and nonlinear, ANNs are a perfect alternative technique to have this analysis executed by the software and to solve the problem. Functional relationships between input variables and dependent variables are usually not known prior to the analysis. The network learns from examples and adjusts itself to generalize the underlying relationship among variables (Learning from Data, Machine Learning Course – California Institute of Technology).

9.1.1 Artificial Neuron

An Artificial Neuron Network model consists of neurons, similar to the nerve cells in the human brain and the connections between these neurons can be considered as synapses between two neurons.

The IT software functions like a biological neuron, first, it receives inputs from other sources, then processes these inputs and finally outputs the result. While the biological neuron is significantly more complicated than this structure, the artificial neuron is designed based on this basic structure of the biological neuron and simulate its basic functions. Figure 33 shows the structure of an artificial neuron. The inputs represented by $\mathbf{x_n}$ symbol multiplied by corresponding connection weight $\mathbf{w_n}$. Then a transfer function applied to the sum of the products to generate a result as output.

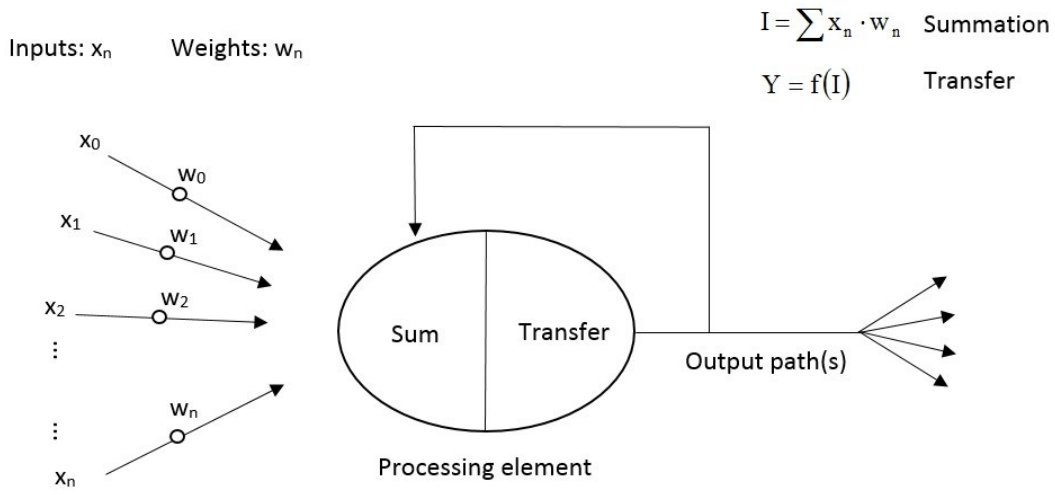

Figure 33: Basic Artificial Neuron (Artificial Neural Networks Technology Course – University of Toronto)

Data processing takes place in the neuron. In case of this study the input neurons were various parameters about the treatments, the environment and the well itself while the output neuron was the Formation Breakdown Pressure representing the response based on the input variables.

9.1.2 Artificial Neural Network Architecture

In Artificial Neural Networks the interconnected neurons organized in layers, namely:

- An input layer representing the raw information for the network.
- Hidden layer(s) to transfer the inputs into something that can be used by the output layer
- An output layer, meaning the result

cVision is a feedforward ANN software, which means the information only moves in forward direction. Figure 34 illustrates a simple feedforward neural network with one hidden layer and shows how information moves from input layer to the hidden layer and then from the hidden layer to the output.

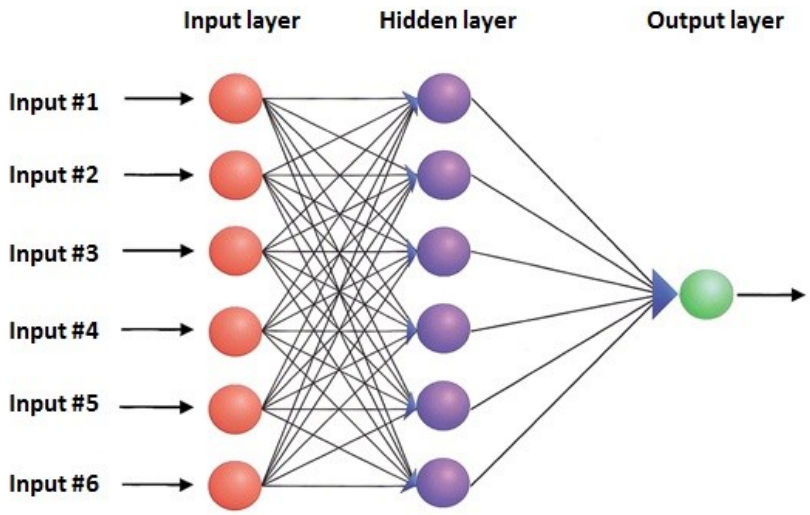

Figure 34: Feedforward neural network with one hidden layer

cVision is capable of using the so called Improved Completely Connected Perceptron (iCCP) architecture which is based on the CCP concept. The Completely Connected Perceptron (CCP) has the advantage, that a network growing process is straight forward since it is not necessary to find an optimal choice for the number of hidden layers. CCP's have an input layer, one single input block consisting of an arbitrary number of hidden neurons and an output layer. The Improved Completely Connected Perceptron (iCCP) has additional input - output shortcut connections, drawn in orange in the right picture below.

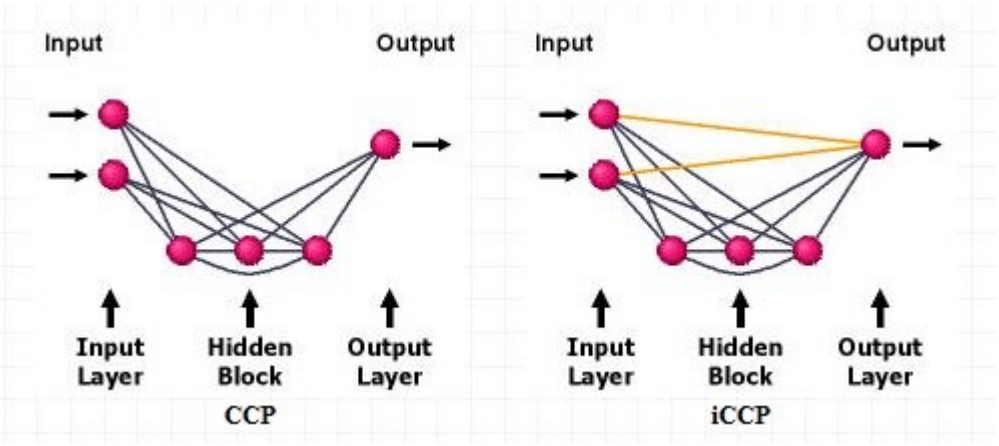

Figure 35: Completely Connected Perceptron (CCP) and Improved Completely Connected Perceptron (iCCP) architecture (cVision Manual)

Figure 35 sketches the structure of a CCP and an iCCP with 2 input neurons, 3 hidden neurons and 1 output neuron.

9.1.3 The Learning Process

The knowledge of a neural network is represented by the values of the connection weights between the neurons. The learning process is the determination of these values. The goal is to adjust the weights of the units (synaptic weights) in a way that the error between the output of the network and the desired output is reduced. The algorithm increase or decrease the weights of the units slightly and then recalculate the error to see how it changes. In order to do so, the sum of squared error, the squared difference between actual and desired network output, is minimized as shown in the equation below:

$$\mathrm{EEF} = \frac{1}{2\sum_{k=1}^{n} |y_k - d_k|^2} \qquad \text{Eq.48}$$

where EEF is the so called Euclidean Error Function, y is the actual and d is the desired data

The objective of the learning process is to find the connection weight which minimizes the objective function **E**. In Artificial Neural Networks, this is always done with iterative algorithms (see Fig. 36).

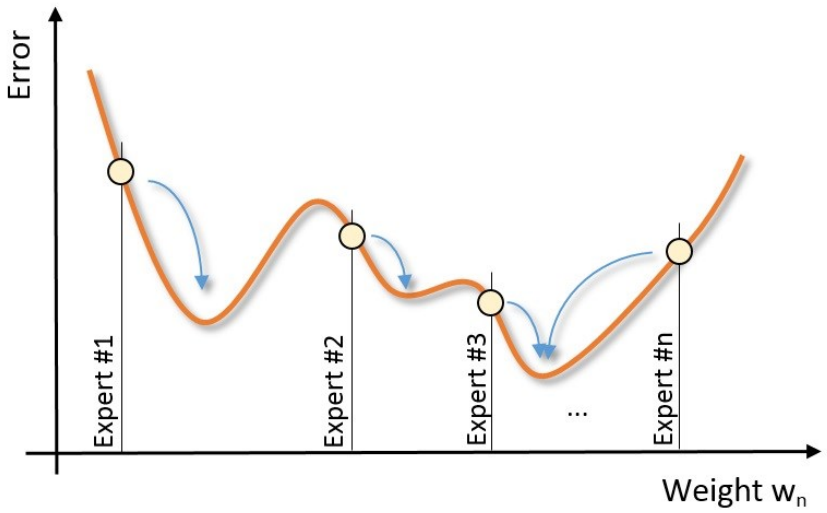

Figure 36: Finding the local minimum error by changing the weight of the connections between the neurons (cVision Manual)

cVision applies supervised learning process to produce an inferred function from the input data. The weight matrix is adjusted during the learning process and this will enable the network predicting the correct output for unseen input data.

9.1.4 Network Quality Control

To check the validity of the prediction a quality control procedure was used to help ensure that there is minimal error in the design and training process. Data is used which the network had not previously been seen. By default setting cVision uses 20 % of the database for testing purposes (60 % of data is used for learning and 20 % for validation). The error calculated using that test data is a measure for the quality of the created model.

9.2 Used Input and Output Variables

cVision can handle numerical as well as categorical data (text) for both, model input and model output. It is useful since all the available information including the categorical ones, such as the well, environment and the treatment itself can be included and not only the measured/calculated parameters.

For this FBP prediction study, 21 input features were used in the network in order to include as many influencing parameters as possible.

To find out which variables have any linear correlation with the Formation Breakdown Pressure a scatter plot about the investigated parameter versus the FBP was used.

Figure 37 shows minimum, maximum horizontal and vertical stress plotted against FBP. As it can be seen, the plot reveals a direct relationship meaning that with increasing $S_{h,min}$. $S_{H,max}$, S_v value the FBP increases consequently.

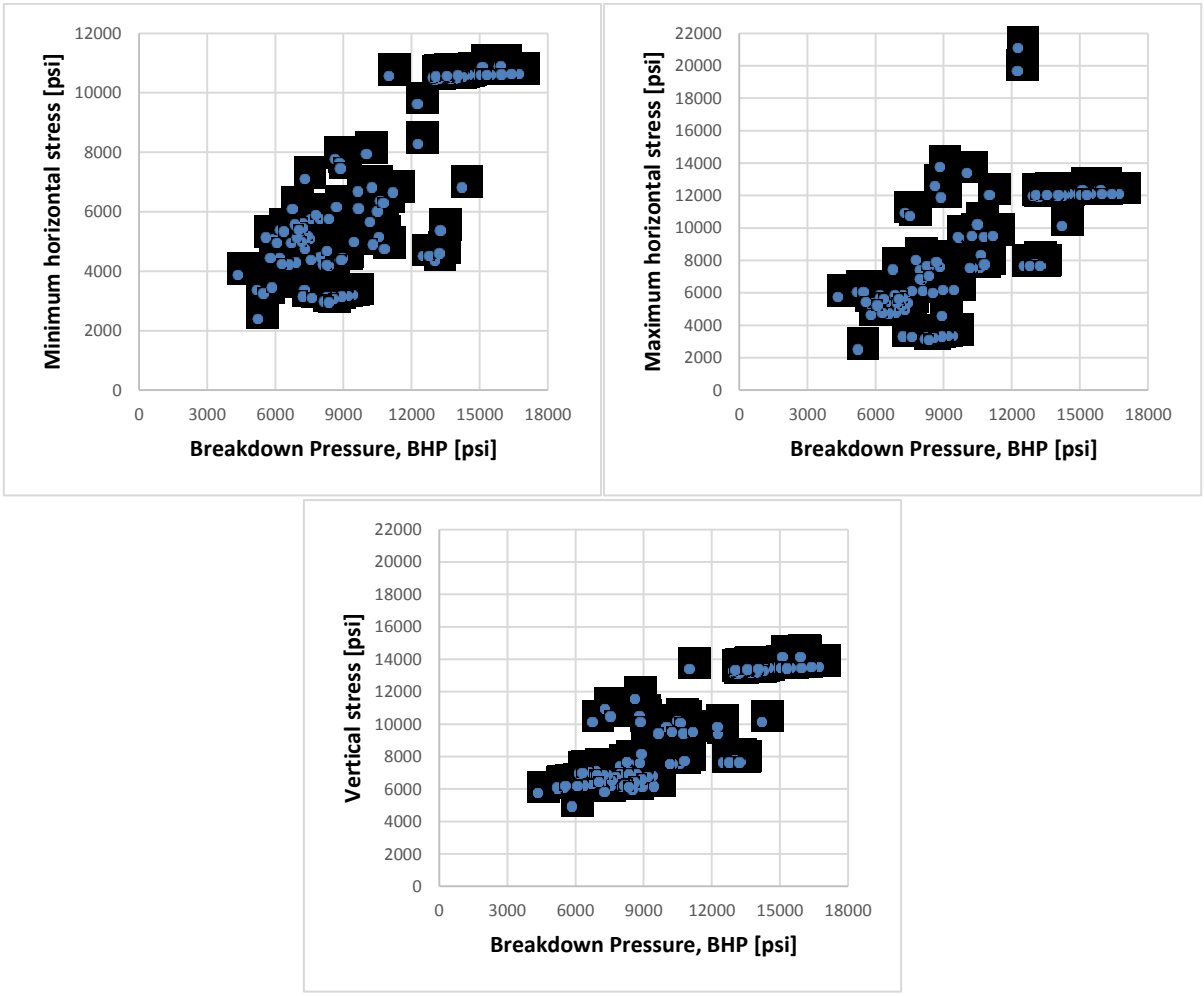

Figure 37: Minimum, maximum horizontal and vertical in-situ stress against Formation Breakdown Pressure

Figure 38 presents true vertical depth, measured depth and closure pressure versus the FBP. The closure pressure is the minimum pressure which needs to be overcome to keep the fracture open.

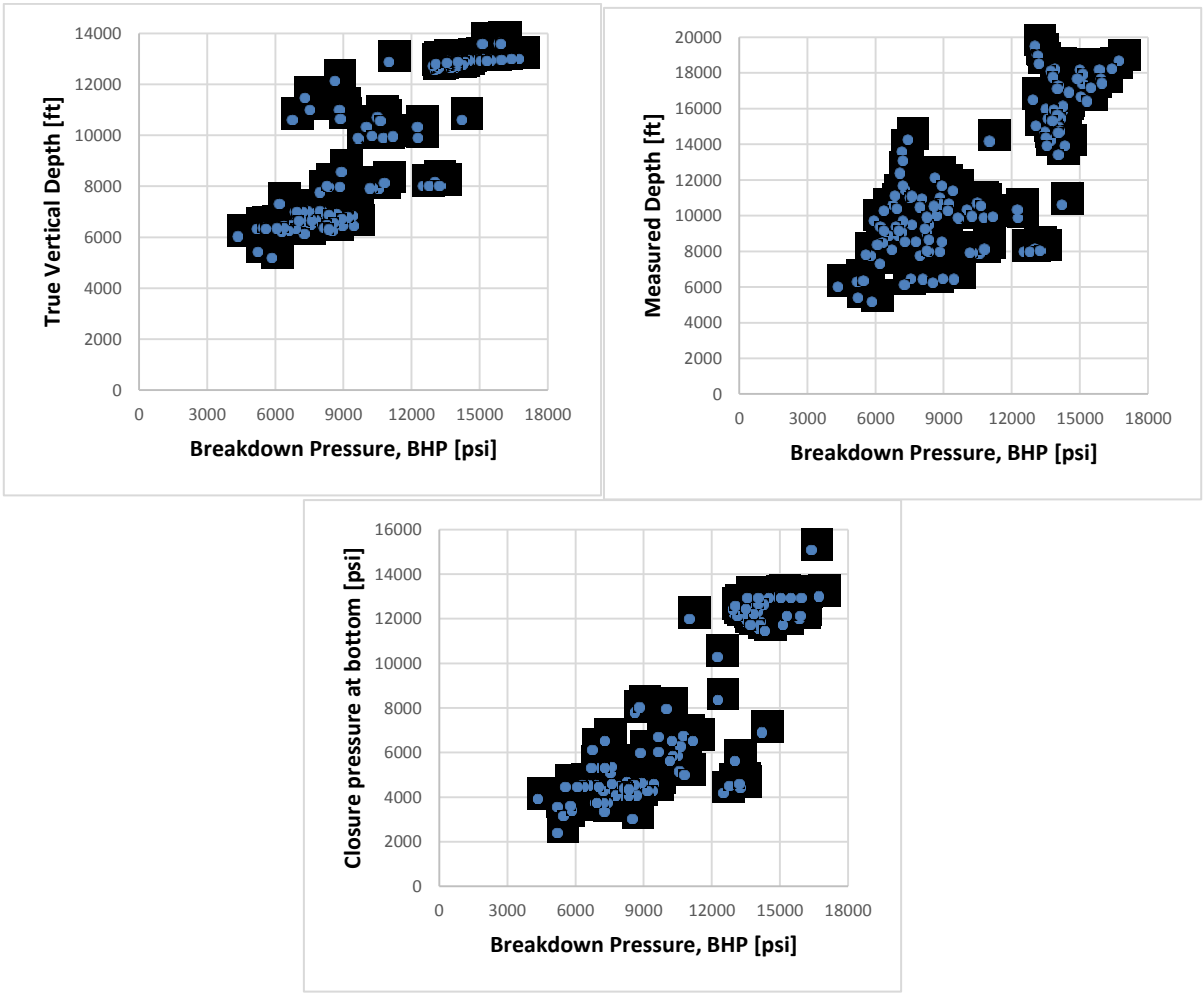

Figure 38: True Vertical Depth, Measured Depth and closure pressure against Formation Breakdown Pressure

As one can see, Formation Breakdown Pressure increases in the investigated data sets with depth. A positive correlation is revealed with investigating the closure pressure versus the FBP too.

On the other hand, in case of many input parameters it is not straightforward to reveal linear correlations. Artificial Neural Networks nevertheless are capable of dealing with such variables using weight functions between these features.

9.3 Results

9.3.1 Formation Breakdown Pressure Predicted by Artificial Neural Networks

First, to evaluate the accuracy and precision of the Formation Breakdown Pressure predicted by the Artificial Neural Networks the same visualization method which was introduced in Chapter 7.1 was used. Figure 39 shows all the predicted Formation Breakdown Pressure points of the 127 data sets. With exception of a few points the correlation is robust. Only four values fall outside the range defined as acceptable in Chapter 7.1 and represented by the black dashed lines. Most of the calculated values follow the red line which represents the

perfect correlation between the predicted and the measured values. Since the FBP predictions were close to the observed data, a different evaluation criterion was applied. As it can be seen in Fig. 39 the new criteria can be described with 10 % error from the actual value marked by the dark grey lines.

Out of the 127 data sets only 12 predicted data fall outside of the newly defined observation range which calculates to a success-rate of about 90 %. Taking into consideration that the over prediction of the FBP is less important for the original scope of the thesis the success-rate improves to 96 %. Furthermore it was observed that R, the Pearson Correlation Coefficient for this dataset equals 0.9685 which proves the strong correlation of the results.

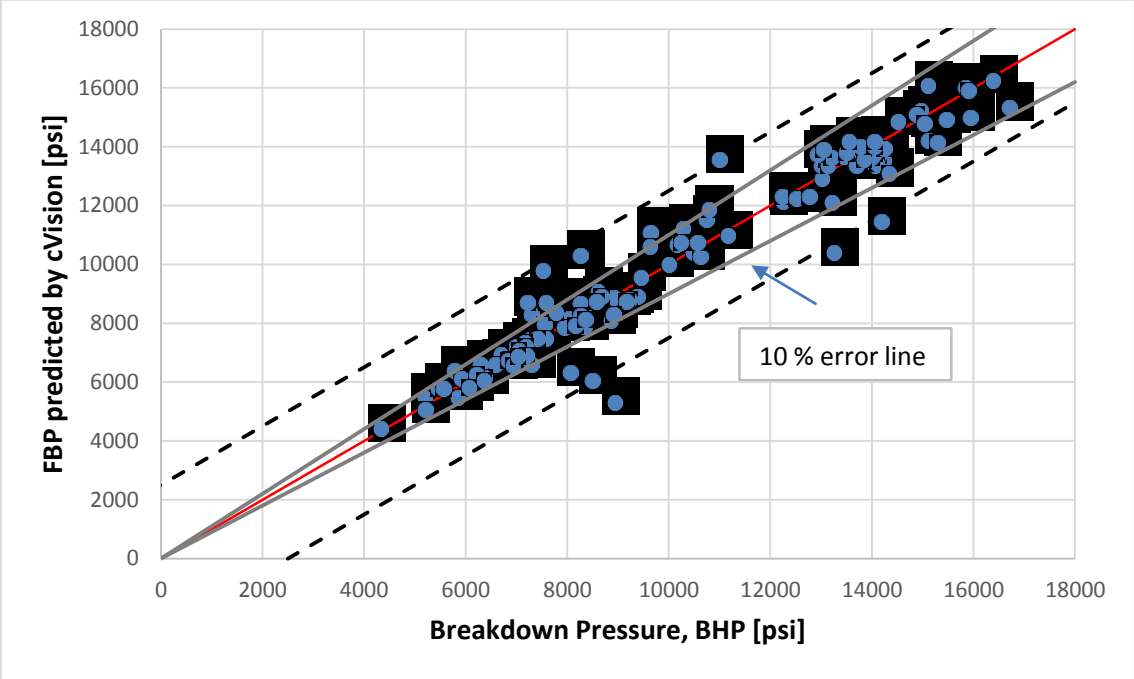

Figure 39: Comparison of the predicted Formation Breakdown Pressure using Artificial Neural Networks to the measured pressure

Second, an additional quality check of the trained Artificial Neural Network was carried out. 14 additional data sets of treatments from three different fields, four from Field F, nine from Field G and one from Field H, which had not been used during training of the ANN, were processed and the expected FBP predicted.

Figure 40 shows the results of the predicted FBP. As in Fig. 39 the red line represents a perfect correlation of the observed and measured FBPs and the dashed and dark grey lines indicate the old and new observation criteria. The ANN prediction performance for the new datasets was in general worse than the one for the data sets also used for training purposes but it still provided a 78 % success. In particular, considering that a slight over prediction is providing less risk to the operation a 100 % success-rate is given, since none of the predicted FBPs is falling below the lower limit of the ±10 % observation range. The calculated Pearson Correlation Coefficient, R, equals 0.9727, which demonstrates again the

strong positive correlation of the calculated values. The results of these tests were evaluated as confirmation of the validity of the correlation found by the ANN.

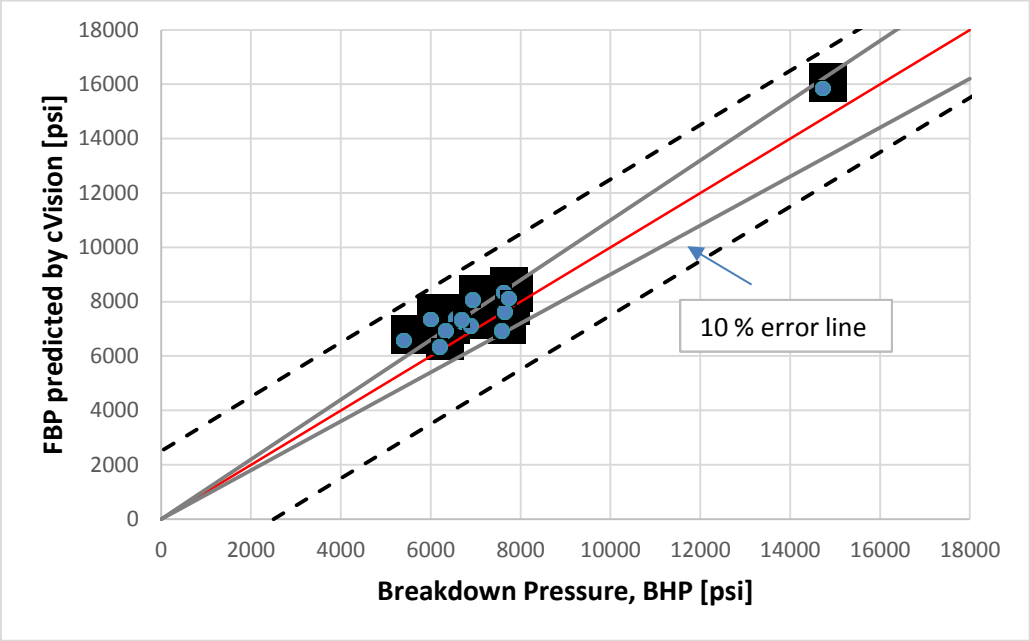

Figure 40: Comparison of the predicted Formation Breakdown Pressure using Neural Networks to the measured pressure for the 14 test treatments

The tabulated measured and the predicted pressure values for the test treatments can be found in Appendix O.

Third, the results for the FBM prediction of the 14 data sets obtained with ANN were compared to the two conventional Formation Breakdown Pressure prediction models which scored best in the error analysis.

Figure 41 shows the absolute error of the predicted and the measured FBP pressure values. For plotting purposes the treatments were sorted with increasing ANN errors. The absolute errors of Aadnoy and Belayneh 1 and Kirsch method for the corresponding treatment were overlaid. The plot demonstrates that the Artificial Neural Networks gave more accurate prediction in most of the cases.

In case of treatment 13 both Aadnoy and Belayneh 1 and Kirsch method resulted in a very high absolute error. This phenomena was not in detail investigated and therefore the actual cause for these errors not understood, but taking this into consideration it can be concluded that the ANN software, if calibrated can also mitigate such high discrepancies and add to confidence to the simulated FBPs.

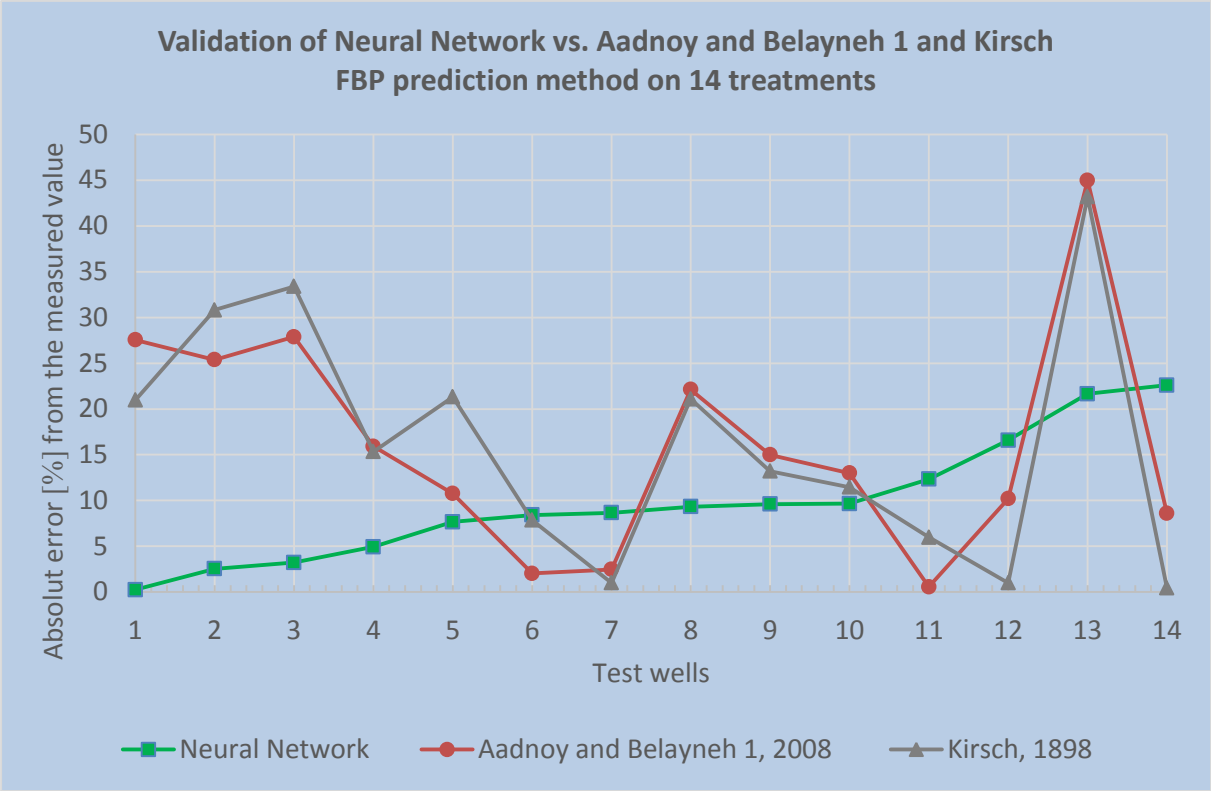

Figure 41: Validation of Neural Network vs. Aadnoy and Belayneh 1 and Kirsch FBP prediction method on 14 treatments using the absolute error [%] from the measured value

Table 19 summarizes the statistical analysis of the absolute errors given by the three methods for the test treatments. The mean of the absolute errors calculated for the Artificial Neural Network is less than 10 % and for the conventional models is more than 16 %. The standard deviation of the ANN is half in magnitude compared to the conventional models demonstrating that the ANN results in less scatter in the error values. While the minimum absolute error values were similar for all three methods the maximum absolute error was in case of Aadnoy and Belayneh 1 and Kirsch method somewhat double than for the ANN.

Table 19: Descriptive statistics of the absolute errors [%] from the measured value of Neural Network and the Aadnoy and Belayneh 1 FBP prediction method

	Neural Network	Aadnoy and Belayneh 1, 2008	Kirsch, 1898
Mean	9.81	16.17	16.21
Standard Dev.	6.65	12.34	13.08
Minimum	0.24	0.57	0.43
Maximum	22.59	44.97	43.17
Count	14	14	14

Summarizing the results, with using ANN software -if a big enough database with trustworthy data is available for training purposes- acceptable FBP prediction can be expected even if some of the input parameters are classified with a low confidence rating.

9.3.2 Determination of Key Influencers

The Artificial Neural Network outcomes include also the determination of key influencers for its calculation and ranking these features based on their importance.

Figure 42 summarizes this capability. It shows the error which certain parameters can cause and orders them according to their importance. In the specific case of FBP the codes represent the following: p2=Max. horizontal in-situ stress, p15=Effective min. horizontal stress, p12=Faulting environment type, p10=True Vertical Depth, p3=Vertical stress, p14=Max. circumferential stress around the wellbore, p13=Min. circumferential stress around the wellbore, p1=Min. horizontal in-situ stress, p11=Measured Depth, p17=On/Offshore location, p16=Well type (vertical/deviated), p8=Closure pressure at bottom, p4=Pore pressure, p21=Scaling factor for temperature, p9=Tensile strength of the rock, p5=Poisson's ratio, p18=Borehole diameter

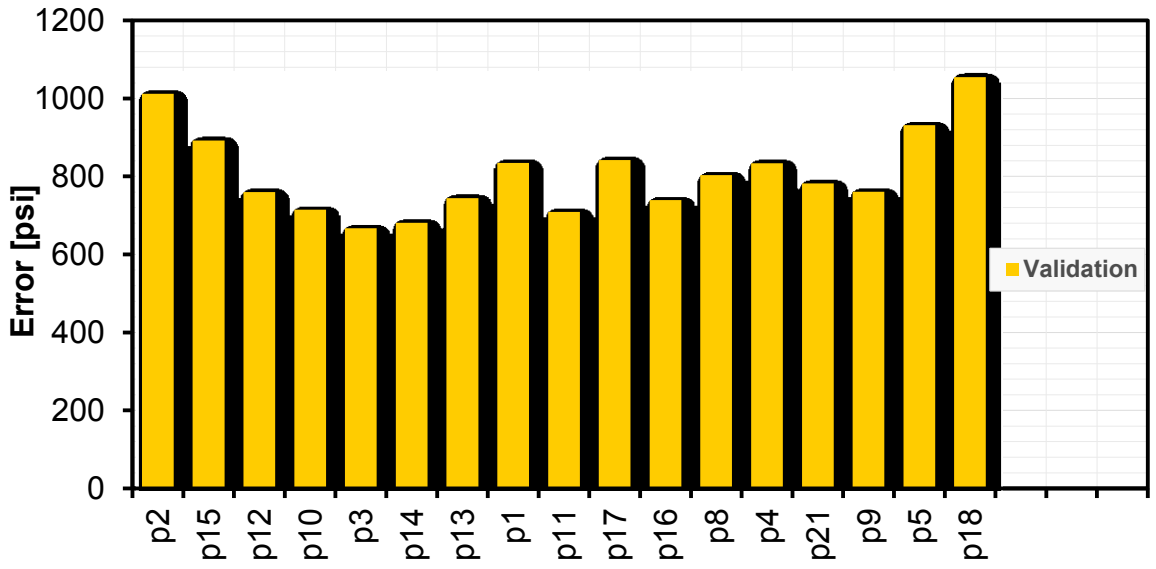

Figure 42: Ranking of the key influencer parameters

The first ranked parameters which have descending column heights (errors) are the most influencing ones and any effort should be focused on those parameters to obtain as accurate data as possible since the quality of these data will influence the Artificial Neural Network results positively.

As already expected but not really proven by the conventional models the five most important parameters are the three principal stresses, pore pressure (NB: effective minimum horizontal stress can be calculated by subtracting the pore pressure from the stress value, since pore pressure reduces the effective stress) and the knowledge about the faulting environment (which can be described by the information of the principal stress magnitudes).

When the column height starts to ascend this means that focusing on those parameters leads to reduced accuracy.

10. Comparison of the Results of the Best Formation Breakdown Pressure Prediction Model and Artificial Neural Network Pressure Prediction

This chapter compares the predicted pressures of all datasets calculated with the best ranked Formation Breakdown Pressure prediction model from Aadnoy and Belahney to the results obtained by the Artificial Neural Network software (ANN). Figure 43 presents the predicted pressures on cross plots for the identical 127 treatments. The correlation of the model is pure and shows high differences to the actual measured data, while the ANN software provides consistent and robust data in most cases within a 10 % error range from the actual measured value.

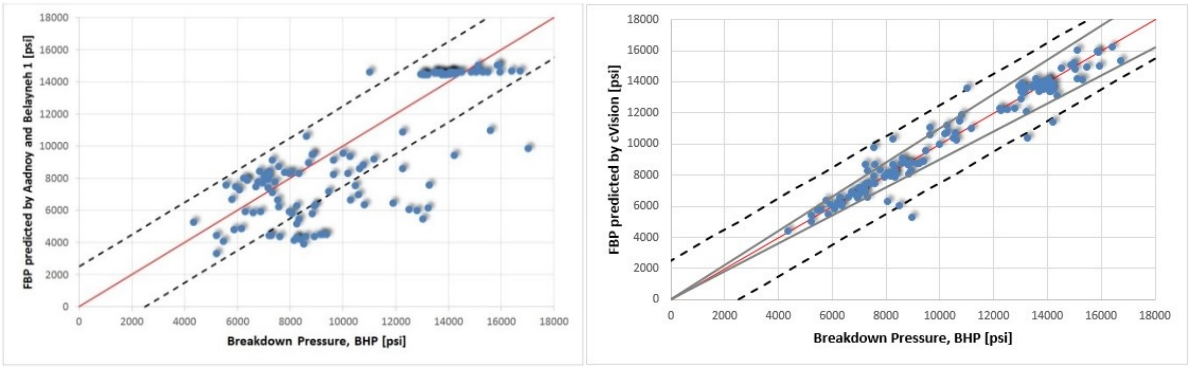

Figure 43: Comparison of the calculated Formation Breakdown Pressure and the measured values by Aadnoy and Belayneh 1 method and Artificial Neural Network

The histograms of the result distribution as demonstrated in Fig. 44 and 45 mirror the findings of the cross plots and show that in case of the Aadnoy and Belayneh 1 model (Fig. 44), predicted pressures in the range of 6000–10000 psi, where the majority of the data is located, can be considered acceptable, while below 6000 psi and above 10000 psi this model carries significant errors and that in case of the Artificial Neural Network software the predicted pressures are acceptable throughout the entire observed pressure range.

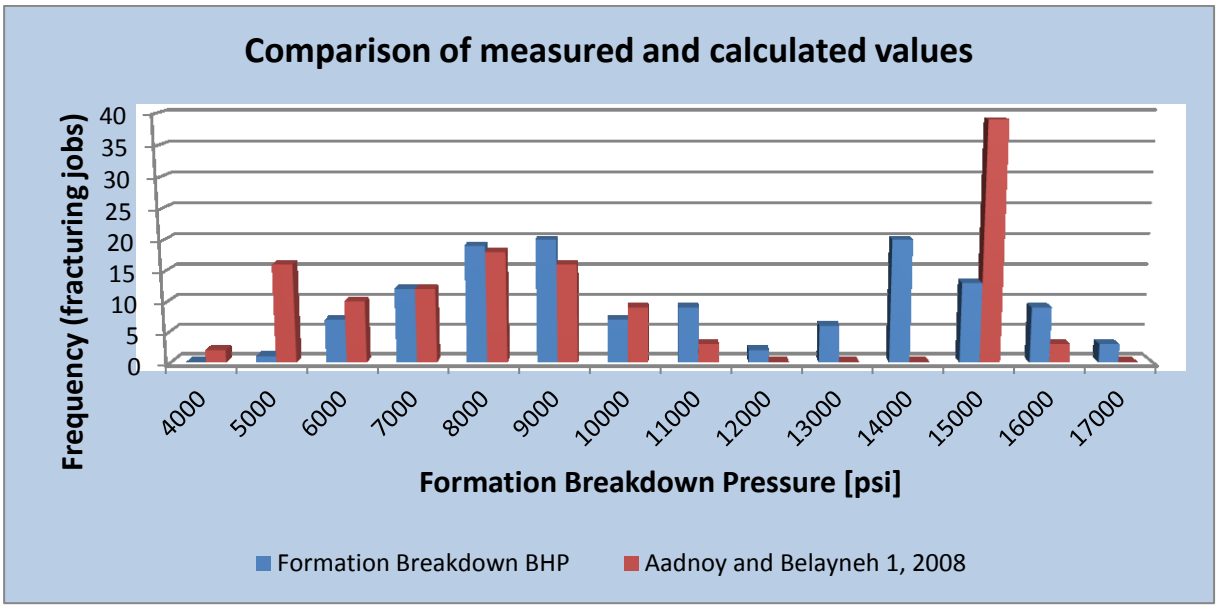

Figure 44: Comparison of measured and calculated Formation Breakdown Pressure values on histogram

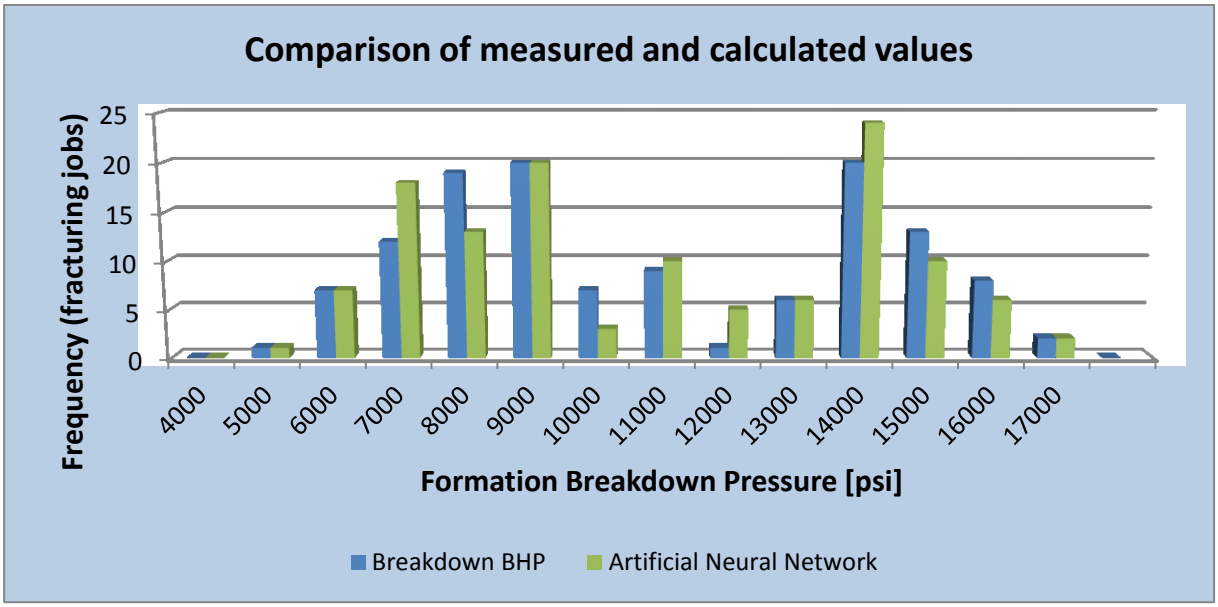

Figure 45: Comparison of measured and calculated Formation Breakdown Pressure values on histogram

The ANN prediction accuracy of ±10 % of the actual reading was checked with 14 data sets which were not used in the learning and verification of the ANN software iterations. Comparing the FBP predictions to the actual measured FBPs the ± 10 % error was confirmed.

All in all, the usage of Artificial Neural Networks is the best approach among the investigated methods. If more high quality data is used for the training of the network, the prediction accuracy can be further improved.

11. Economic Impact of Formation Breakdown Pressure Prediction

Knowing an accurate Formation Breakdown Pressure impacts the economic spend of any well completion by the possibility to optimize material selection for tubing, rating of packers, completion components and surface installations. Fit for purpose completion design based on trustfully FBP predictions with a narrow error range might yield in requirement of less expensive material however fulfilling the required design factors by API or company standards (Fig. 46). Furthermore, the narrow error range on the expected maximum pressures during well interventions will ensure that HSSE risks related to the completion and well construction design are minimized. Although these costs are not easily tangible, any HSSE issue related to under dimensioned completion design, because of an erroneous base data, can impact the economics dramatically. In the worst case, either part of the completion needs to be replaced, the planned well intervention can't be executed or the well architecture needs to be changed. In any case on one side additional completion cost, such as but not limited to, rig time, equipment replacement, rental and/or addition, treatment materials change, contingency interventions, etc. and on the other side cost for lost production will be accumulated. Obviously these costs can culminate to a value difficult to estimate, particularly if an environmental accident or safety incident occurs.

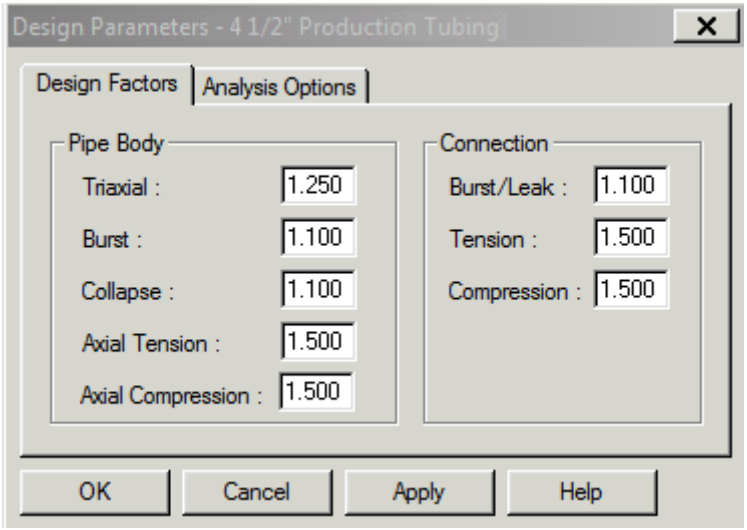

Figure 46: Applied Design Parameters for Tubing (OMV Aktiengesellschaft)

12. HSE Aspects of Hydraulic Fracturing

Performing any task has some health or injury risk potential. The only way to reduce that risk to zero is to avoid the task entirely. This is hardly a practical or possible solution for every task, but it may be reasonable to proceed with a hazardous task if the risk can be reduced and controlled.

There are many risks presented by a hydraulic fracturing treatment, since fracturing is a complex operation comprising multiple tasks performed by a mixed group of contractors and employees at all levels of job experience. General tasks are, but not limited to, job preparation at the yard, loading equipment/chemicals, traveling to location, rigging up equipment, handling and mixing chemicals and proppants, transferring of various fluids, priming up pumps, pressure testing high pressure lines, pumping the frac job, clean and rig down equipment, remove and load excess chemicals, load equipment, de-mobilization of equipment and post job activities at the yard. The fracturing treatment is inherently hazardous and relate to a vast variety of health safety and environmental risks caused by pressure, chemicals, working at heights, confined spaces, noise, heat, lifting and manual handling, stress, weather etc. Since hydraulic fracturing always requires high pressure, pressure integrity testing of the surface installation of the treating lines and the equipment prior to the job is a must. Because pressure is one of the key risks pressure testing is discussed in detail.

12.1 Pressure Testing

Uncontrolled release of pressure carries high-risks for ***H***ealth ***S***afety and ***E***nvironment and can lead to consequences with fatal impacts. Its prevention is one of the main objectives during hydraulic fracturing. Pressure testing is one of the most important controls applied. It assures that the surface installation is prepared with the minimum risk for failure and it provides the highest level of confidence that the used equipment will safely contain the maximum expected pressures.

Good praxis is that pressure tests are performed using incompressible and non-damaging liquids. The most common ones are water or brine. Although generally pressure tests are carried out on equipment prior to mobilization as part of standard maintenance procedures, it is vital that the assembled equipment at the well site is pressure tested to the maximum expected pressures plus a safety margin to assure the pressure integrity of the whole treatment installation. However, because all individual safety devices, such as valves need to be tested, pressure tests can be quite complex and need to be planned thoroughly. Detailed test procedures are often included into the general operating program to assure that tests are performed in the right order to prove the pressure integrity of all sections and interception safety devices. The criteria seen essential for every pressure test and should be defined in a pressure test standard or guideline such as describe by Nardone, 2009:

1. The magnitude of the test pressure (for high-pressure equipment the test pressure shall be 20 % above the maximum expected pressure, but the maximum test pressure cannot exceed the working pressure of the components).
2. The duration for which the test pressure must hold (5 or 10 minutes is adequate for most pressure tests to detect a leak or to provide evidence that there is none, although many operators specify 15 minutes; OMV well engineering standards specifies that a satisfactory test is obtained when a stabilized test is held for 5 minutes).
3. Acceptance criteria, or degree of variation of pressure acceptable. Most standards accept some drop from the initial value (i.e. pressure drop of 1 % of the initial applied test pressure over 10 minutes) but require that the pressure profile show a stabilizing trend.
4. The test fluid (with certain exceptions all pressure tests shall be performed using an incompressible nonflammable medium (i.e. water), when formation of hydrates is possible it is permitted to use water-glycol mix).
5. Test procedure (pressure must be applied in at least two stages: low pressure initially followed by high pressure).

To show a carefully conducted pressure test, an example can be seen below which was a surface line pressure test carried out prior to a hydraulic frac treatment. The pressure was increased in three steps (low, intermediate and high pressure test) and kept for a minimum time required by company standards. Since no leak was detected, the pressure was bleed off and the test was accepted.

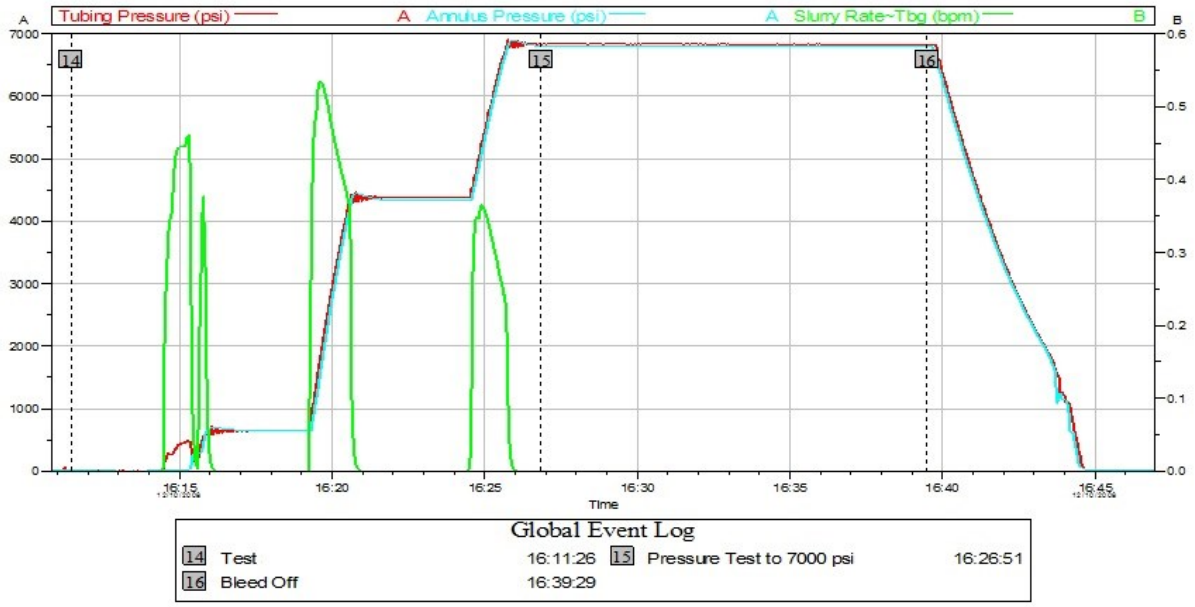

Figure 47: Surface line pressure test example

It is also important to point out that the economic impact of improper HSE measures can be really high, so HSE has to have a priority in all cases.

13. Conclusion

1. The importance of an accurate Formation Breakdown Pressure determination is increasing when the exploration takes place in challenging high pressure environments such as shale gas and tight gas.

2. The knowledge of the expected Formation Breakdown Pressure with high confidence in the prediction data accuracy allows optimization of material selection and fit for purpose completion design, reducing operational risk.

3. With optimized completion material selection the economics of the project can be improved.

4. Of eleven conventional Formation Breakdown Pressure prediction models evaluated, the latest developed prediction model, namely the Aadnoy and Belayneh 1&2 method performed best (based on an error analysis).

5. The usage of Aadnoy and Belayneh 1 method requires the determination of more parameters ($S_{h,min}$, $S_{H,max}$, P_o, v) than the usage of the second ranked Kirsch model ($S_{h,min}$, P_o).

6. The Kirsch method, also built into the GOHFER software which is currently used by OMV Aktiengesellschaft for frac treatment planning and evaluation, is considered the most valid prediction model when limited geomechanical data are available.

7. Minimum and maximum horizontal stress as well as pore pressure is necessary to know with high data quality confidence because these are the most important geomechanical parameters to obtain valid estimated FBP prediction data.

8. Nevertheless, the analysis of the conventional Formation Breakdown Pressure prediction models showed that none of the methods was universally applicable nor gave accurate results in all types of reservoir rocks.

9. The employment of self-learning Artificial Neural Networks software reduces uncertainties of FBP prediction to < 10% error in all types of reservoir rock. This method can be used only if a reference database of historical treatments is available. The historical data are necessary for training purposes of the software.

10. Accurate and higher data volume processed by the Neural Networks improves the accuracy of the FBP prediction.

14. References

Aadnoy, B.S. and Belayneh, M. 2004. Elasto-plastic fracturing model for wellbore stability using non-penetrating fluids. Journal of Petroleum Science and Engineering 45. pp. 179–192.

Aadnoy, B.S. and Belayneh M. 2008 A. A New Fracture Model that Includes Load History, Temperature, and Poisson's Effects. IADC/SPE Asia Pacific Drilling Technology Conference and Exhibition, Jakarta, 25–27 August. SPE-114829-MS.

Aadnoy, B.S. and Belayneh M. 2008 B. A New Fracture Model that Includes Load History, Temperature, and Poisson's Effects. IADC/SPE Asia Pacific Drilling Technology Conference and Exhibition, Jakarta, 25–27 August. SPE-114829-PA.

Barree, R.D. and Miskimins, J.L., 2015. Calculation and Implications of Breakdown Pressures in Directional Wellbore Stimulation. SPE Hydraulic Fracturing Technology Conference. The Woodlands, Texas, USA, 3–5 February. SPE-173356-MS.

Bourgoyne, A.T.Jr., Millheim, K.K., Chenevert, M.E. and Young, F.S.Jr. 1986. Applied Drilling Engineering, SPE Textbook Series, Volume 2, ISBN: 978-1-55563-001-0

Chavez, J., Mjeni, R. and Briner, A. 2013. Formation Breakdown Prediction for the Implementation of Hydraulic Fracturing on a HPHT Tight Gas Reservoir in Oman. SPE Middle East Unconventional Gas Conference and Exhibition, Muscat, Oman, 28–30 January. SPE-164012-MS.

Comisky, J. T., Newsham, K. E., Rushing, J. A. and Blasingame, T. A. 2007. A Comparative Study of Capillary-Pressure-Based Empirical Models for Estimating Absolute Permeability in Tight Gas Sands, SPE Annual Technical Conference and Exhibition, Anaheim, California, USA, 11–14 November 2007, SPE 110050

Economides, M. J. and Martin, T. 2007. Modern Fracturing - Enhancing Natural Gas Production, ISBN: 978-1-60461-688-0, BJ Services Company, Houston, USA

Economides, M. J. and Nolte, K. G. 2000. Reservoir Stimulation, Third Edition, Wiley, pp 856, ISBN: 978-0471491927

Gaarenstroom, L., Tromp, R.A.J., Jong, M.C.d. 1993. Overpressures in the Central North Sea: Implications for Trap Integrity and Drilling Safety. In Petroleum Geology Northwest Europe, Proceedings of the 4th Conference, ed. J.R. Parker, v. 4, pp. 1305–1313. London, UK. DOI: 10.1144/0041305.

Haimson, B.C. and Huang, X. 1989. Hydraulic Fracturing Breakdown Pressure and In Situ Stress at Great Depth. In Rock at Great Depth, Maury and Fourmaintraux (eds), pp 939–946. Balkema, Rotterdam, ISBN 90 6191 975 4.

Haimson, B.C. and Zhao Z. 1991. Effect of Borehole Size and Pressurization Rate on Hydraulic Fracturing Breakdown Pressure. In Rock Mechanics as a Multidisciplinary Science, Roegiers (ed.), pp 191–199. Rotterdam, Balkema. ISBN 90 6191 194 X.

Jin, X., Shah, S.N., Roegiers, J.C. and Hou, B. 2013. Breakdown Pressure Determination – A Fracture Mechanics Approach. SPE Annual Technical Conference and Exhibition, New Orleans, Louisiana, USA, 30 September–2 October. SPE-166434-MS.

Kirsch, G. 1898. Die Theorie der Elastizitat und die Bedurfnisse der Festigkeitslehre, Zeitschrift des Verlines Deutscher Ingenieure

Mats, G. A. 2009. Reservoir Production Optimization Using Genetic Algorithms and Artificial Neural Networks, Norwegian University of Science and Technology, pp. 104

Muhammad, A. 2003. Neural Networks Predict Well Inflow Performance, Texas A&M University, pp. 66

Nardone, P. J. 2009. Well Testing Project Management: Onshore and Offshore Operations, ISBN: 978-1-85617-600-2, Burlington, USA, Elsevier

Olubusola, O. A. T. 2002. The Data as The Model: Interpreting Permanent Downhole Gauge Data Without Knowing The Reservoir Model, Stanford University, pp. 42

Rummel, F. 1987. Fracture mechanics approach to hydraulic fracturing stress measurements. Fracture Mechanics of Rock, B.K. Atkinson ed. Academic Press. pp. 217–239.

Zoback, M. D. 2007. Reservoir Geomechanics, ISBN: 978-0-521-77069-9, Cambridge University Press, Cambridge, UK

Zoback, M. D., Barton, C. A, Brudy, M., Castillo, D. A., Finkbeiner, T., Grollimund, B. R., Moos, D. B., Peska, P., Wardb, C. D., Wipruth, D. J. 2003. Determination of Stress Orientation and Magnitude in Deep Wells, International Journal of Rock Mechanics & Mining Sciences 40 (2003) 1049–1076

Websites:

Artificial Neural Networks Technology Course – University of Toronto, Web page last visited: 20/10/2015

- http://www.psych.utoronto.ca/users/reingold/courses/ai/cache/neural2.html

Data Science and Machine Learning Essentials – Arizona State University, Web page last visited: 01/10/2015

- https://www.edx.org/course/data-science-machine-learning-essentials-microsoft-dat203x

Learning from Data, Machine Learning Course – California Institute of Technology, Web page last visited: 15/10/2015

- http://work.caltech.edu/telecourse.html

ResGeo202 Reservoir Geomechanics Course – Stanford University, Web page last visited: 07/06/2015

- https://lagunita.stanford.edu/courses/EarthSciences/ResGeo202/Spring2015/about

Appendices

Appendix A Formation Microimager (FMI) Log Example

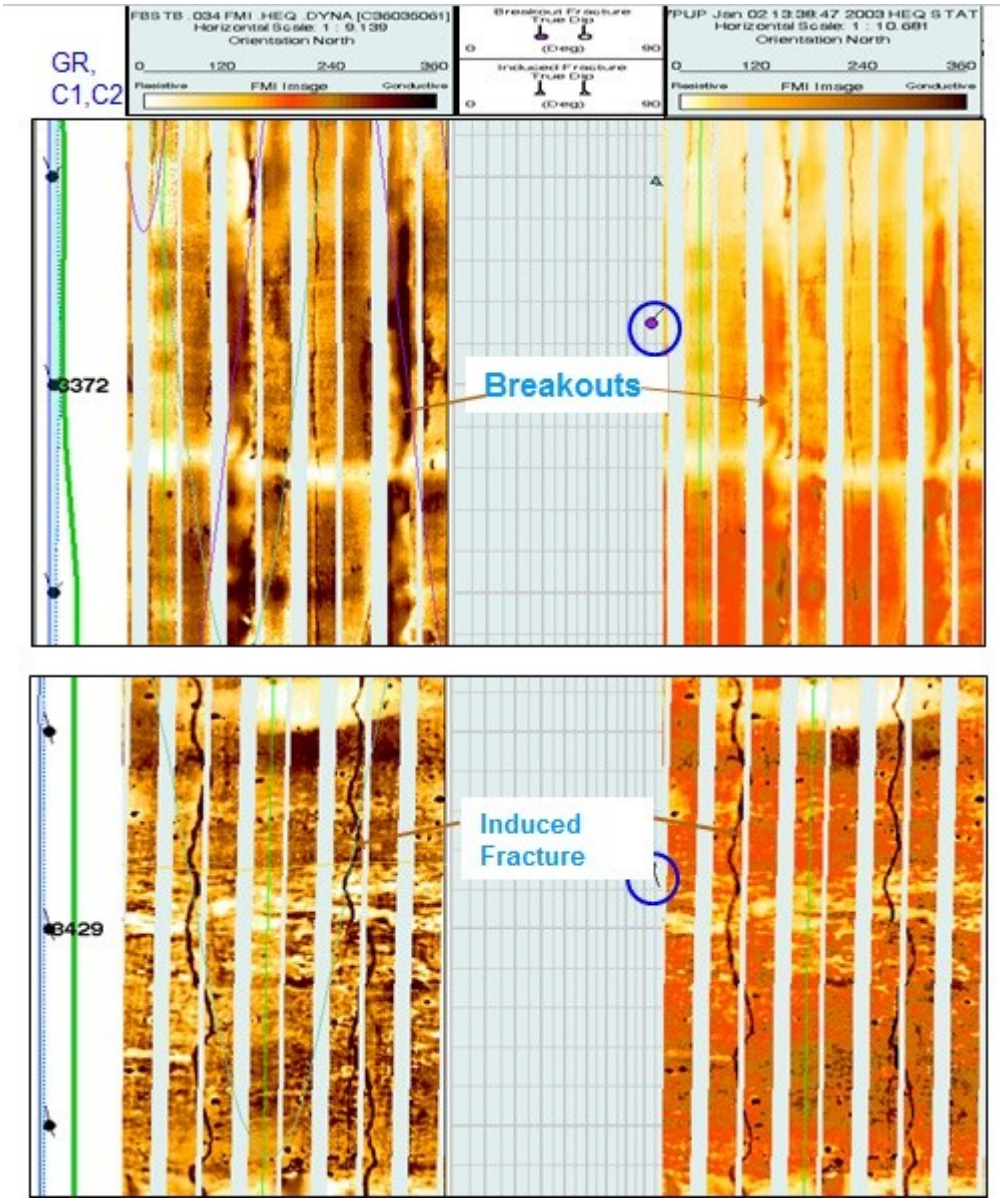

Figure 48: Image log showing wellbore breakouts and drilling induced tensile fractures

Appendix B Relative Stress Magnitudes and E. M. Anderson´s Classification Scheme

E.M. Anderson`s classification scheme describes the style of faulting which would be induced by a given stress state. This scheme leads naturally to some general constraints on stress magnitudes as a function of depth and pore pressure.

E. M. Anderson considered the magnitudes of the greatest, intermediate and least principal stress at depth ($\mathbf{S_1}$, $\mathbf{S_2}$ and $\mathbf{S_3}$) in terms of $\mathbf{S_v}$, $\mathbf{S_{H,max}}$ and $\mathbf{S_{h,min}}$ (Table 20). As shown in Fig. 49 Anderson scheme classifies areas by the geomechanic faulting regimes and characterizes them into three categories, normal, strike-slip or reverse faulting. This classification methodology defines the horizontal principal stress magnitudes with respect to the vertical stress.

Table 20: Relative stress magnitudes and faulting regimes

Regime/Stress	S_1	S_2	S_3
Normal	S_v	$S_{H,max}$	$S_{h,min}$
Strike-slip	$S_{H,max}$	S_v	$S_{h,min}$
Reverse	$S_{H,max}$	$S_{h,min}$	S_v

The vertical stress, $\mathbf{S_v}$: is a) the maximum principal stress ($\mathbf{S_1}$) in normal faulting regimes, b) the intermediate principal stress ($\mathbf{S_2}$) in strike-slip regimes, and c) the least principal stress ($\mathbf{S_3}$) in reverse faulting regimes.

NB: Among Anderson's classification, other faulting environments are possible shown as Limiting cases and Intermediate cases in Fig. 49. While radial extension and compression (Limiting cases) are rare, normal/strike-slip intermediate ($\mathbf{S_v=S_{H,max}}$) and strike-slip/reverse intermediate ($\mathbf{S_v=S_{h,min}}$) can frequently occur (ResGeo202 Reservoir Geomechanics Course – Stanford University).

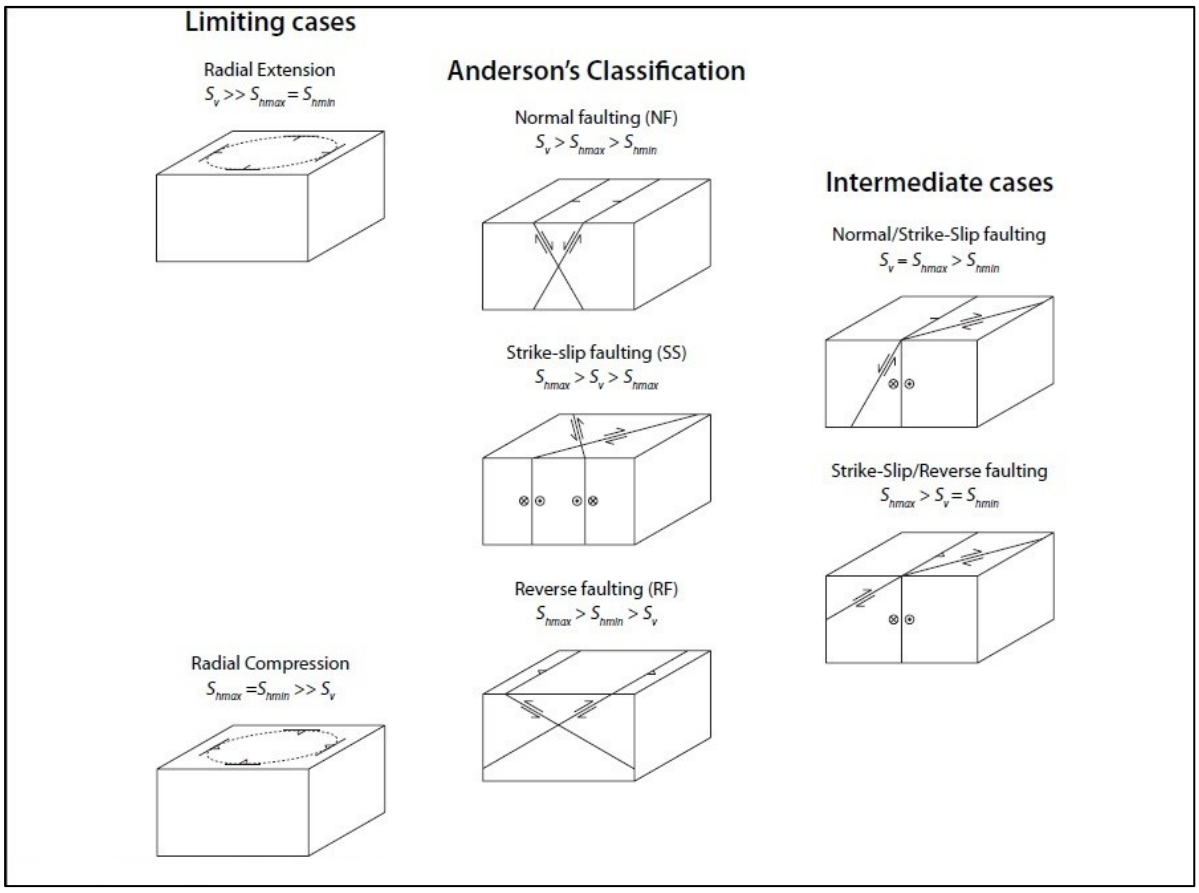

Figure 49: Possible faulting environments (ResGeo202 Reservoir Geomechanics Course – Stanford University)

In order to consider the ranges of stress magnitudes at depth in the different tectonic environments Fig. 50 and 51 can be generally used. The plots show different stress magnitudes for normal, strike-slip and reverse faulting environments when pore pressure is hydrostatic and when it approaches lithostatic (overburden) values at depth. At each depth, the range of possible values for $\mathbf{S_{h,min}}$ and $\mathbf{S_{H,max}}$ are established by Anderson faulting theory based on the limiting fact that the least principle stress must always exceed the pore pressure and cannot exceed the strength of the crust.

As seen in Fig. 50 the differences between the three principal stresses can be large and grow rapidly with depth when pore pressure is close to hydrostatic. When there are severely over-pressured formations at depth (Fig. 51) there are consequently small differences among the three principal stresses. In normal and strike-slip faulting domains, $\mathbf{S_{h,min}}$, the least principal stress must increase as pore pressure increases because, it can never be less than the pore pressure. In strike-slip and reverse faulting regimes ($\mathbf{S_{H,max}=S_1}$), the upper bound values of $\mathbf{S_{H,max}}$ is severely reduced by high pore pressure. Thus, when pore pressure approaches the vertical stress, both horizontal stresses are close to the vertical stress, regardless of whether the formation is in a normal, strike-slip or reverse faulting environment.

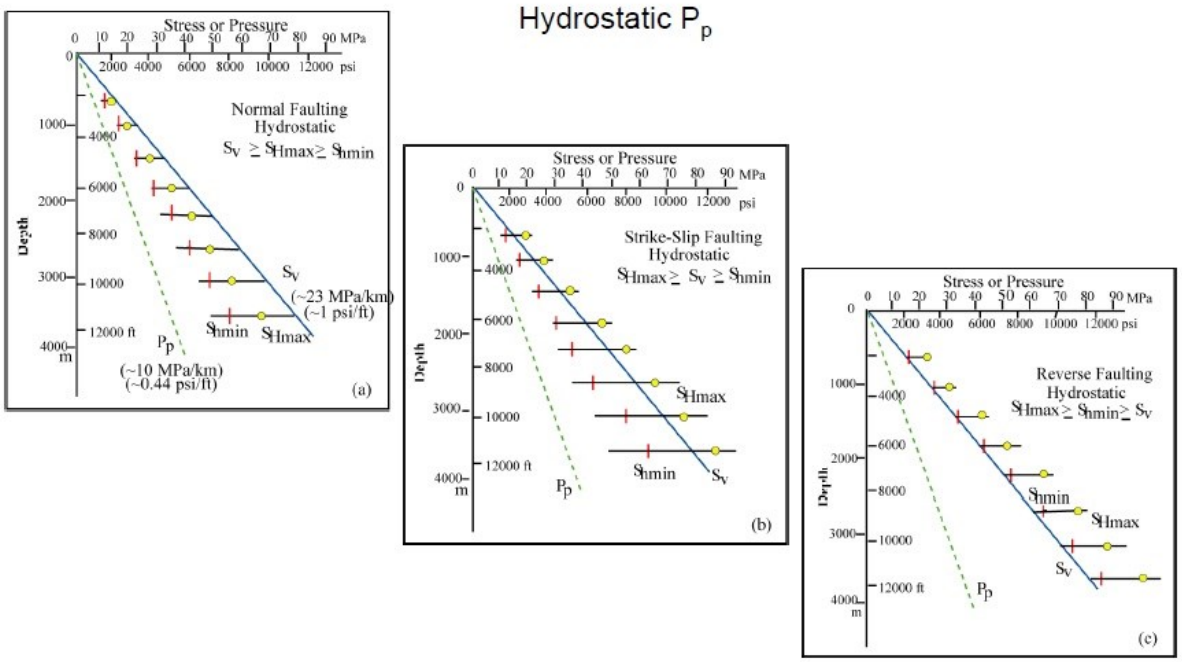

Figure 50: Variation of stress magnitudes with depth in normal, strike-slip and reverse faulting stress regimes for hydrostatic conditions (ResGeo202 Reservoir Geomechanics Course – Stanford University)

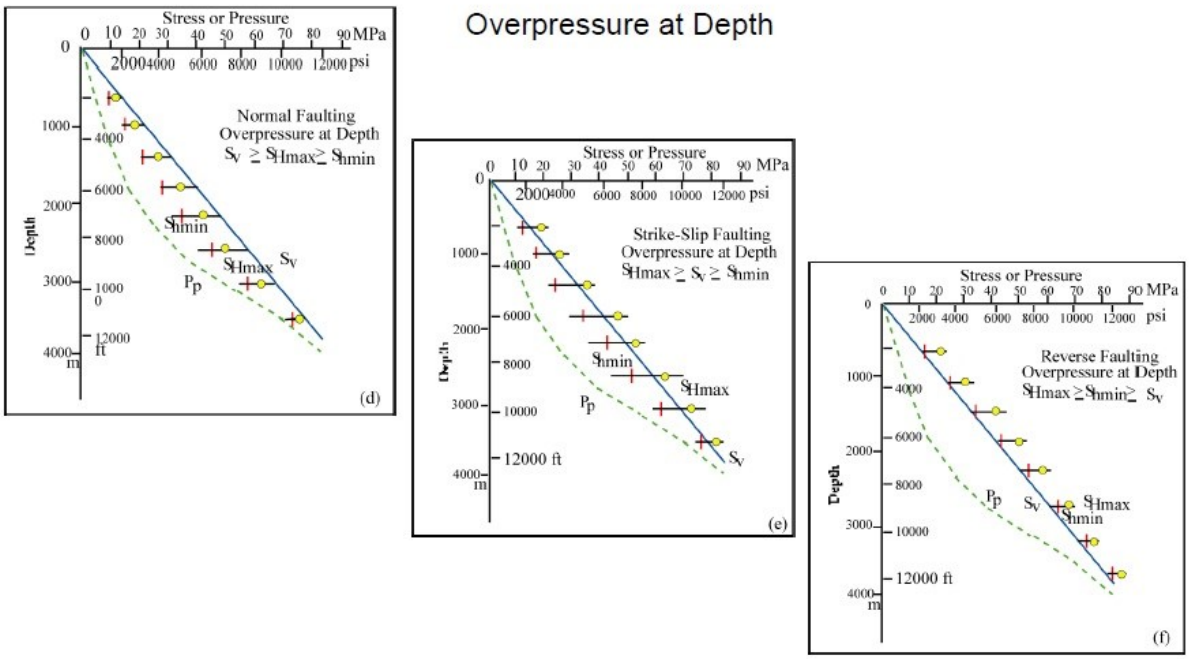

Figure 51: Variation of stress magnitudes with depth in normal, strike-slip and reverse faulting stress regimes for overpressure conditions (ResGeo202 Reservoir Geomechanics Course – Stanford University)

Note, that at extremely high pore pressure, relatively small stress perturbations are sufficient to change the style of faulting from one stress regime to the other (for example to go from

normal faulting to reverse faulting). Although this distinction might seem to be relatively insignificant, it is important because if $\mathbf{S_3 = S_{hmin}}$, vertical hydrofracs propagate into the formation whereas if $\mathbf{S_3 = S_v}$, the formation will open in horizontal fractures.

Stress-polygon (Zoback-o-gram)

Nevertheless it is possible to estimate the range of possible magnitudes of $\mathbf{S_{h,min}}$ and $\mathbf{S_{H,max}}$ at a particular depth for a given pore pressure and assumed coefficient of friction. Considering that stress in the crust is limited by the frictional strength of the faults the stress-polygon can be used (Zoback et al., 2003). Figure 52 illustrates the stress-polygon with which the range of allowable values for horizontal principal stresses in the earth`s crust for normal, strike-slip and reverse faulting environment can be determined. Allowable stress states are shown for hydrostatic pore pressure and significant overpressure. As it can be seen, elevated pore pressure reduces the difference between principal stresses.

NB: Figure 52 shows the expected stress values for a depth of 3 km assuming an average overburden rock density of 2.3 g/cm^3.

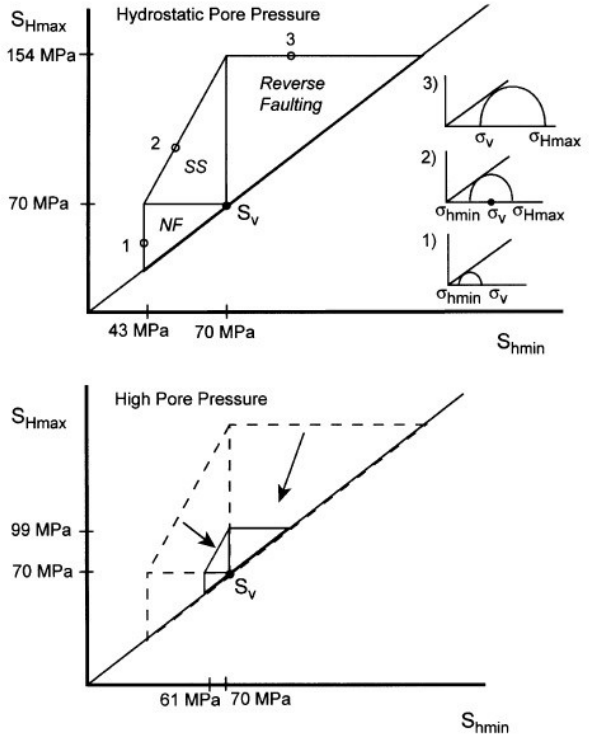

Figure 52: Stress-polygon (Zoback et al., 2003)

Appendix C Stresses Around the Wellbore and Orientation of Hydraulic Fracture

Barree and Miskimins (2015) presents how Kirsch described the stresses around a circular hole when a vertical well is drilled parallel to the vertical principal stress, $\mathbf{S_v}$. Radial stress ($\mathbf{S_r}$), tangential (hoop) stress ($\mathbf{S_t}$), and shear stress ($\boldsymbol{\tau_{r\theta}}$) are calculated according to the following equations:

$$S_r = \frac{S_{h,min} + S_{H,max}}{2}\left(1 - \frac{r_w^2}{r^2}\right) + \frac{S_{h,min} - S_{H,max}}{2}\left(1 - 4\frac{r_w^2}{r^2} + 3\frac{r_w^4}{r^4}\right)\cos 2\theta + \frac{r_w^2}{r^2}(P_w - \alpha P_o) \quad \text{Eq.49}$$

$$S_t = \frac{S_{h,min} + S_{H,max}}{2}\left(1 - \frac{r_w^2}{r^2}\right) - \frac{S_{h,min} - S_{H,max}}{2}\left(1 + 3\frac{r_w^4}{r^4}\right)\cos 2\theta - \frac{r_w^2}{r^2}(P_w - \alpha P_o) \quad \text{Eq.50}$$

$$\tau_{r\theta} = -\frac{S_{h,min} + S_{H,max}}{2}\left(1 + 2\frac{r_w^2}{r^2} - 3\frac{r_w^4}{r^4}\right)\sin 2\theta - \frac{r_w^2}{r^2}(P_w - \alpha P_o) \quad \text{Eq.51}$$

where $\mathbf{P_o}$ is the far-field pore pressure, $\mathbf{P_w}$ is the wellbore fluid pressure, **r** is the distance from wellbore, $\mathbf{r_w}$ is the wellbore radius, **α** is the Biot's poroelastic parameter (which describes the relationship between the rock matrix and rock bulk compressibilities), $\mathbf{S_{h,min}}$ is the minimum horizontal in-situ stress, $\mathbf{S_{H,max}}$ is the maximum horizontal in-situ stress, **θ** is the angle from direction of minimum in-situ stress.

Radial, tangential and vertical stresses acting on the wellbore can be seen in Fig. 53.

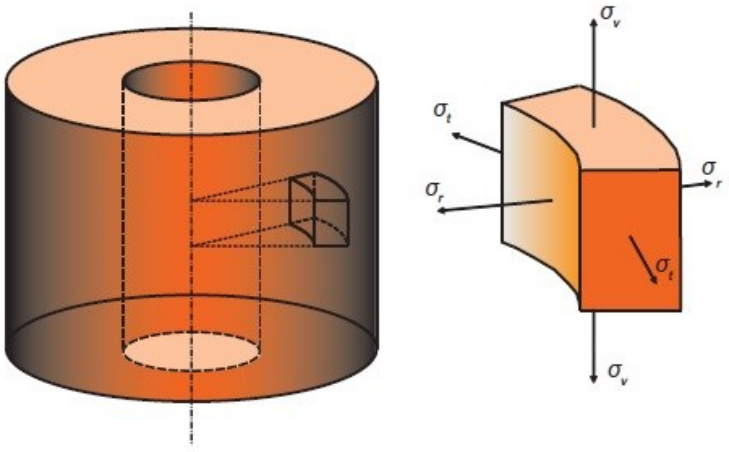

Figure 53: Three-dimensional stresses around a wellbore (Economides et al., 2007)

As can be seen in Fig. 54, the magnitude of effective principal stresses $\boldsymbol{\sigma_{\theta\theta}}$ (hoop stress), $\boldsymbol{\sigma_{rr}}$ (radial stress) and $\boldsymbol{\sigma_{zz}}$ (stress acting parallel to the wellbore) vary around a vertical wellbore as a function of azimuth. The amplitude of hoop stress change in a sinusoidal manner and one can identify regions with minimum compression around the wellbore (i.e. parallel to

$\mathbf{S_{h,min}}$) at θ=0°, 180° (measured from the azimuth of $\mathbf{S_{H,max}}$) where the minimum hoop stress at the wellbore wall can be written as the following:

$$\sigma_{\theta\theta}^{min} = 3S_{h,min} - S_{H,max} - 2P_o - \Delta P - \sigma^{\Delta T} \quad \text{Eq. 52}$$

At the same time the hoop stress in the region with maximum stress concentration around the wellbore (i.e. parallel to $\mathbf{S_{H,max}}$) at θ=90°, 270° can be calculated by equation 53 :

$$\sigma_{\theta\theta}^{max} = 3S_{H,max} - S_{h,min} - 2P_o - \Delta P - \sigma^{\Delta T} \quad \text{Eq. 53}$$

such that the difference between the two is:

$$\sigma_{\theta\theta}^{max} - \sigma_{\theta\theta}^{min} = 4\left(S_{H,max} - S_{h,min}\right) \quad \text{Eq. 54}$$

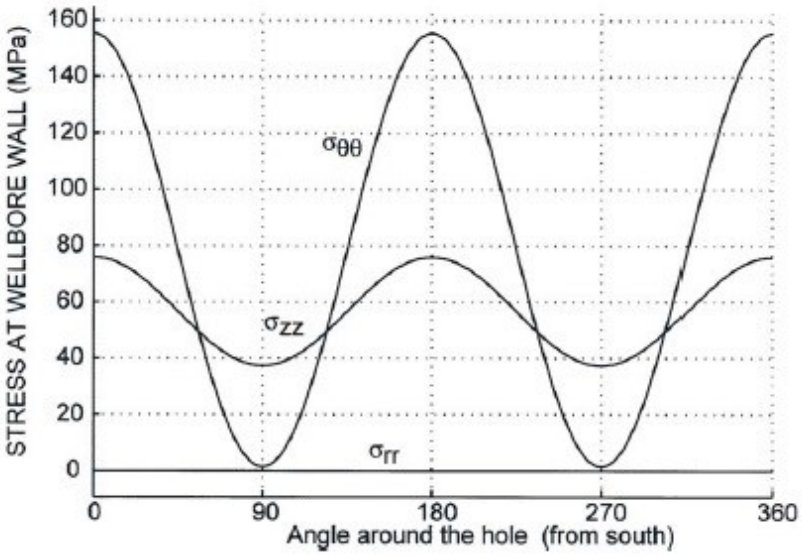

Figure 54: Variation of effective principal stresses $\sigma_{\theta\theta}$ (hoop stress), σ_{rr} (radial stress) and σ_{zz} (stress acting parallel to the wellbore) around a vertical wellbore as a function of azimuth (Zoback et al., 2003)

The variation of the hoop stress ($\boldsymbol{\sigma_{\theta\theta}}$) around the wellbore is four times the difference between $\mathbf{S_{H,max}}$ and $\mathbf{S_{h,min}}$ in the far field. As the mud weight is assumed to equal the pore pressure $\boldsymbol{\sigma_{rr}=0}$. $\boldsymbol{\sigma_{zz}}$ varies around the well in the same manner as $\boldsymbol{\sigma_{\theta\theta}}$ but without the extreme variation of values.

In order to show how the stresses change around and along the wellbore in practice, Fig. 55 shows the calculated breakdown pressure for one of the investigated wells using GOHFER software. FBP is displayed with colors on a disk at a particular depth of the wellbore and the magnitude of the pressure can be read from the color bar on the right.

These stress values are the breakdown pressure required to initiate a fracture in an intact section of the well, with no pre-existing fractures.

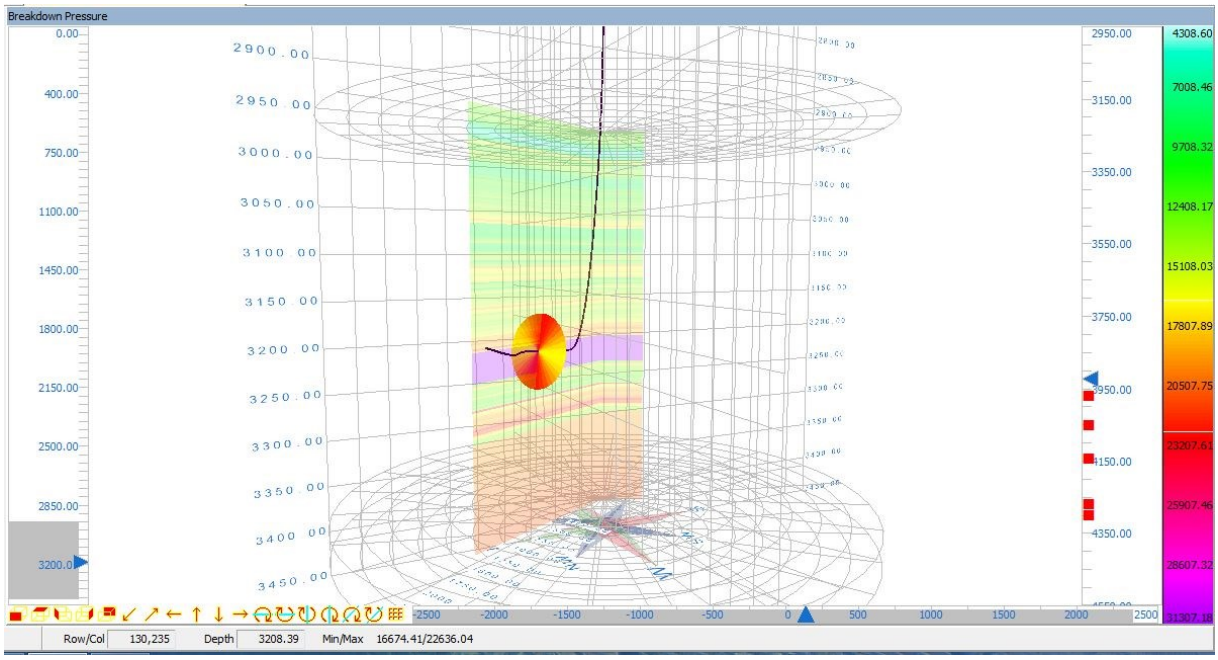

Figure 55: Calculated Formation Breakdown Pressure around the wellbore at a particular depth for one of the investigated wells

Orientation of Hydraulic Fracture

A fracture always propagates perpendicular to the plane of the least principal stress and parallel to the greatest principal stress. This is a fundamental principle; therefore, the key to understanding fracture orientation is to understand the stress regime.

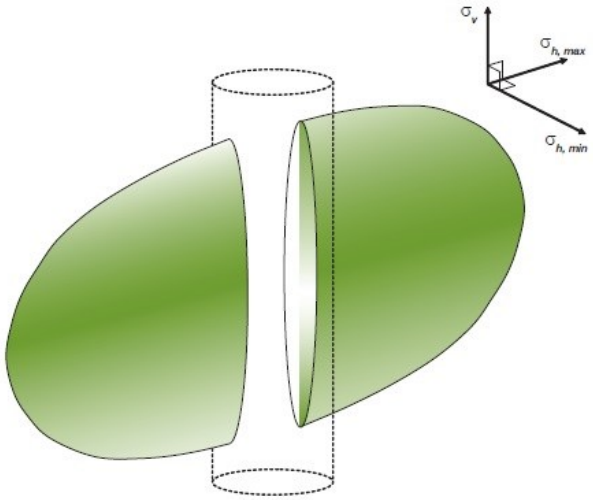

Figure 56: A fracture propagates perpendicular to the minimum horizontal stress (Economides et al., 2007)

Propagation perpendicular to the least principal stress (usually $S_{h,min}$) means that the fracture will most of the cases propagate on a vertical plane (see Fig. 56). However, there are some exceptions like in case of Fig. 55 as well since looking at the disk the fractures will initiate in horizontal planes, indicated by the breakdown pressure at the sides of the hole being less

than at the top of the hole. This condition can be changed by drilling the well at a different azimuth.

Appendix D Data Requirements of a Geomechanical Study

Table 21: Data checklists and formats for a Geomechanical Study

	Category	Data	Format
Minimum Data For The Geomechanical Model			
General Field Information			
	Field/Regional Data	Field map with well locations	.bmp, .jpeg, .tiff, .ppt
		General stratigraphic column	.xls, .txt
		Geological reports (structural, sedimentary, stratigraphic)	.doc, .pdf
		Structural maps / Cross sections	.bmp, .jpeg, .tiff, .ppt
Existing Wells			
	Typical Log Data	Gamma (e.g., GR)	.las, .txt, .xls
		Density (e.g., RHOB)	.las, .txt, .xls
		Sonic (DTC or DTC/DTS)	.las, .txt, .xls
		Porosity	.las, .txt, .xls
		Resistivity	.las, .txt, .xls
		Single arm caliper	.las, .txt, .xls
	Non Typical log data	Cross dipole sonic, oriented (MSIP, DSI in BCR mode, XMAC, WaveSonic)	.las, .txt, .xls
		Oriented 4-arm/6-arm caliper	.las, .txt, .xls
		Image logs (e.g., FMI, EMI, UBI, CAST, CBIL, OBMI, etc.)	.lis, .dlis, .flip, .tap, .nti
		Image log length Feet Meters	feet, meters
		Verification file (paper or digital) with caliper,HAZI,DEVI or P1AZ/RB,header, 1:10 to 1:12	pds, pdf, tif
	Drilling Data	DDR-Daily drilling reports (**MW, reported LOT with time**)	.doc, .pdf, .xls, .txt
		Wellbore survey (**MD, DEVI, AZI**, DOGLEG)	.las, .txt, .doc, .xls
		Well schematic (hole sizes, casing depths and sizes)	.las, .txt, .doc, .xls
	Lithology	Formation tops (**MD and TVD**)	.las, .txt, .doc, .xls
	Pore Pressure	Pore pressure measurements (**RFT, DST, MDT**) and predictions **with time**	.las, .txt, .doc, .xls
	Fracing	**Minifrac or hydraulic fracturing tests (pressure and flow rate vs. time) with time**	.las, .txt, .doc, .xls
Additional Data, If Available, For The Geomechanical Model			
Existing Wells			
	Drilling Data	**ECD vs. MD**	.las, .txt, .doc, .xls
		XLOT, LOT, FIT raw data (**time, flow rate, volume, pressure**)	.xls, .txt
		PWD (time based data preferred)	.las, .txt, .doc, .xls
		Rate of penetration	.las, .txt, .doc, .xls
		Pore pressure model in shales	.las, .txt, .doc, .xls
		Formation temperatures	.las, .txt, .doc, .xls
		Mud temperatures	.las, .txt, .doc, .xls
	Lithology	**Mud logging report**	.doc, .pdf, .xls
		Cuttings description / pictures	.bmp, .jpeg, .tiff, .ppt
	Cuttings Tests	Cuttings based rock mechanical properties (DCM, others)	.las, .txt, .doc, .xls
	Core Tests	**Rock mechanics test results (triaxial, UCS, Brazil, TWC, Biot, etc.)**	.doc, .pdf, .xls
		Cores available, no geomechanical tests	.doc, .pdf, .xls
	Previous Studies	**Previous geomechanics reports for the study area**	.las, .txt, .doc, .xls
		Wellbore failure analysis	.las, .txt, .doc, .xls
		Fracture or bedding orientations analysis	.las, .txt, .doc, .xls
		Other: please list	
Data for special mechanical problems:	**Weak Planes**	Orientation of the planes (strike, dip, depth)	.las, .txt, .doc, .xls, .pdf
		Characteristics of the planes (sliding friction)	.las, .txt, .doc, .xls, .pdf
	Chemical instability of shales (osmosis)	salinity (solid concentrations) of the used mud	.doc, .pdf, .xls, .txt
		activity of the mud	.doc, .pdf, .xls, .txt
		salinity (solid concentrations) of the formation fluid	.doc, .pdf, .xls, .txt
		temperature of mud and formation fluid	.doc, .pdf, .xls, .txt

Required Data from GEM | Required Data for WBS | Required Data for SPP | Required Data for FracPerm | 3D Pore Pressure | Sheet2

Appendix E Logs and Mechanical Earth Model Example

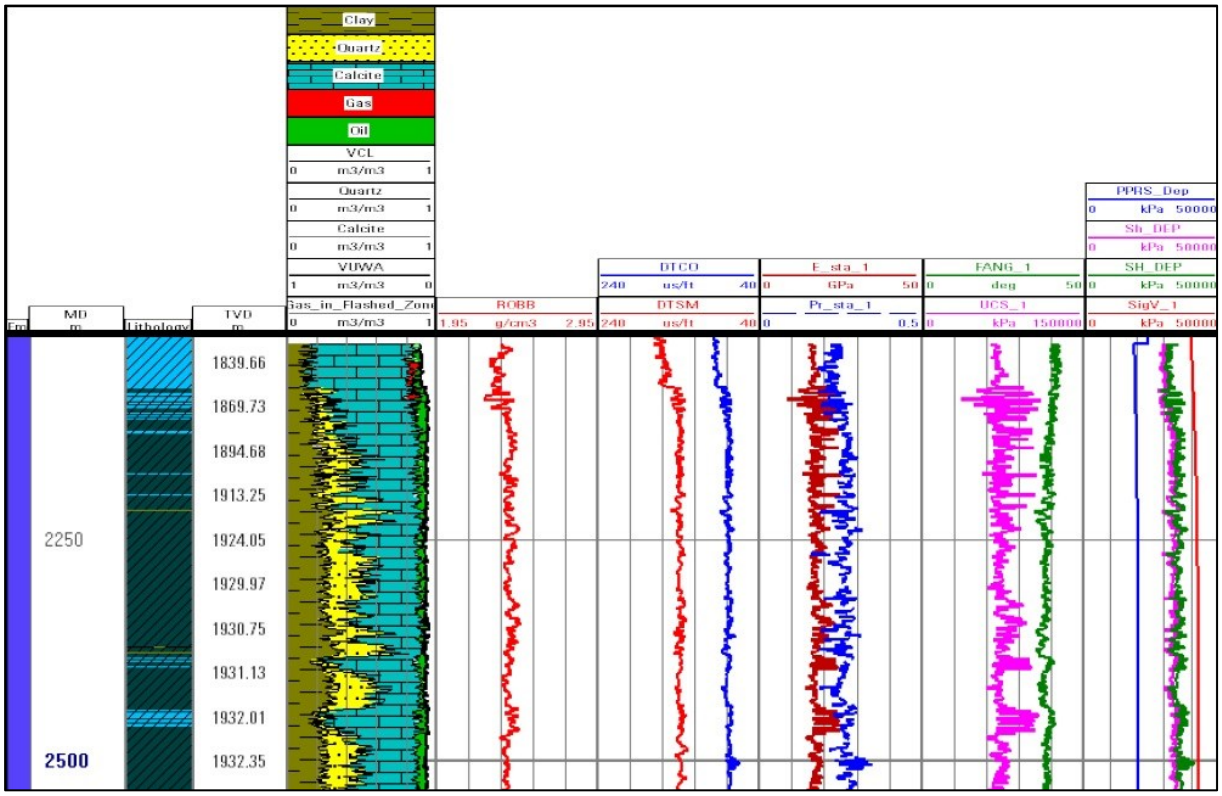

Figure 57: Mechanical properties and stress interpretation

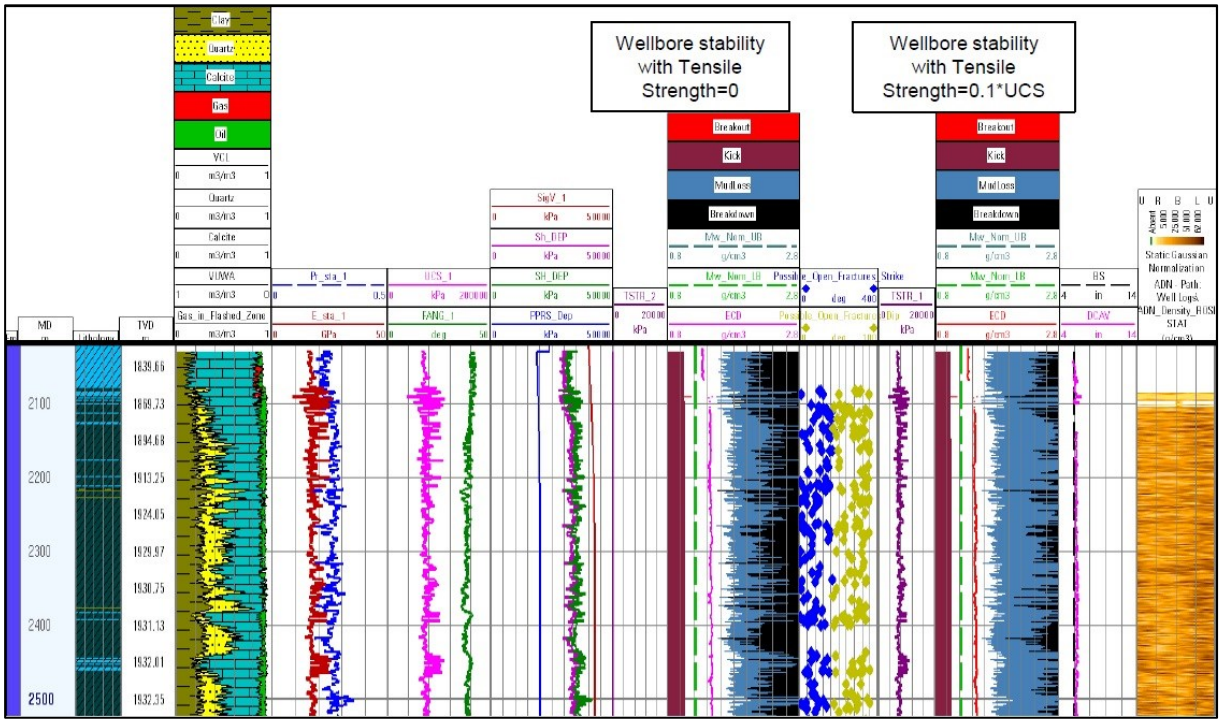

Figure 58: Wellbore stability interpretation

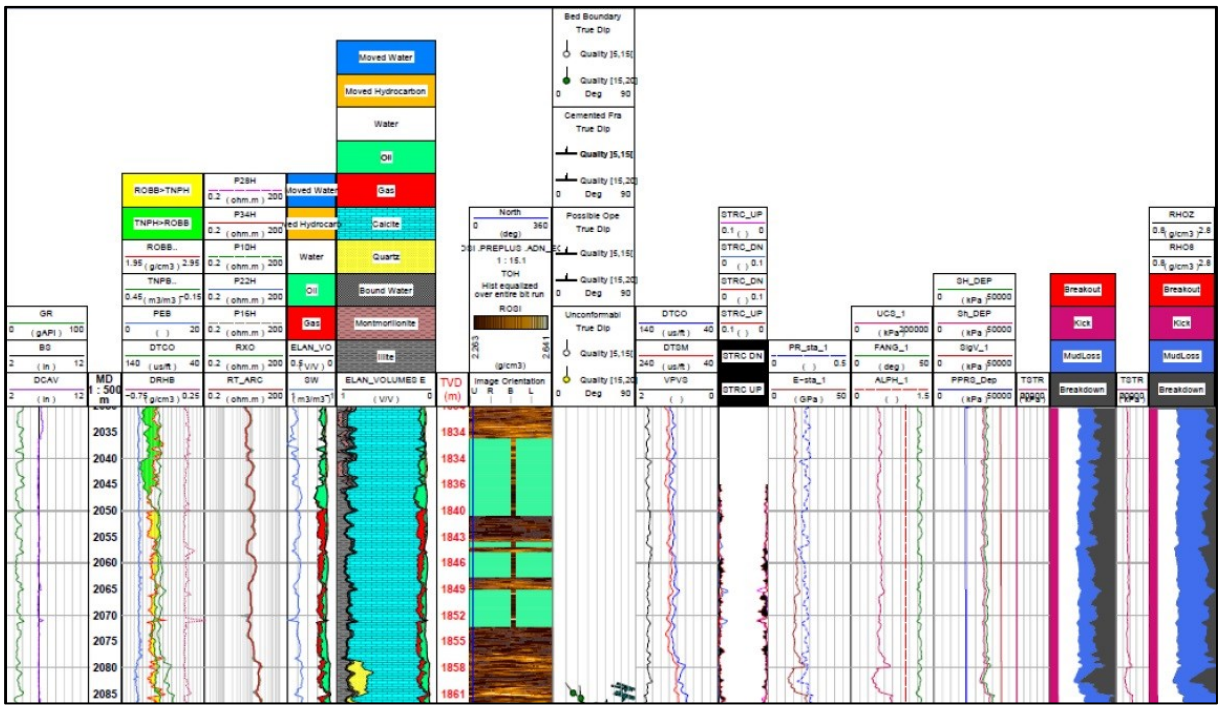

Figure 59: Final integrated montage

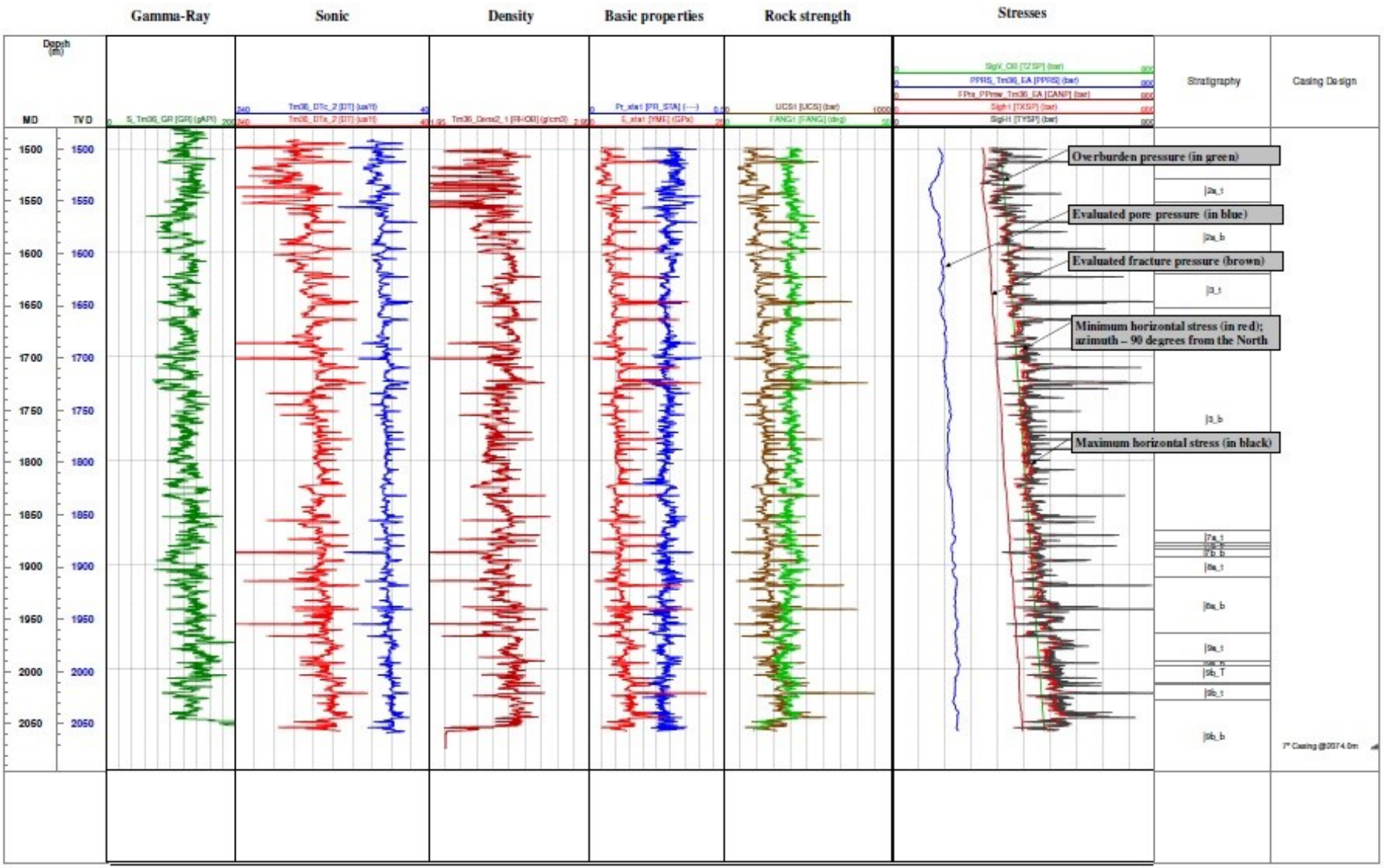

Figure 60: Mechanical Earth Model for one of the investigated wells

Appendix F Formation Breakdown Pressure Data Distribution by Fields

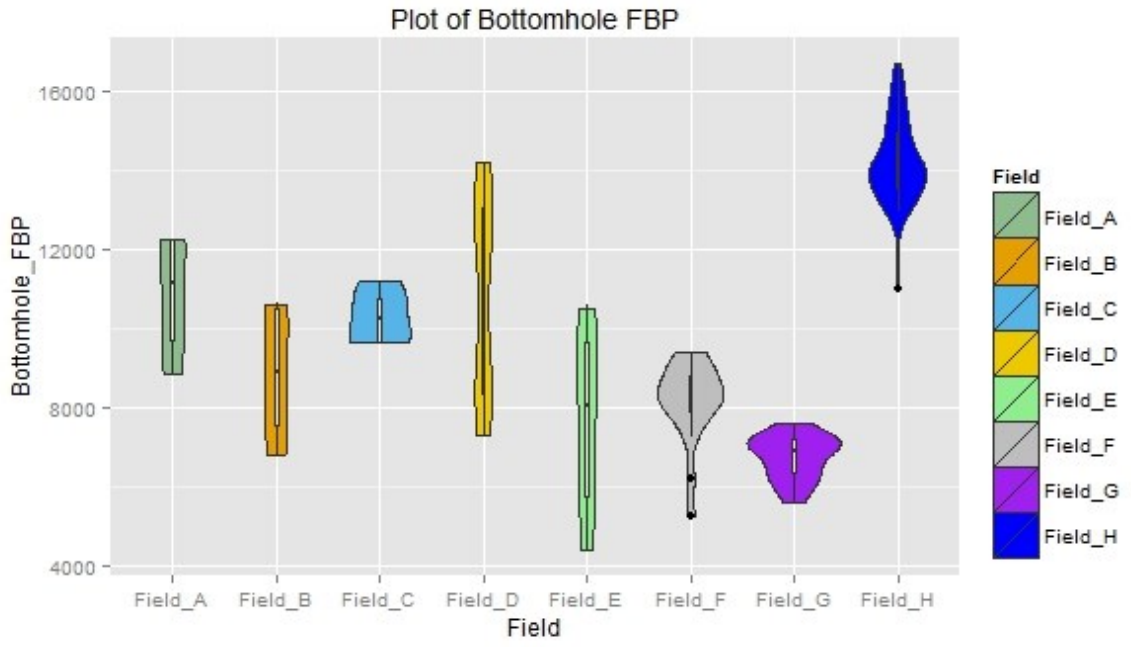

Figure 61: Formation Breakdown Pressure data distribution by fields

Appendix G Measured and Calculated Formation Breakdown Pressure Values

Table 22: Measured and calculated Formation Breakdown Pressures by the conventional models

Well name	Breakdown BHP	Kirsch, 1898	Hubbert and Willis, 1957	Haimson and Fairhurst, 1967	Rummel 1, 1987	Rummel 2, 1987	Rummel 3, 1987	Rummel 4, 1987	Schmitt and Zoback, 1989	Ito and Hayashi, 1990	Aadnoy and Belayneh 1, 2008	Aadnoy and Belayneh 2, 2008
Well 1	8818	10552	5943.1	4616	8884	10502	16625	21401	6395	7458	9499	9491
Well 2	12252	14386	3091	2511	9397	11126	17674	22782	2977	4078	8620	8602
Well 3	12236	14407	5859	4759	10752	12779	20451	26435	5608	7401	10886	10870
Well 4	10000	10543	6612	5371	9205	10893	17282	22266	6334	8262	9534	9517
Well 5	8860	9558	6640	5157	8731	10315	16310	20987	7150	8283	9489	9481
Well 6	10484	8016	5299	4116	7316	8590	13412	17173	5681	6656	7552	7544
Well 7	10625	7292	6805	4979	7689	9045	14177	18180	8260	8456	8636	8623
Well 8	7526	7782	3631	2591	6389	7460	11514	14676	4437	4651	6612	6592
Well 9	6750	6740	6896	5663	7460	8765	13707	17562	6405	8558	7750	7734
Well 10	15585	12656	6327	4841	10113	12000	19141	24712	7063	7943	10994	10986
Well 11	8609	10061	6784	4717	9050	10703	16963	21846	8994	8461	10628	10615
Well 12	7300	8927	6622	5143	8410	9923	15652	20121	7128	8254	9118	9110
Well 13	10749	9732	8107	5931	7629	8971	14053	18016	8883	7698	8861	8851
Well 14	9645	8041	6259	4579	7441	8743	13669	17511	7389	7372	8251	8235
Well 15	11170	9142	7793	5702	7974	9392	14760	18948	8915	8291	9207	9195
Well 16	10244	8840	7640	5590	8135	9588	15090	19381	8930	8578	9365	9342
Well 17	9628	9073	7812	5857	8003	9428	14820	19026	8674	8379	9147	9127
Well 18	14194	10414	8604	6528	8126	9577	15070	19356	9139	8200	9445	9425
Well 19	12511	6323	4705	3442	5867	6823	10444	13268	5431	5525	6018	6002
Well 20	13014	6092	4152	3225	5705	6625	10112	12831	4401	5132	5442	5428
Well 21	13258	8049	7255	5309	6722	7866	12195	15573	7978	7077	7568	7554
Well 22	7274	4669	3698	2706	4754	5467	8165	10270	4253	4540	4449	4433

Well 23	11872	6817	5520	4138	6143	7160	11011	14014	6074	6060	6435	6420
Well 24	8332	6060	4115	3011	5518	6398	9730	12329	4724	4898	5481	5467
Well 25	12777	6308	4677	3422	5866	6823	10443	13267	5408	5517	6013	5997
Well 26	13217	6395	4848	3547	5953	6929	10621	13502	5602	5675	6152	6136
Well 27	8502	4365	3025	2295	4520	5181	7685	9638	3340	4028	3906	3896
Well 28	8261	5729	3775	2932	5562	6452	9820	12447	4032	4948	5180	5166
Well 29	8257	6657	5177	3834	6026	7018	10770	13698	5809	5805	6265	6252
Well 30	8828	5989	4277	3129	5751	6682	10207	12956	5031	5326	5791	5777
Well 31	5200	4804	3631	2657	4746	5456	8148	10247	4147	4408	4429	4420
Well 32	8070	5787	5384	3939	5620	6522	9938	12602	6106	5949	5835	5822
Well 33	7951	6381	4953	3758	5842	6793	10393	13201	5382	5609	5905	5897
Well 34	8941	6207	6002	4119	5836	6786	10381	13186	7170	6336	6343	6334
Well 35	10563	7541	6655	5168	6506	7603	11754	14992	6918	6755	7003	6982
Well 36	10278	7513	6359	4938	6260	7302	11249	14328	6577	6290	6655	6634
Well 37	10163	9572	9175	6961	7014	8222	12793	16360	9464	7675	8282	8267
Well 38	7552	6120	5832	4108	5778	6715	10262	13028	6815	6214	6196	6181
Well 39	9451	7034	7372	5327	6373	7441	11481	14633	8264	7325	7165	7157
Well 40	5464	3752	2444	1766	4640	5328	7931	9962	3279	4197	4103	4095
Well 41	4333	5205	4839	3584	5279	6107	9240	11684	5444	5551	5276	5268
Well 42	5847	4640	4652	3361	4858	5594	8378	10550	5337	5258	4776	4760
Well 43	10792	6454	4964	3677	6111	7121	10945	13927	5684	5904	6319	6301
Well 44	8905	5860	7141	5546	10041	10041	10041	10041	7418	7175	6310	6303
Well 45	5208	2466	3846	2814	6166	6166	6166	6166	4471	4829	3329	3303
Well 46	6163	6221	6337	6035	9020	9020	9020	9020	4388	6536	4837	4837
Well 47 Stage 1	9388	3377	4724	3350	7747	7747	7747	7747	5789	5107	4514	4500
Well 47 Stage 2	9225	3359	4762	3412	7767	7767	7767	7767	5738	5158	4474	4459
Well 47 Stage 3	9164	3347	4720	3346	7715	7715	7715	7715	5778	5109	4474	4459
Well 47 Stage 4	7216	3333	4827	3475	7807	7807	7807	7807	5758	5244	4433	4417
Well 47 Stage 5	8265	3309	5065	3799	8023	8023	8023	8023	5656	5546	4335	4317

Well 48 Stage 1	8034	8292	8034	5799	11270	11270	11270	11270	9024	6255	8375	8358
Well 48 Stage 2	7954	8279	7954	5844	11183	11183	11183	11183	8786	6197	8322	8303
Well 48 Stage 3	8682	9094	8682	6018	11904	11904	11904	11904	9999	6857	8934	8915
Well 48 Stage 4	8336	8285	8336	6102	11549	11549	11549	11549	9197	6755	8286	8268
Well 48 Stage 5	7778	8620	7778	5599	10938	10938	10938	10938	8769	6275	8374	8355
Well 49 Stage 1	8910	3325	4299	3141	7274	7274	7274	7274	5110	4588	4400	4390
Well 49 Stage 2	7585	3287	4497	3218	7438	7438	7438	7438	5462	4845	4380	4367
Well 49 Stage 3	8578	3247	4427	3070	7332	7332	7332	7332	5611	4767	4367	4354
Well 49 Stage 4	8262	3200	4124	2844	6988	6988	6988	6988	5329	4401	4311	4301
Well 49 Stage 5	8161	3152	4215	3087	7035	7035	7035	7035	4968	4524	4168	4157
Well 49 Stage 6	8359	3118	4085	2791	6871	6871	6871	6871	5321	4368	4208	4197
Well 50 Stage 1	7580	9249	10373	7617	12664	12664	12664	12664	10967	7630	8702	8683
Well 50 Stage 2	7169	8331	9527	7006	11734	11734	11734	11734	10091	7158	7930	7915
Well 50 Stage 3	7002	8656	9868	7042	12034	12034	12034	12034	10595	7317	8163	8148
Well 50 Stage 4	7294	7378	8686	6240	10792	10792	10792	10792	9356	6686	7127	7117
Well 50 Stage 5	6698	7890	9107	6671	11123	11123	11123	11123	9644	6842	7467	7453
Well 50 Stage 6	5779	6950	8283	5909	10215	10215	10215	10215	8933	6389	6684	6675
Well 51 Stage 1	6891	4554	5162	3777	9194	9194	9194	9194	6248	5516	5938	5928
Well 51 Stage 2	6590	4467	5075	3713	9078	9078	9078	9078	6153	5455	5851	5842
Well 51 Stage 3	6292	4526	5134	3710	9108	9108	9108	9108	6338	5471	5910	5900
Well 52 Stage 1	7413	8019	8937	6378	11264	11264	11264	11264	9718	6659	7769	7758
Well 52 Stage 2	7174	7621	8635	6416	10960	10960	10960	10960	9162	6586	7442	7430
Well 52 Stage 3	7194	8891	10050	7061	12375	12375	12375	12375	10923	7443	8449	8436
Well 52 Stage 4	7055	8302	9278	6564	11600	11600	11600	11600	10109	6883	7988	7977
Well 52 Stage 5	7208	8573	9621	6768	11940	11940	11940	11940	10484	7121	8198	8186
Well 52 Stage 6	6852	8841	10052	7136	12369	12369	12369	12369	10861	7485	8404	8390
Well 52 Stage 7	6931	7959	8975	6523	11290	11290	11290	11290	9641	6758	7709	7697
Well 52 Stage 8	7034	8652	9752	6738	11862	11862	11862	11862	10631	7123	8125	8112
Well 53 Stage 1	6368	7741	9235	6715	12245	12245	12245	12245	10097	7634	7938	7921

Well 53 Stage 2	5922	7189	8185	5848	11168	11168	11168	11168	9177	6702	7495	7483
Well 53 Stage 3	6213	7792	8902	6142	11879	11879	11879	11879	10152	7163	7986	7972
Well 53 Stage 4	6359	7703	8922	6277	11896	11896	11896	11896	10028	7251	7904	7890
Well 53 Stage 5	6069	6944	7871	5673	10831	10831	10831	10831	8788	6473	7281	7269
Well 53 Stage 6	5565	7323	8275	5796	11230	11230	11230	11230	9408	6704	7595	7583
Well 54 Stage 1	15842	11586	10116	8499	20302	20302	20302	20302	14360	9873	15027	15008
Well 54 Stage 2	15908	11581	10111	8496	20293	20293	20293	20293	14354	9868	15020	15002
Well 54 Stage 3	15108	11577	10107	8492	20283	20283	20283	20283	14348	9863	15013	14995
Well 54 Stage 4	16707	11328	9858	8310	19786	19786	19786	19786	14032	9613	14666	14648
Well 54 Stage 5	16390	11322	9852	8306	19774	19774	19774	19774	14025	9607	14658	14640
Well 54 Stage 6	14969	11321	9851	8305	19772	19772	19772	19772	14024	9606	14656	14638
Well 54 Stage 7	15121	11317	9847	8302	19764	19764	19764	19764	14018	9602	14651	14633
Well 54 Stage 8	14882	11312	9842	8299	19755	19755	19755	19755	14013	9598	14645	14626
Well 54 Stage 9	15940	11308	9838	8296	19747	19747	19747	19747	14008	9594	14639	14621
Well 54 Stage 10	15470	11303	9833	8292	19737	19737	19737	19737	14001	9589	14632	14614
Well 54 Stage 11	14515	11300	9830	8290	19730	19730	19730	19730	13997	9585	14627	14609
Well 54 Stage 12	15036	11296	9826	8287	19723	19723	19723	19723	13993	9582	14622	14604
Well 54 Stage 13	15297	11293	9823	8285	19717	19717	19717	19717	13989	9579	14618	14600
Well 54 Stage 14	13500	11287	9817	8280	19704	19704	19704	19704	13980	9572	14609	14591
Well 54 Stage 15	14224	11286	9816	8280	19703	19703	19703	19703	13980	9572	14608	14590
Well 54 Stage 16	14131	11283	9813	8277	19695	19695	19695	19695	13975	9568	14603	14585
Well 54 Stage 17	13572	11282	9812	8277	19695	19695	19695	19695	13975	9568	14603	14584
Well 54 Stage 18	14062	11279	9809	8274	19688	19688	19688	19688	13970	9564	14598	14580
Well 54 Stage 19	14100	11277	9807	8273	19684	19684	19684	19684	13968	9562	14595	14577
Well 54 Stage 20	13450	11277	9807	8273	19683	19683	19683	19683	13967	9562	14595	14576
Well 54 Stage 21	13696	11275	9805	8271	19679	19679	19679	19679	13965	9560	14592	14574
Well 54 Stage 22	11000	11274	9804	8271	19678	19678	19678	19678	13964	9559	14591	14573
Well 54 Stage 23	14339	11274	9804	8271	19679	19679	19679	19679	13964	9559	14591	14573
Well 55 Stage 1	13000	11148	9678	8179	19426	19426	19426	19426	13804	9433	14415	14397

Well 55 Stage 2	13100	11161	9691	8188	19453	19453	19453	19453	13821	9446	14434	14416
Well 55 Stage 3	13134	11163	9693	8190	19456	19456	19456	19456	13823	9448	14436	14418
Well 55 Stage 4	13200	11175	9705	8198	19480	19480	19480	19480	13838	9460	14453	14435
Well 55 Stage 5	13900	11180	9710	8202	19490	19490	19490	19490	13844	9465	14460	14442
Well 55 Stage 6	13725	11182	9712	8204	19494	19494	19494	19494	13847	9467	14463	14445
Well 55 Stage 7	13800	11191	9721	8210	19512	19512	19512	19512	13859	9476	14475	14457
Well 55 Stage 8	14050	11201	9731	8218	19533	19533	19533	19533	13872	9486	14490	14472
Well 55 Stage 9	14000	11205	9735	8220	19540	19540	19540	19540	13876	9490	14495	14477
Well 55 Stage 10	12927	11216	9746	8229	19563	19563	19563	19563	13891	9501	14511	14492
Well 55 Stage 11	14250	11222	9752	8233	19574	19574	19574	19574	13898	9507	14518	14500
Well 55 Stage 12	13850	11225	9755	8235	19580	19580	19580	19580	13901	9510	14522	14504
Well 55 Stage 13	14000	11232	9762	8240	19595	19595	19595	19595	13911	9517	14533	14515
Well 55 Stage 14	13770	11239	9769	8245	19608	19608	19608	19608	13920	9524	14542	14524
Well 55 Stage 15	13050	11244	9774	8249	19619	19619	19619	19619	13926	9529	14549	14531
Well 55 Stage 16	14050	11253	9783	8255	19635	19635	19635	19635	13937	9538	14561	14543
Well 55 Stage 17	13500	11257	9787	8258	19643	19643	19643	19643	13942	9542	14567	14549
Well 55 Stage 18	13550	11264	9794	8263	19658	19658	19658	19658	13951	9549	14577	14559
Well 55 Stage 19	14050	11278	9808	8273	19685	19685	19685	19685	13969	9563	14596	14578

Appendix H Data Clustering

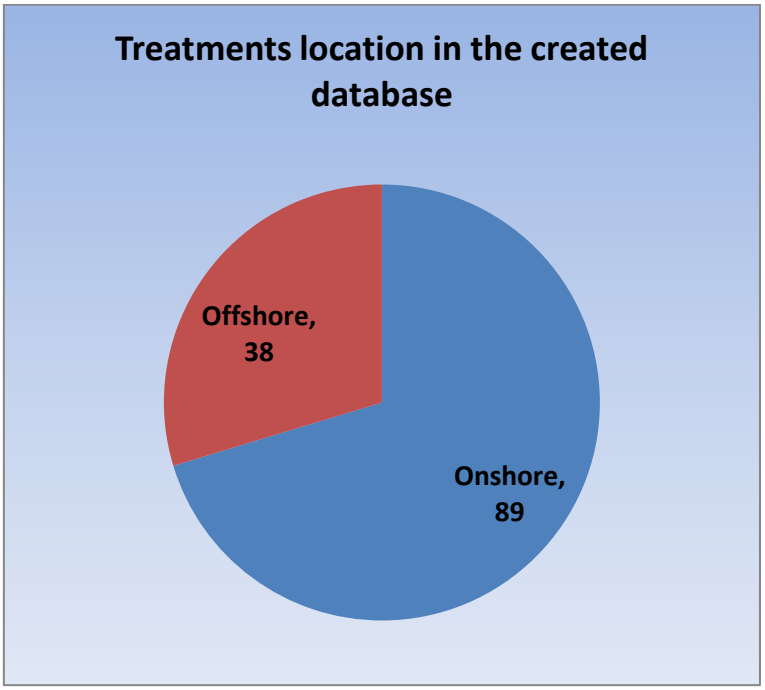

Figure 62: Distribution of onshore and offshore treatments in the created database

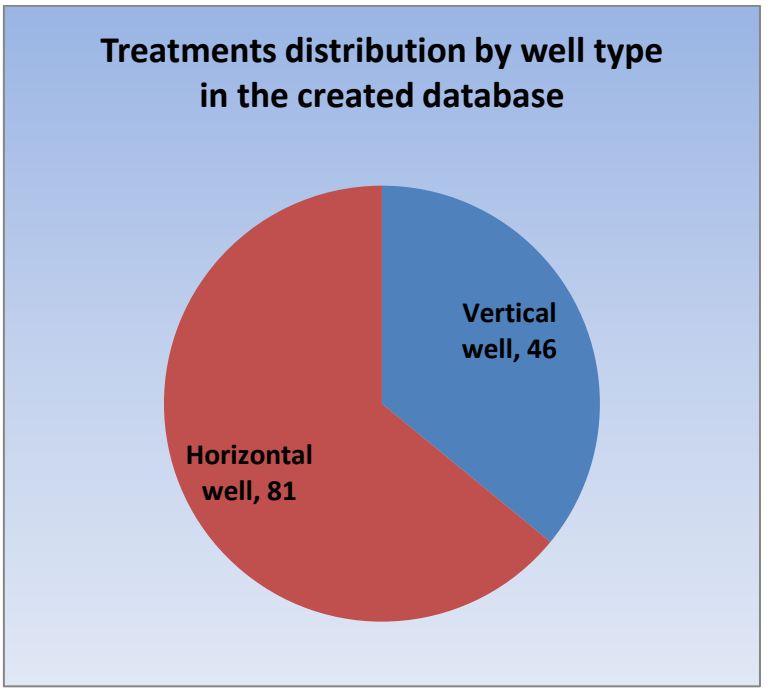

Figure 63: Distribution of treatments by vertical and deviated wells in the created database

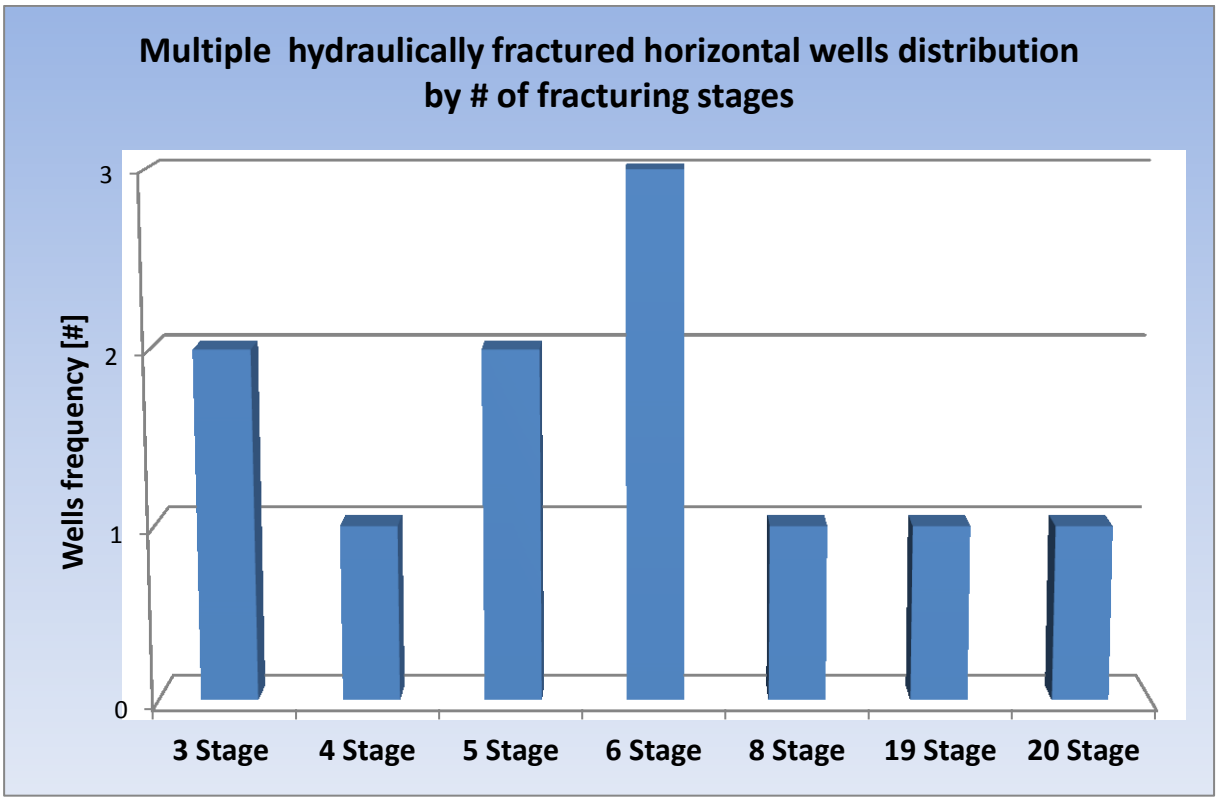

Figure 64: Distribution of the multiple hydraulically fractured horizontal wells by number of fracturing stages

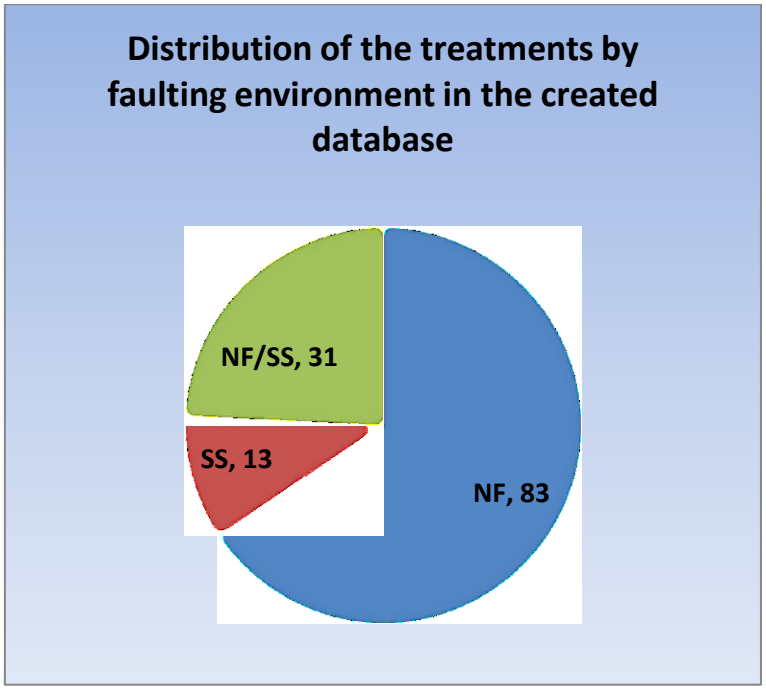

Figure 65: Distribution of treatments by normal, strike-slip and normal/strike-slip intermediate faulting environment in the created database

Appendix I Performance of the Models in Different Well Locations

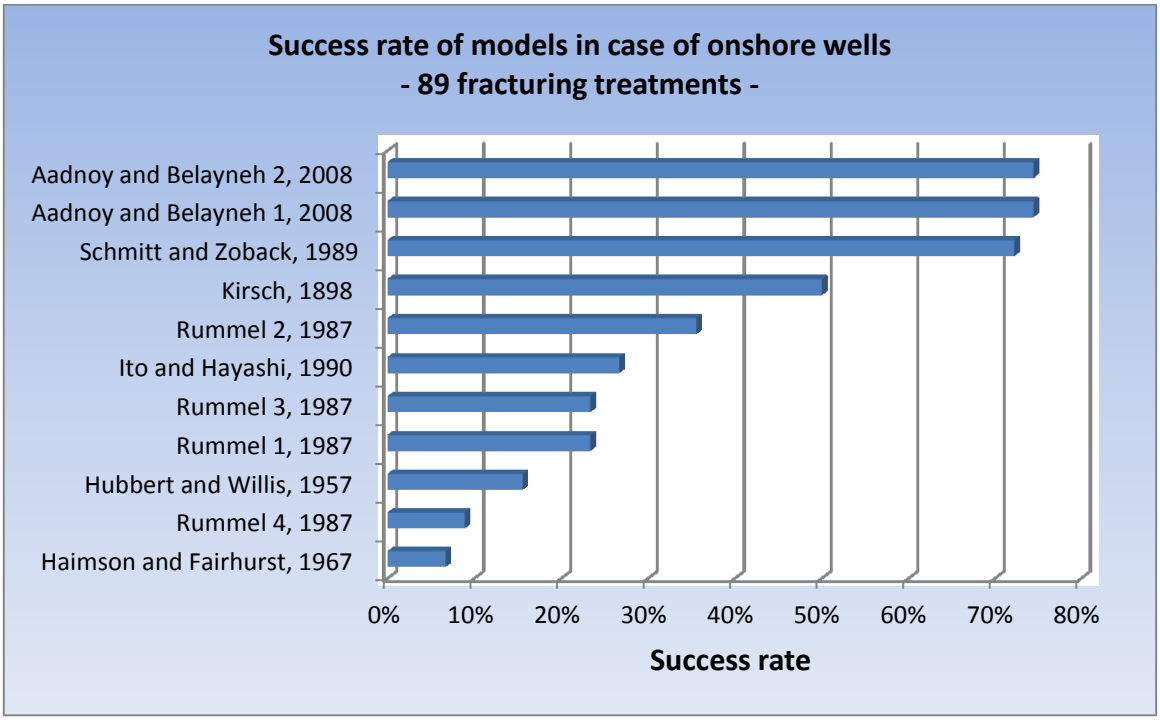

Figure 66: Success rate of the FBP prediction methods in case of onshore wells based on the percentage of the sample subset that falls within the acceptable region

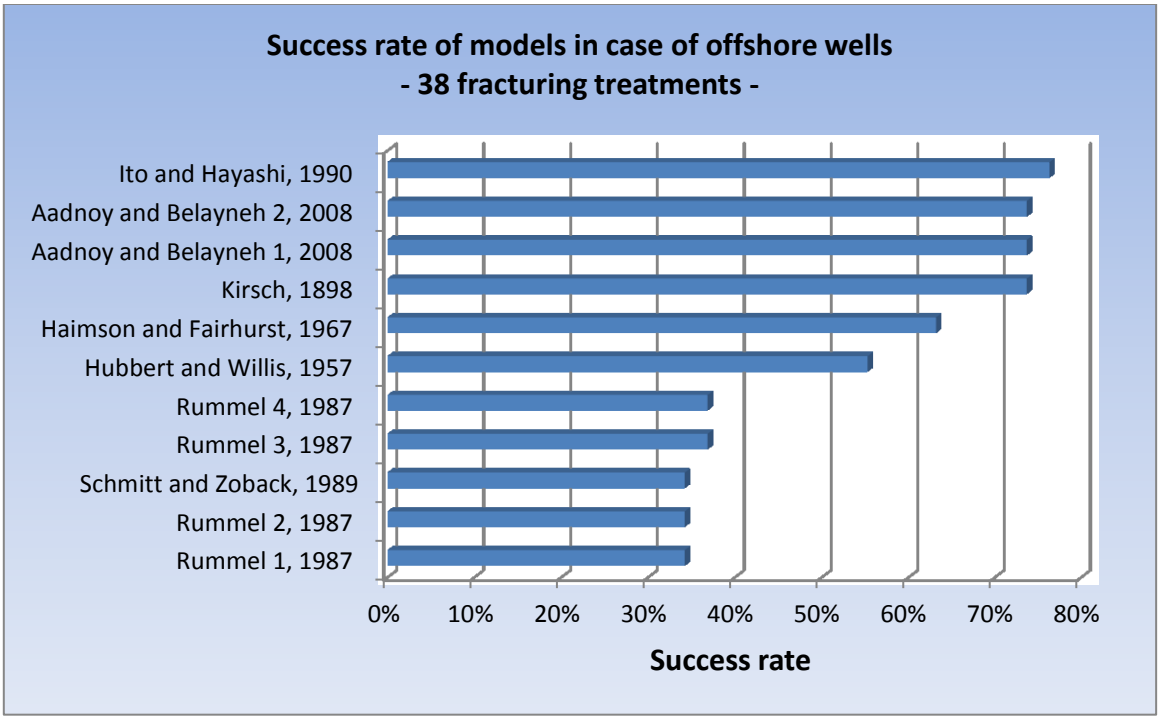

Figure 67: Success rate of the FBP prediction methods in case of offshore wells based on the percentage of the sample subset that falls within the acceptable region

Appendix J Performance of the Models in Different Well Types

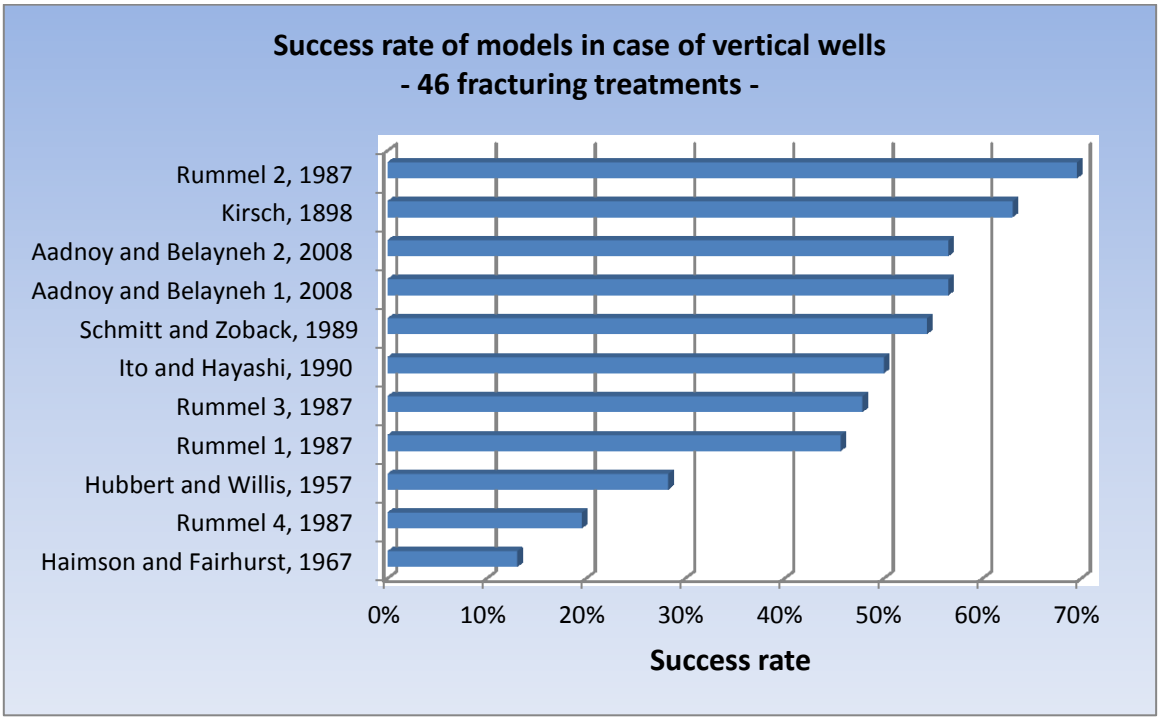

Figure 68: Success rate of the FBP prediction methods in case of vertical wells based on the percentage of the sample subset that falls within the acceptable region

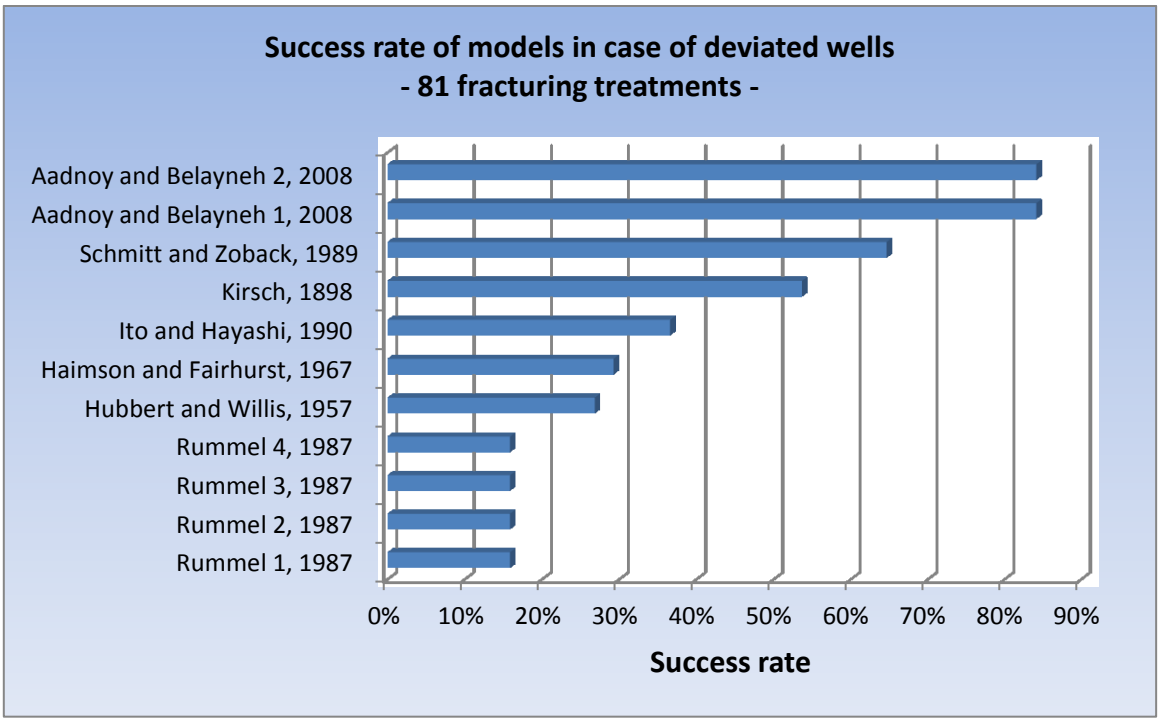

Figure 69: Success rate of the FBP prediction methods in case of deviated wells based on the percentage of the sample subset that falls within the acceptable region

Appendix K Performance of the Models in Different Depths

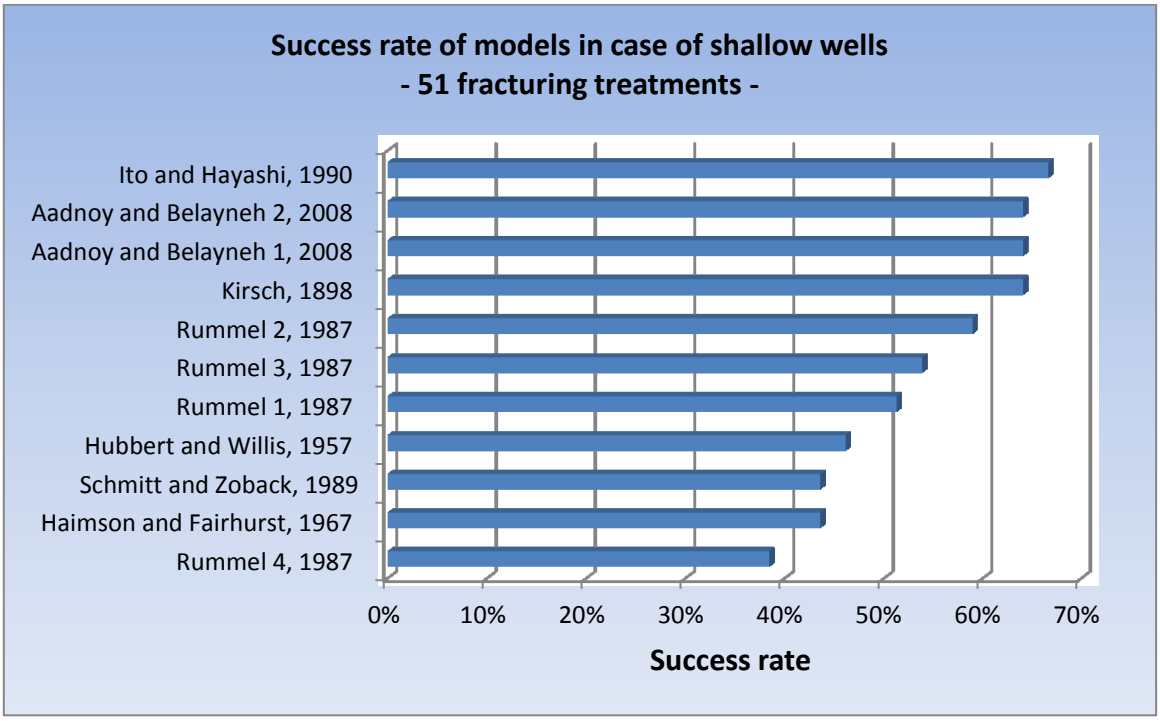

Figure 70: Success rate of the FBP prediction methods in case of shallow wells (1500–2300 m TVD) based on the percentage of the sample subset that falls within the acceptable region

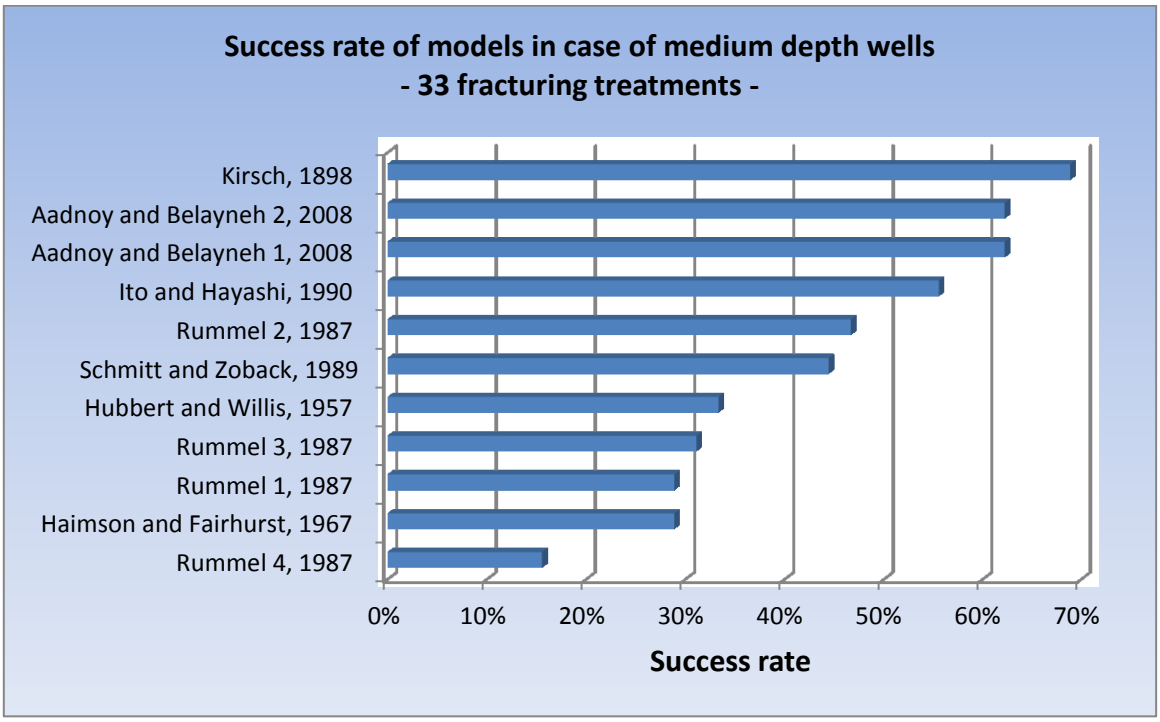

Figure 71: Success rate of the FBP prediction methods in case of medium depth wells (2300–3750 m TVD) based on the percentage of the sample subset that falls within the acceptable region

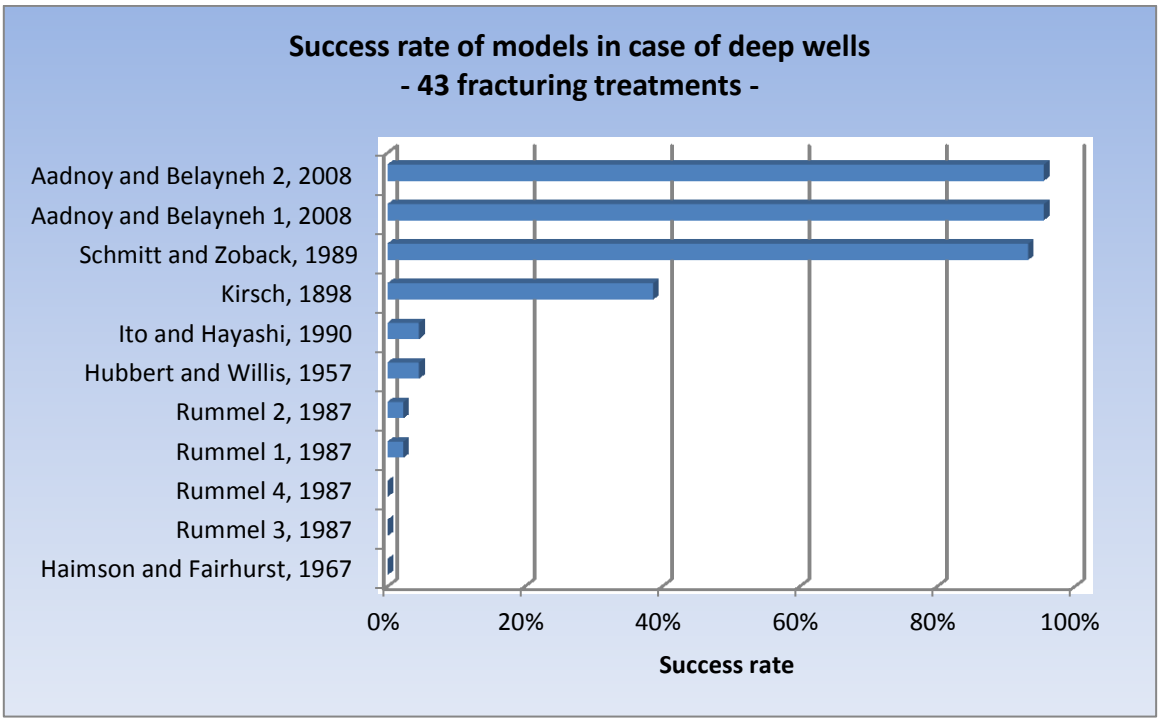

Figure 72: Success rate of the FBP prediction methods in case of deep wells (3750–4200 m TVD) based on the percentage of the sample subset that falls within the acceptable region

Appendix L Performance of the Models in Different Faulting Environments

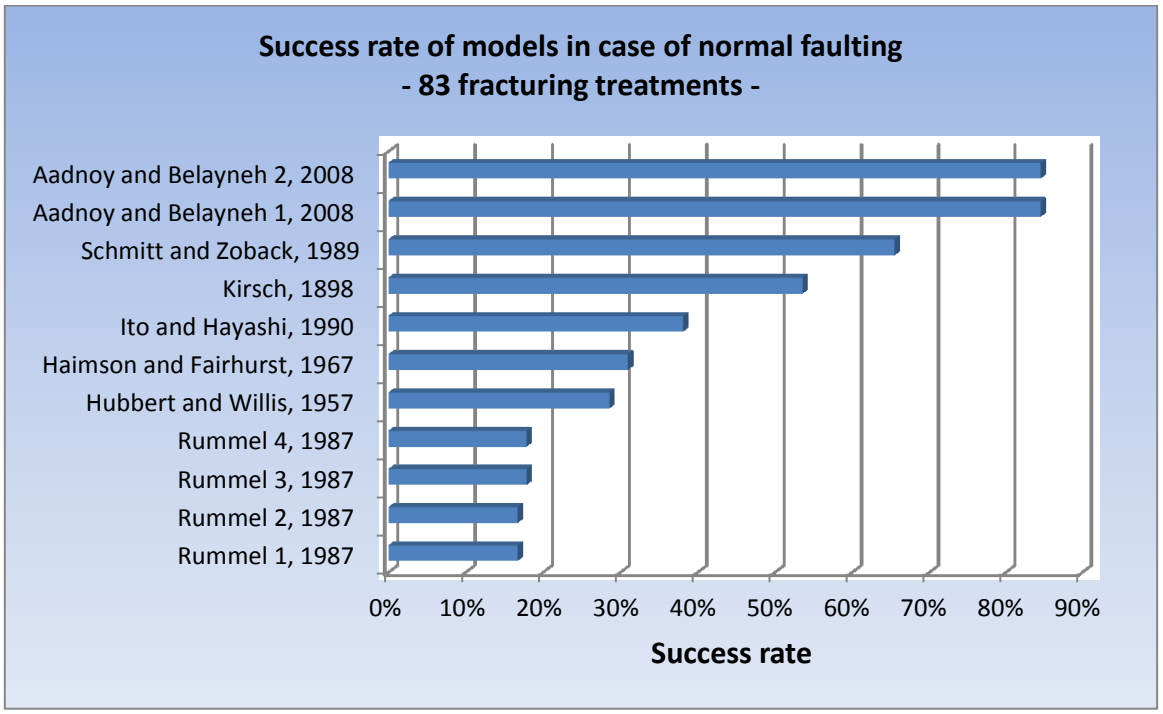

Figure 73: Success rate of the FBP prediction methods in case of normal faulting based on the percentage of the sample subset that falls within the acceptable region

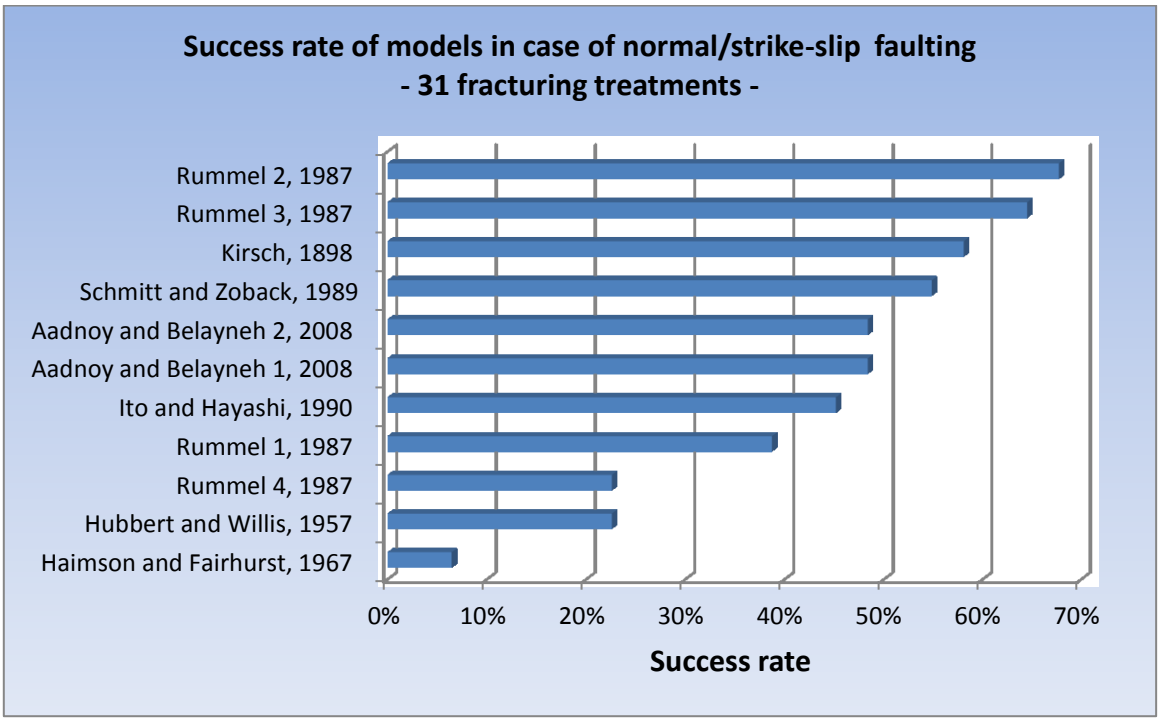

Figure 74: Success rate of the FBP prediction methods in case of normal/strike-slip faulting based on the percentage of the sample subset that falls within the acceptable region

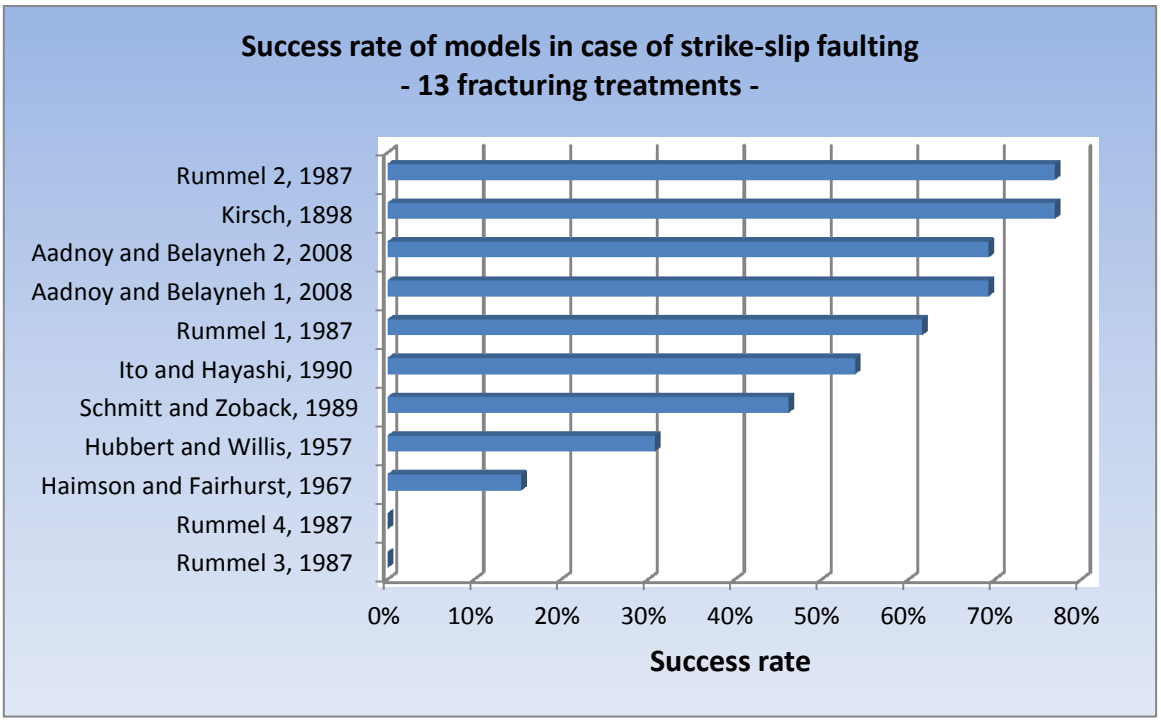

Figure 75: Success rate of the FBP prediction methods in case of strike-slip faulting based on the percentage of the sample subset that falls within the acceptable region

Appendix M Performance of the Models in Different Formation Types

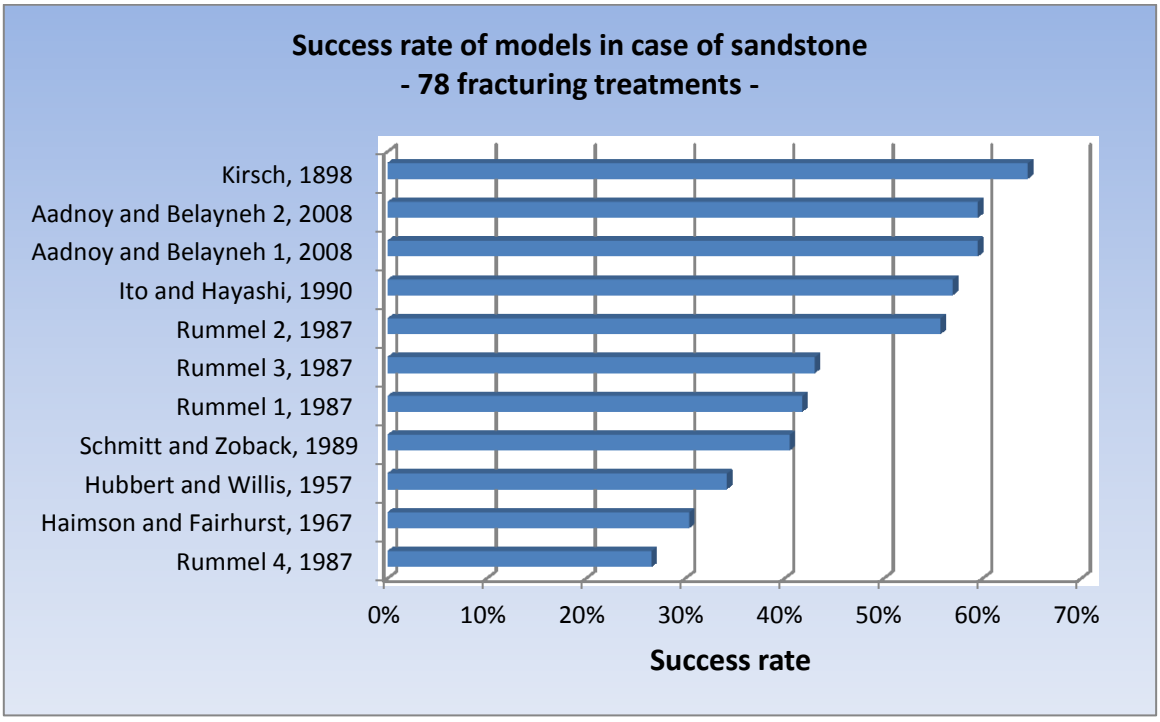

Figure 76: Success rate of the FBP prediction methods in case sandstone based on the percentage of the sample subset that falls within the acceptable region

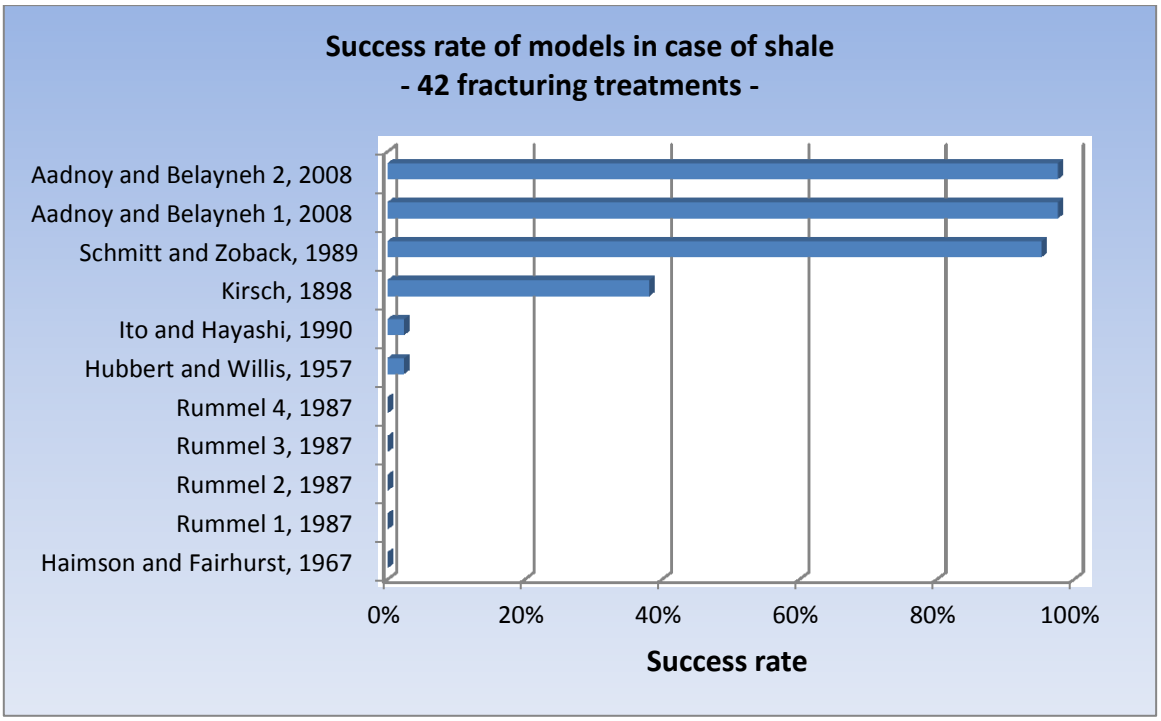

Figure 77: Success rate of the FBP prediction methods in case of shale based on the percentage of the sample subset that falls within the acceptable region

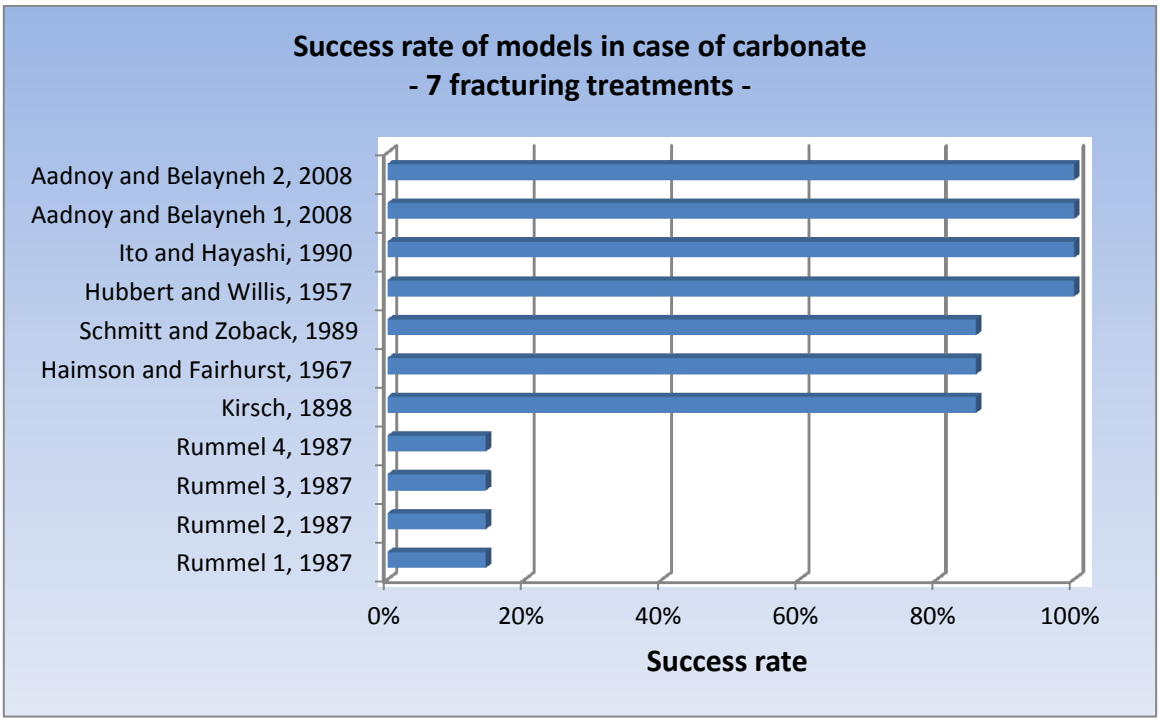

Figure 78: Success rate of the FBP prediction methods in case of carbonate based on the percentage of the sample subset that falls within the acceptable region

Appendix N Performance of the Models in Different Fields

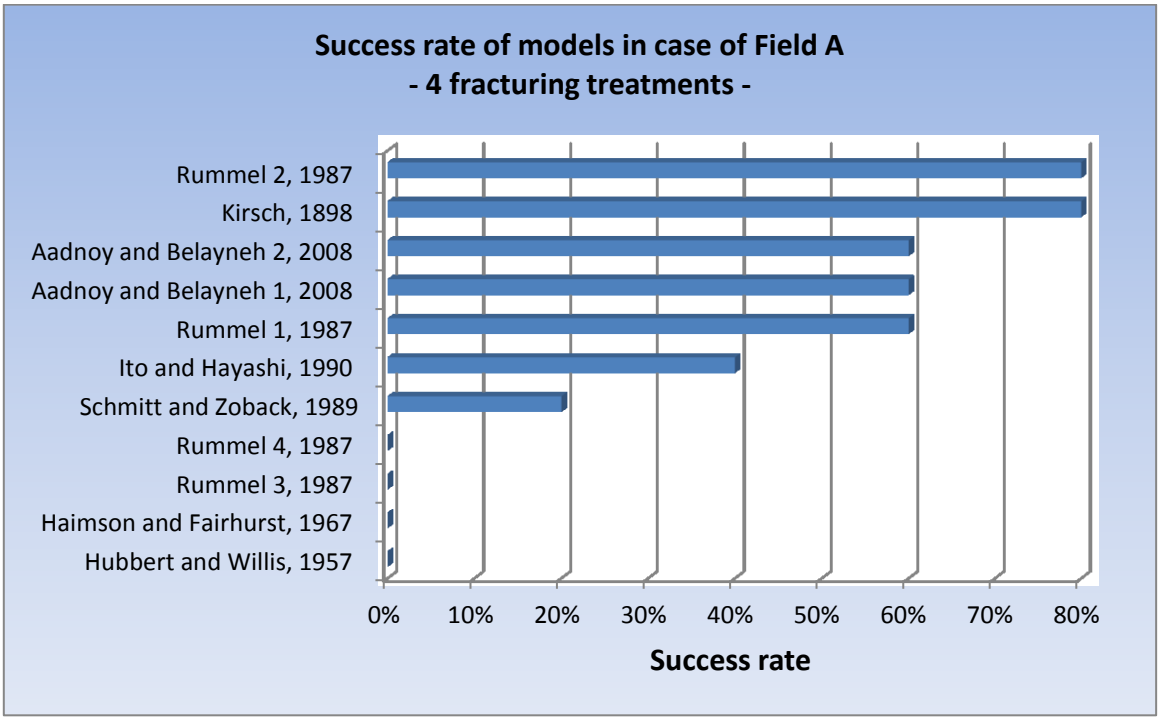

Figure 79: Success rate of the FBP prediction methods in case of Field A based on the percentage of the sample subset that falls within the acceptable region

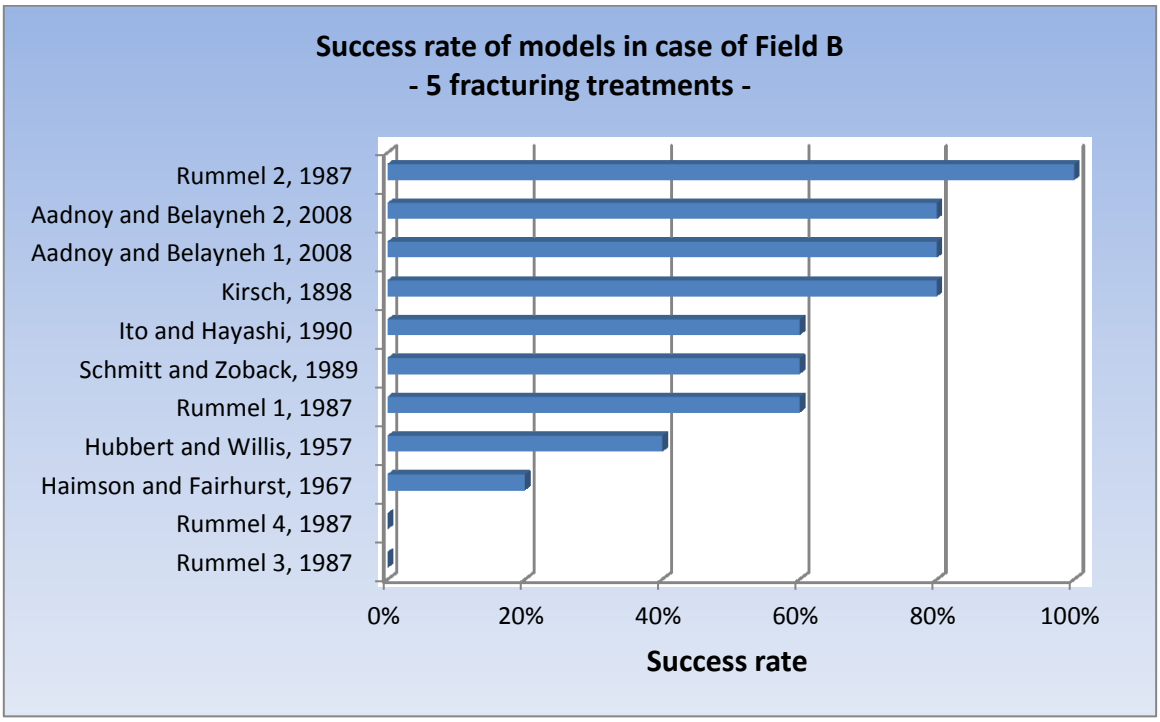

Figure 80: Success rate of the FBP prediction methods in case of Field B based on the percentage of the sample subset that falls within the acceptable region

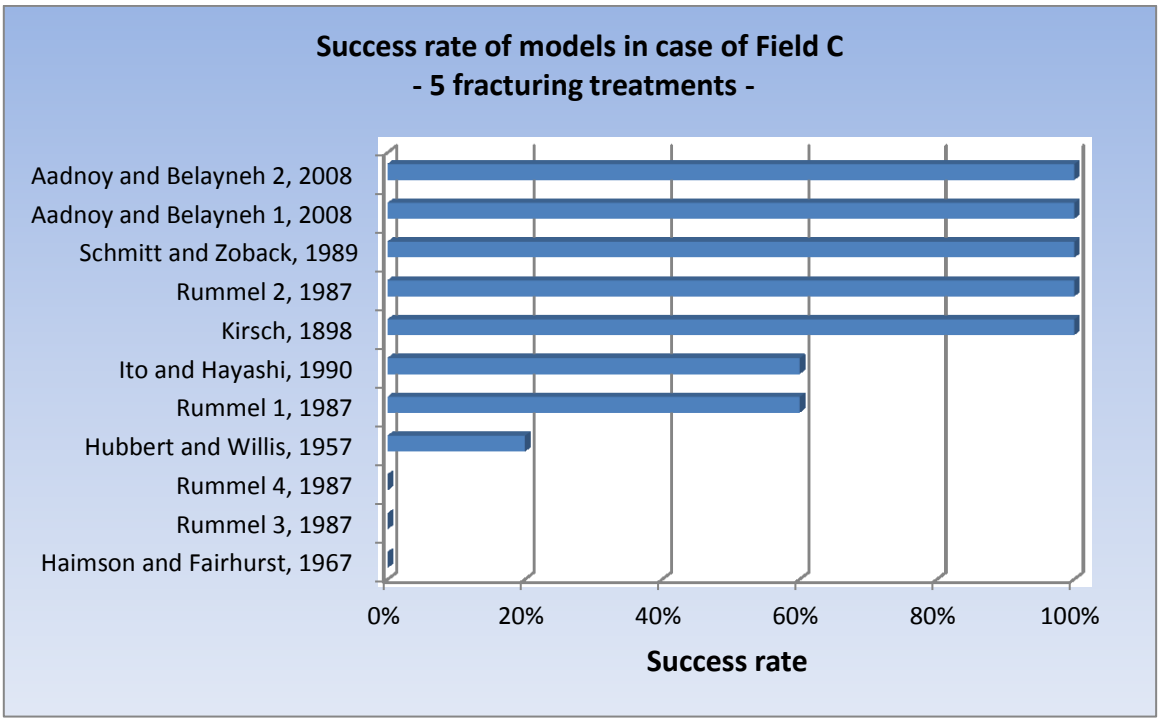

Figure 81: Success rate of the FBP prediction methods in case of Field C based on the percentage of the sample subset that falls within the acceptable region

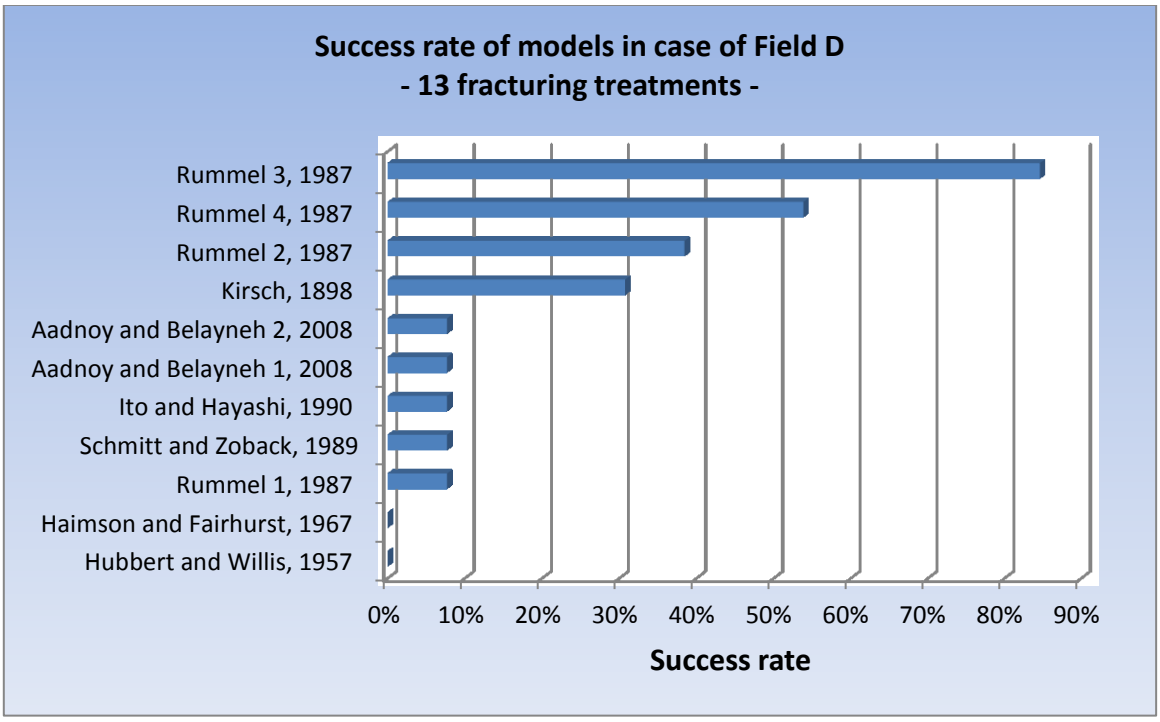

Figure 82: Success rate of the FBP prediction methods in case of Field D based on the percentage of the sample subset that falls within the acceptable region

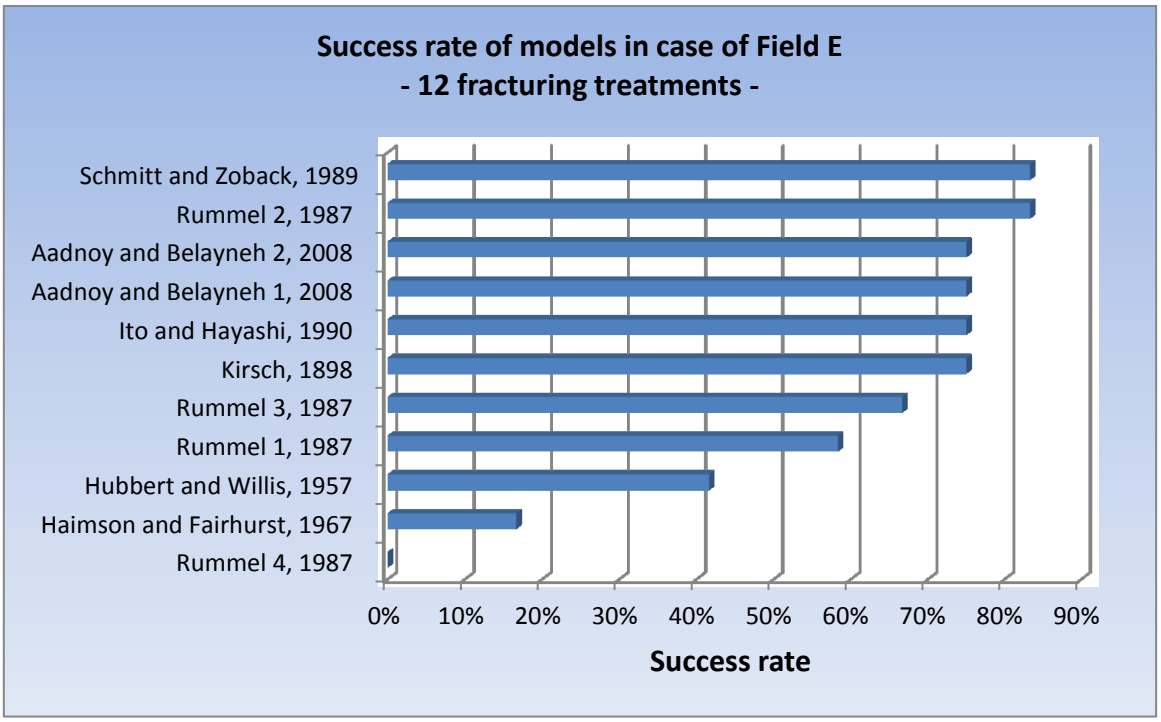

Figure 83: Success rate of the FBP prediction methods in case of Field E based on the percentage of the sample subset that falls within the acceptable region

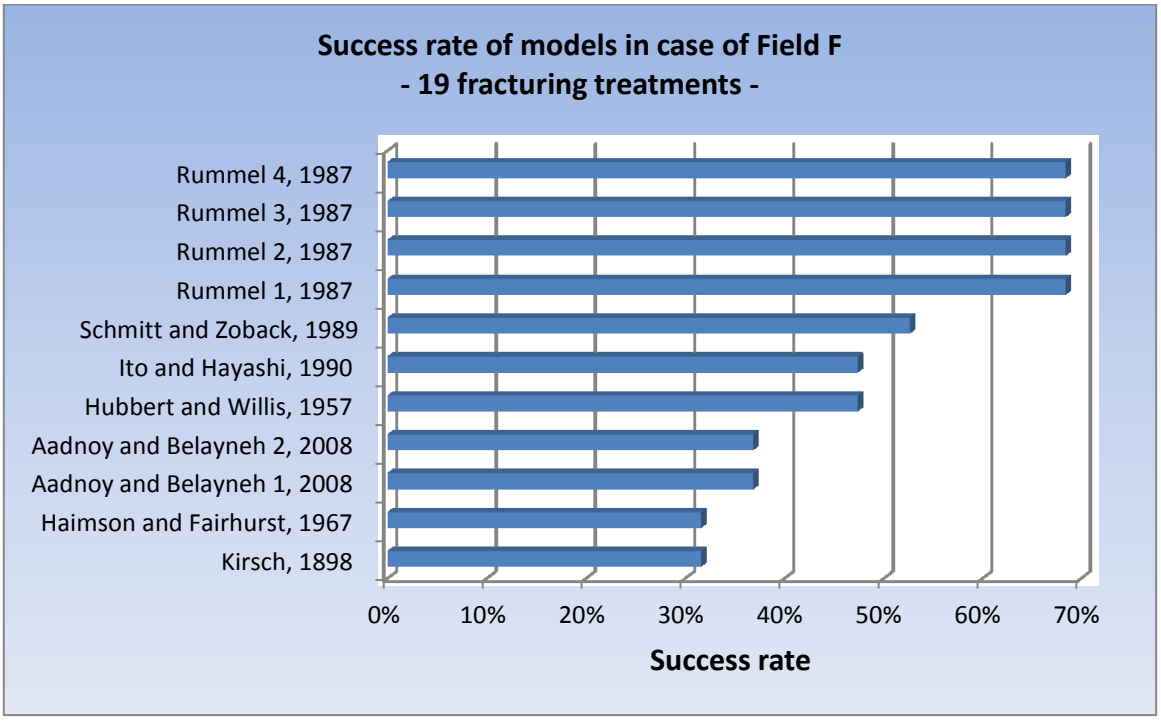

Figure 84: Success rate of the FBP prediction methods in case of Field F based on the percentage of the sample subset that falls within the acceptable region

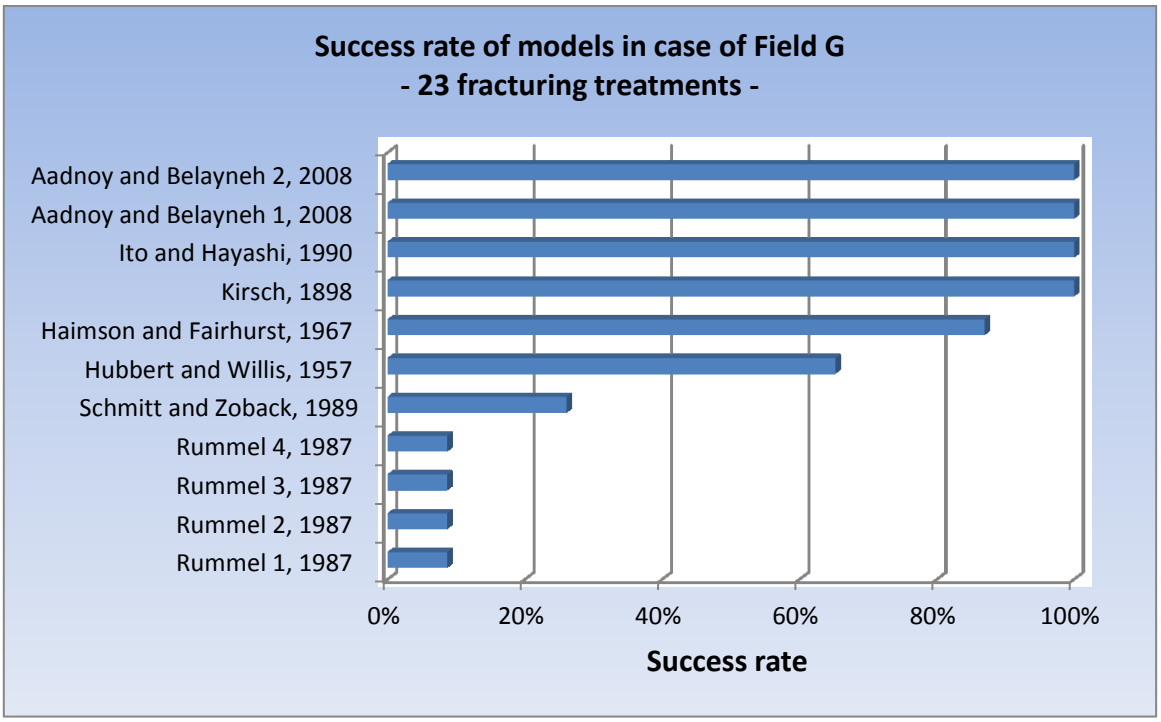

Figure 85: Success rate of the FBP prediction methods in case of Field G based on the percentage of the sample subset that falls within the acceptable region

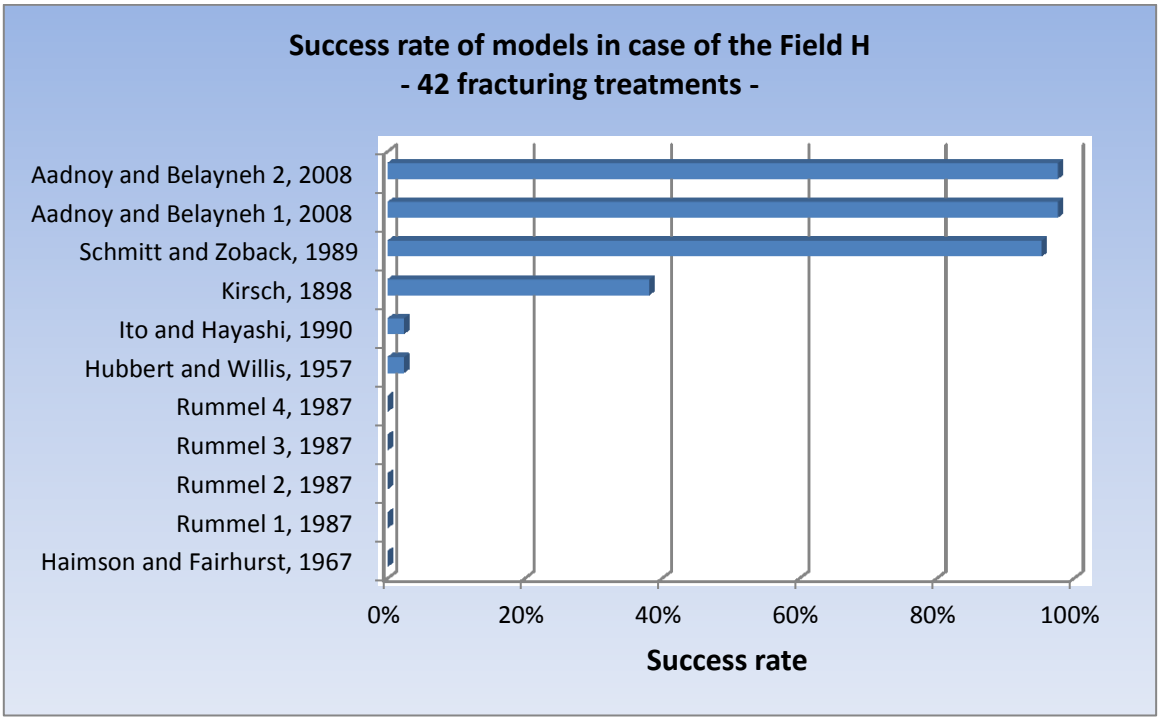

Figure 86: Success rate of the FBP prediction methods in case of Field H based on the percentage of the sample subset that falls within the acceptable region

Appendix O Test Treatments Results

Table 23: Measured and calculated Formation Breakdown Pressures by the conventional models and the Artificial Neural Network

Well name	Breakdown BHP	Kirsch, 1898	Hubbert and Willis, 1957	Haimson and Fairhurst, 1967	Rummel 1, 1987	Rummel 2, 1987	Rummel 3, 1987	Rummel 4, 1987	Schmitt and Zoback, 1989	Ito and Hayashi, 1990	Aadnoy and Belayneh 1, 2008	Aadnoy and Belayneh 2, 2008	Artificial Neural Network
Well 1	14716	11577	9055	7723	16432	16432	16432	16432	12542	7697	13134	13116	15844
Well 2	6922	6853	6655	6927	7742	7742	7742	7742	7921	3844	6216	6201	8071
Well 3	7582	7658	7394	8470	10294	10294	10294	10294	6787	5112	7394	7389	6925
Well 4	6879	4582	4409	4590	6729	6729	6729	6729	6131	3342	4962	4939	7101
Well 5	6197	4287	5623	4776	7900	7900	7900	7900	5134	5181	4625	4609	6355
Well 6	6556	6164	5939	5778	8767	8767	8767	8767	7709	4354	6519	6508	7364
Well 7	7613	6741	6518	6811	8693	8693	8693	8693	7551	4317	6624	6609	8348
Well 8	6705	6178	5951	5787	8851	8851	8851	8851	7728	4395	6568	6552	7269
Well 9	7657	6051	5873	6263	6960	6960	6960	6960	7139	3456	5547	5532	7638
Well 10	7735	6548	6328	6649	8590	8590	8590	8590	7342	4266	6503	6492	8116
Well 11	6324	7658	7394	7304	10294	10294	10294	10294	8633	5112	7723	7719	6914
Well 12	6688	7571	7307	7232	10294	10294	10294	10294	8539	5112	7690	7686	7331
Well 13	5409	7744	7478	6973	10378	10378	10378	10378	9255	5154	7842	7838	6580
Well 14	5995	5969	7293	5989	8380	8380	8380	8380	7195	5430	5479	5463	7350